FERMILAB-Pub-00/251-T
SLAC-PUB-8643

arXiv:hep-ph/0008070 v2 16 Oct 2000

Low-Scale and Gauge-Mediated Supersymmetry Breaking at the Fermilab Tevatron Run II

CONVENERS:

Ray Culbertson[1](CDF), Stephen P. Martin[2,3], Jianming Qian[4](DØ), Scott Thomas[5]

CONTRIBUTORS: Howard Baer[6], Wasiq Bokhari[7](CDF), Sailesh Chopra[8](DØ), Chih-Lung Chou[9], Amy Connolly[10](CDF), Ray Culbertson[1](CDF), Dave Cutts[11](DØ), Regina Demina[12](CDF,DØ), Bhaskar Dutta[13], Gary Grim[14](CDF), Greg Landsberg[11](DØ), Stephen P. Martin[2,3], Konstantin Matchev[3], P.G. Mercadante[6,15], D.J. Muller[16], S. Nandi[16], Michael Peskin[9], Jianming Qian[4](DØ), Uri Sarid[17], David Stuart[1](CDF), Benn Tannenbaum[18](CDF), Xerxes Tata[15], Scott Thomas[5], Randy Thurman-Keup[19](CDF), Ming-Jer Wang[20](CDF), Yi-li Wang[15]

[1] *MS 318, Fermi National Accelerator Laboratory, Batavia IL 60510*
[2] *Physics Department, Northern Illinois University, DeKalb IL 60115*
[3] *Theoretical Physics, MS 106, Fermilab, Batavia IL 60510*
[4] *Physics Department, University of Michigan, Ann Arbor MI 48109*
[5] *Physics Department, Stanford University, Stanford CA 94305*
[6] *Department of Physics, Florida State University, Tallahassee FL 32306*
[7] *Department of Physics, University of Pennsylvania, Philadelphia PA 19104*
[8] *Brookhaven National Laboratory, Upton NY 11973*
[9] *Stanford Linear Accelerator Center, Stanford University, Stanford CA 94309*
[10] *Ernest Orlando Lawrence Berkeley National Laboratory, Berkeley CA 94720*
[11] *Physics Department, Brown University, Providence RI 02912*
[12] *Physics Department, Kansas State University, Manhattan KS 66506*
[13] *Center for Theoretical Physics, Dept. of Physics, Texas A&M University, College Station TX 77843*
[14] *Physics Department, University of California, Davis CA 95616*
[15] *Dept. of Physics and Astronomy, University of Hawaii, Honolulu HI 96822*
[16] *Department of Physics, Oklahoma State University, Stillwater OK 74078*
[17] *Department of Physics, University of Notre Dame, Notre Dame IN 46556*
[18] *Department of Physics, University of California, Los Angeles CA 90095*
[19] *Argonne National Laboratory, Argonne IL 60439*
[20] *Institute of Physics, Academia Sinica, Taipei, Taiwan 11529 Republic of China*

Abstract. The prospects for discovering and studying signals of low-scale supersymmetry breaking models at the Tevatron Run II and beyond are explored. These models include gauge-mediated supersymmetry breaking as the most compelling and concrete realization, but more generally are distinguished by the presence of a nearly massless Goldstino as the lightest supersymmetric particle. The next-lightest supersymmetric particle(s) (NLSP) decays to its partner and the Goldstino. Depending on the supersymmetry breaking scale, these decays can occur promptly or on a scale comparable to or larger than the size of a detector. A systematic analysis based on a classification in terms of the identity of the NLSP and its decay length is presented. The various scenarios are discussed in terms of signatures and possible event selection criteria. The Run II and beyond discovery and exclusion reaches, including the effects of background, are detailed for the most compelling cases. In addition to standard event selection criteria based on missing energy and photons, leptons, jets, taus, tagged b-jets, or reconstructed Z-bosons, more exotic signals of metastable NLSPs such as displaced photons, large negative impact parameter tracks, kink tracks, both opposite and same-sign highly ionizing tracks, time of flight measurements, charge-changing tracks, charge-exchange tracks, and same-sign di-top events are investigated. The interesting possibility of observing a Higgs boson signal in events that are efficiently "tagged" by the unique signatures of low-scale supersymmetry breaking is also considered.

Contents

I Introduction **3**

II Model Lines for Run II Studies and Minimal Gauge Mediation **9**

III Object Identification and Acceptances **11**
- A CDF study object identification and acceptance parameters . . . 11
- B DØ study object identification and acceptance parameters . . . 12
- C ISAJET study object identification and acceptance parameters . . . 13
- D PYTHIA-SHW study object identification and acceptance parameters . . . 14

IV Bino-like Neutralino NLSP **15**
- A Prompt Decays to Photons . . . 17
  - 1 CDF study of promptly-decaying Bino-like NLSP . . . 19
  - 2 DØ study of promptly-decaying Bino-Like NLSP . . . 22
  - 3 ISAJET Studies of Bino-like NLSP . . . 23
- B Non-prompt Decays and Photon Pointing . . . 26
  - 1 CDF study of Displaced Photons . . . 26
  - 2 DØ study of Displaced Photons . . . 27
- C Associated Higgs Production from Supersymmetric Cascades . . . 28
  - 1 CDF study of Associated Higgs production in SUSY events . . . 28

V Higgsino-like Neutralino NLSP **30**
- A Prompt Decays to Higgs Bosons, Z Bosons, and Photons . . . 35
  - 1 CDF study of Higgsino-like Neutralino NLSP . . . 35
  - 2 DØ study of Higgsino-like Neutralino NLSP . . . 39
  - 3 ISAJET studies of Higgsino-like Neutralino NLSP . . . 40
  - 4 PYTHIA-SHW studies of Higgsino-like Neutralino NLSP . . . 44
- B Higgs Bosons from Higgsino Decay . . . 45
- C Non-Prompt Decays to Higgs and Z Bosons . . . 47

VI Stau NLSP **47**
- A CDF study of Stau NLSP Model Line with prompt $\widetilde{\tau}_1$ decay . . . 49
- B DØ study of Stau NLSP Model Line with prompt $\widetilde{\tau}_1$ decays . . . 54
- C ISAJET study of Stau NLSP Model Line with prompt $\widetilde{\tau}_1$ decays . . . 56
- D CDF study of quasi-stable staus in the Stau NLSP Model Line . . . 61
- E DØ study of quasi-stable stau signals in the Stau NLSP Model Line . . . 63

VII Slepton Co-NLSP **64**
- A CDF study of prompt slepton decay signals in the Slepton co-NLSP Model Line . . . 68
- B DØ study of prompt slepton decay signals for the Slepton co-NLSP Model Line . . . 70
- C DØ study of quasi-stable slepton signals for the Slepton co-NLSP Model Line . . . 73

VIII Squark NLSP **73**
- A Prompt Squark Decay . . . 76
  - 1 CDF study of Prompt Squark Decay . . . 78
- B Mesino and Sbaryon Displaced Decay Signals . . . 78
- C Quasi-stable Mesino and Sbaryon Signals . . . 79
- D Mesino Oscillations . . . 81
  - 1 CDF study of Mesino Oscillations . . . 82

IX Other NLSP Scenarios **82**
- A Gluino NLSP . . . 83
- B Singletino NLSP . . . 83
- C Neutralino-Stau Co-NLSP . . . 83
- D Sneutrino NLSP . . . 84

X Direct Goldstino Pair Production **84**
1 CDF studies of direct Goldstino production 84

XI Summary **85**

Appendix A: Minimal gauge mediation and variations **87**
1 Minimal model of gauge mediation 88
2 Beyond minimal gauge mediation 90

Appendix B: Decays to the Goldstino **93**

Appendix C: List of Model Lines Studied **95**

Appendix D: Glossary of Acronyms **96**

I INTRODUCTION

Supersymmetry has emerged as the most promising candidate solution to the hierarchy problem associated with the large separation between the electroweak and Planck scales. Supersymmetry (SUSY) stabilizes the Higgs boson mass against potentially dangerous quantum contributions from ultraviolet physics. Supersymmetry requires that for each known particle there exists a superpartner which differs in spin by $\frac{1}{2}$ unit of angular momentum. Spontaneous SUSY breaking in general splits the particle and superpartner masses, consistent with the non-observation of Bose-Fermi degeneracy in the physical spectrum at low energies. In supersymmetric extensions of the Standard Model with spontaneously broken supersymmetry, quantum effects of the top squark scalar superpartners of the top quark lead naturally, through the large top quark Yukawa coupling, to the observed electroweak symmetry breaking. In this way the electroweak scale is *determined* by the superpartner masses.

The search for superpartners with electroweak scale masses constitutes a major effort at present and future high energy colliders. This report presents studies of interesting and unique signatures of low-scale supersymmetry breaking which can be probed at the Fermilab Tevatron Run II. The results of these studies suggest a wide range of new analysis which should be implemented in the search for supersymmetry. In some channels the Tevatron has a very significant discovery reach for supersymmetry in Run II. All the studies presented here were completed as part of the Supersymmetry and Higgs Workshop in preparation for Run II.

The manner and scale at which supersymmetry is spontaneously broken has crucial implications for the phenomenology of collider searches for the superpartners. The spontaneous breaking of any global symmetry implies the existence of a Nambu-Goldstone particle to realize the symmetry in the broken phase. Since supersymmetry is a fermionic symmetry which relates Bosons and Fermions, the Nambu-Goldstone particle is a fermion, the Goldstino.

In order to preserve supersymmetry in a theory which includes gravity, supersymmetry must be promoted to a local symmetry. For any local symmetry realized in the broken phase, the gauge particle becomes massive by eating the Nambu-Goldstone particle. With spontaneously broken local supersymmetry, the spin $\frac{1}{2}$ Goldstino becomes the longitudinal components of the spin $\frac{3}{2}$ gravitino superpartner of the graviton. The gravitino-Goldstino gains a mass by this super-Higgs mechanism of

$$m_{\widetilde{G}} = \frac{F}{\sqrt{3}M_P} \simeq 2.4 \left(\frac{\sqrt{F}}{100 \text{ TeV}}\right)^2 \text{ eV}, \tag{1.1}$$

where $M_P = 2.4 \times 10^{18}$ GeV is the reduced Planck mass, and F is the order parameter for spontaneous supersymmetry breaking with units of [mass]^2. F is a vacuum expectation value (of an auxiliary field) which measures the magnitude of supersymmetry breaking in the vacuum state. Supersymmetry is restored for $F \to 0$. Couplings of the helicity $\pm 1/2$ Goldstino components discussed below are only directly relevant to accelerator phenomenology for a gravitino which is much lighter than the energy scale of a collider experiment. In addition, the helicity $\pm 3/2$ components only couple with gravitational strength and are never relevant to accelerator phenomenology. It is therefore most appropriate to consider only the essentially massless Goldstino,

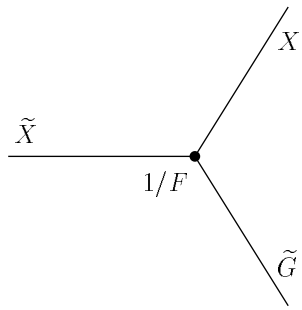

FIGURE 1. The Goldstino $\widetilde{G}$ derivatively couples each particle X to its superpartner $\widetilde{X}$, with an interaction strength inversely proportional to F.

although gravitino and Goldstino are used interchangeably in the literature. Use of the gravitino mass rather than the supersymmetry breaking scale, $\sqrt{F}$, to characterize accelerator signatures is also not very appropriate since this mass scale does not appear in any relevant process.

All the signatures studied in this report follow either directly or indirectly from the existence of the Goldstino. The analog of the Goldberger-Treiman relation implies that each particle is derivatively coupled to its superpartner through the Goldstino with a strength inversely proportional F, as illustrated in Fig. 1. If the scale of supersymmetry breaking is not too high, these interactions can be relevant to accelerator physics. In particular a massive superpartner, $\widetilde{X}$, can decay to its partner particle, X, by emitting an essentially massless Goldstino [1] with decay rate:

$$\Gamma(\widetilde{X} \to X\widetilde{G}) = \frac{\kappa m_{\widetilde{X}}^5}{16\pi F^2}\left(1 - \frac{m_X^2}{m_{\widetilde{X}}^2}\right)^4 , \tag{1.2}$$

where κ is a mixing parameter to be evaluated for the particular model parameters. If X and $\widetilde{X}$ are unmixed states within the same supermultiplet, such as for slepton decay to a lepton and Goldstino, $\kappa = 1$. However, for superpartner mass eigenstates which are mixtures of superpartners in different supermultiplets, $\kappa < 1$ is possible. For a pure $U(1)_Y$ Bino decay to a photon and Goldstino, $\kappa = \cos^2\theta_W$. A complete list of the decay rates for the particles of the minimal supersymmetric standard model (MSSM) through Goldstino emission is given in Appendix B. The decay rate (1.2) corresponds to a decay length of

$$c\tau(\widetilde{X} \to X\widetilde{G}) \simeq \left(\frac{100\ \mu\text{m}}{\kappa}\right)\left(\frac{100\ \text{GeV}}{m_{\widetilde{X}}}\right)^5\left(\frac{\sqrt{F}}{100\ \text{TeV}}\right)^4\left(1 - \frac{m_X^2}{m_{\widetilde{X}}^2}\right)^{-4} \tag{1.3}$$

For a supersymmetry breaking scale, $\sqrt{F}$, much larger than a few 1000 TeV, superpartner decays through the Goldstino take place well outside a collider detector, and are not directly relevant to accelerator physics. However, for supersymmetry breaking scales below a few 1000 TeV, decays through the Goldstino can occur within a detector, and therefore have a very direct impact on the types of SUSY signatures which can be observed [2].

Supersymmetric particles are generally unstable to decays to lighter superparticles. These decays can take place through interactions related by supersymmetry to the ordinary strong, electromagnetic, or weak couplings. If kinematically allowed, these decays are generally much more rapid than decay through the Goldstino for any reasonable $\sqrt{F}$ above the electroweak scale. Heavy superpartners therefore generally rapidly cascade decay to the lightest standard model superpartner. If R-parity is conserved, the lightest standard model superpartner is stable with respect to all the MSSM couplings. However, as discussed above, if decay through the Goldstino can take place within a detector, the Goldstino is essentially massless, and is therefore the lightest supersymmetric particle (LSP). The lightest standard model superpartner is therefore the next to lightest superpartner (NLSP). Because of the Goldstino coupling, the NLSP is only meta-stable, and can decay to its partner through LSP Goldstino emission with decay rate eq. (1.2) or decay length eq. (1.3). The NLSP decay length is shown in Fig. 2 as a function of the SUSY breaking scale $\sqrt{F}$ for a number of different NLSP masses. Because all cascades pass through the NLSP, the identity of the NLSP and the SUSY breaking scale, which determines the NLSP decay length, are the crucial parameters in classifying the types of SUSY signatures which may arise [2].

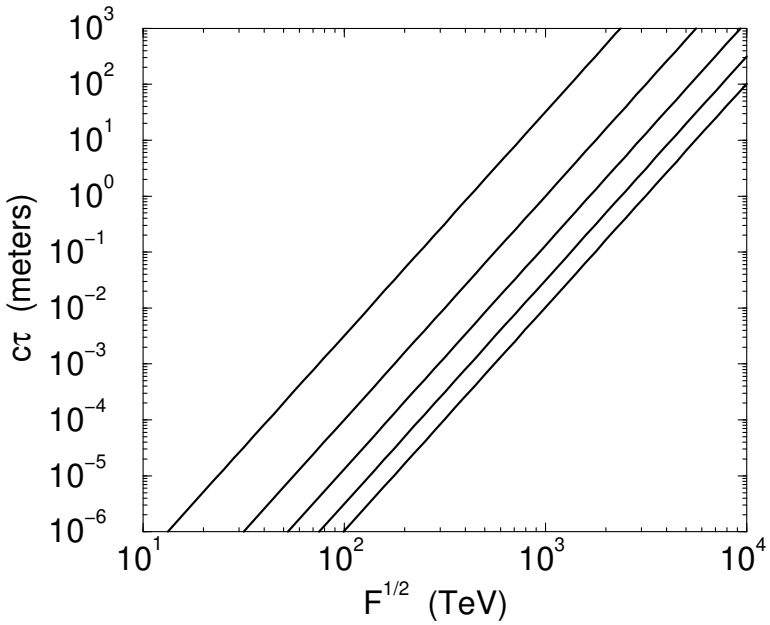

FIGURE 2. NLSP decay length, $c\tau(\widetilde{X} \to X\widetilde{G})$, in meters, as a function of the supersymmetry breaking scale, $\sqrt{F}$, in TeV. From top to bottom the lines are for an NLSP mass $m_{\tilde{X}} = 50$, 100, 150, 200, 250 GeV and with $m_X = 0$ and $\kappa = 1$.

It is important to note that more than one superpartner can effectively act as the NLSP. This can occur if the lightest standard model superpartners are nearly degenerate, with any allowed decays between these states taking place well outside the detector. Each of these superpartners can however decay to the Goldstino, and so each is effectively an NLSP. This situation is most natural if there is some (perhaps approximate) symmetry which enforces the near degeneracy of some of the superpartners. As an example, the approximate lepton chiral flavor symmetry, indicated by the small lepton Yukawa couplings, can be sufficient to enforce the near degeneracy of the lightest slepton in each of the three generations. If the splitting between these sleptons is smaller than the associated lepton mass, then conservation of individual lepton number forbids decays between the slepton states which involve charged leptons. Decays involving neutrinos are allowed, but are slow enough to take place well outside a detector. The lightest slepton in each generation then form an effective slepton co-NLSP [3–6].

The range of possibilities for the NLSP and SUSY breaking scale present many unique and challenging experimental signatures which must be classified in order to fully cover all discovery modes for supersymmetry. In principle any of the MSSM particles may be the NLSP. Some of possibilities for the NLSP, along with the decay modes to the Goldstino, are listed in Table 1. A neutralino NLSP is in general a mixture of gaugino and Higgsino eigenstates, and so can decay to either the γ or Z gauge bosons, or the h Higgs boson, $\widetilde{\chi}_1^0 \to (\gamma, Z, h)\widetilde{G}$. A slepton NLSP decays to its partner lepton and the Goldstino, $\widetilde{\ell} \to \ell\widetilde{G}$. Likewise, a squark NLSP decays to its partner quark and the Goldstino, $\widetilde{Q} \to q\widetilde{G}$. In the case of a stop-like squark lighter than the top quark, decay to a b-quark, W boson, and Goldstino, $\tilde{t} \to bW\widetilde{G}$ (or $\tilde{t} \to c\widetilde{G}$) results. Finally, a gluino NLSP would decay to the gluon and Goldstino, $\widetilde{g} \to g\widetilde{G}$.

The NLSP decay lengths can generally be divided into three relevant ranges. The first are prompt decays which can not be resolved as secondary vertices, and therefore appear to originate from the interaction region. Since SUSY particles are produced in pairs the signatures are then two hard partons coming from the NLSP decays, significant missing energy carried by the Goldstino pair, and possibly other partons from cascade decays to the NLSPs. Since the Goldstino is essentially massless, the partons arising from the NLSP decays can be very hard. A search for each NLSP possibility may be implemented by an inclusive search for the appropriate hard parton pairs in association with missing energy.

The second range of decay lengths are macroscopic but within the detector. In this case the partons arising from NLSP decay do not necessarily point back to the interaction region. For a neutralino decay $\widetilde{\chi}_1^0 \to \gamma\widetilde{G}$ this leads to displaced photons. This presents the experimental challenge of accurate photon pointing. For

TABLE 1. Decay modes to the Goldstino in various NLSP scenarios.

NLSP	Decay to the Goldstino
Bino-like Neutralino	$\widetilde{\chi}_1^0 \to \gamma\ \widetilde{G}$
Higgsino-like Neutralino	$\widetilde{\chi}_1^0 \to (h, Z, \gamma)\ \widetilde{G}$
Stau	$\widetilde{\tau} \to \tau\ \widetilde{G}$
Slepton Co-NLSP	$\widetilde{\ell} \to \ell\ \widetilde{G}$
Squark	$\widetilde{Q} \to (q, q'W)\ \widetilde{G}$
Gluino	$\widetilde{g} \to g\ \widetilde{G}$

a neutralino NLSP displaced decay $\widetilde{\chi}_1^0 \to h\widetilde{G}$ or $\widetilde{\chi}_1^0 \to Z\widetilde{G}$ secondary vertices arise with decay product invariant mass which can be identified with the parent Higgs or Z boson. This generally requires a special analysis to identify high momentum partons which form secondary vertices. In some cases this can greatly reduce background. In the case of a displaced decay $\widetilde{\chi}_1^0 \to h\widetilde{G}$, with $h \to bb$, a search for high momentum large negative impact parameters (LNIPs) greatly reduces potential backgrounds for Standard Model b-quark production. For a slepton NLSP, displaced decays $\widetilde{\ell} \to \ell\widetilde{G}$ inside the inner tracking region will yield charged particle tracks which do not point back to the interaction region. A non-relativistic slepton which traverses at least part of the tracking region before decay $\widetilde{\ell} \to \ell\widetilde{G}$ gives a highly ionizing track (HIT) with a kink to a minimum ionizing track (MIT) or tau jet. In either case identifying these tracks is very challenging and probably requires that such events have some other characteristic on which to trigger and identify in analysis. A strongly interacting squark or gluino NLSP can hadronize as either a neutral or charged bound state. In the neutral case macroscopic decay to a jet $\widetilde{Q} \to q\widetilde{G}$ or $\widetilde{g} \to g\widetilde{G}$ gives a displaced jet which can be searched for using an LNIP analysis. In the case of a charged squark or gluino bound state the additional possibility arises of observing the charged bound state as a highly ionizing track which decays to a jet. Observation of a macroscopic decay length for any NLSP type would be a smoking gun for low scale supersymmetry breaking. In addition, a measure of the decay length distribution, along with the superpartner mass and identity, would give an essentially model independent measure of the supersymmetry breaking scale.

The final range of NLSP decay lengths is well outside the detector. A neutralino NLSP which decays well outside the detector appears as missing energy. This is the conventional form of missing energy considered in standard phenomenological studies of SUSY signatures, and will not be considered in this report. A study of these signatures at the Tevatron Run II is presented in the SUGRA working group report [7]. For the other possible types of NLSPs, even if decay to the Goldstino takes place well outside a detector, the eventual decay can evade cosmological constraints on the nature of the NLSP. So in this case the existence of the Goldstino, while not directly relevant to accelerator physics, does allow the possibility for the NLSP to be of any type listed in Table 1 and to be effectively stable on the scale of a detector. A slepton NLSP which traverses the detector is generally not ultra-relativistic and therefore appears as a HIT. Since slepton pairs result for any SUSY production, the resulting signature is HIT pairs often *without* significant missing energy, and possibly other partons from cascade decays. Time of flight (TOF) can also be utilized in the search for slow moving sleptons. A squark NLSP hadronized with light quark(s) can exchange isospin and charge through strong interactions with background material as it traverses the detector. This gives rise to intermittent charge exchange in the calorimeters associated with highly ionizing tracks in the vertex and tracking volume (CE-HITs). Because of the reduced average ionization, and intermittent nature of the charged tracks, CE-HIT momenta would generally be mismeasured, leading to an apparent missing energy. Identification of CE-HITs is likely to be challenging and requires specialized analysis. A squark NLSP hadronized with light antiquark(s) cannot as readily charge exchange with matter. Charged bound states of this type however can still have soft hadronic activity along a highly ionizing track (H-HIT). Both CE-HITs and H-HITs are likely to appear as HITs in the inner tracking region.

Some of the distinctive signatures associated with the NLSP decay to the Goldstino may be useful in obtaining samples of Higgs bosons. In the case of a Bino-like neutralino NLSP, $\widetilde{\chi}_1^0$, cascade decays to $\widetilde{\chi}_1^0$ can often include

a Higgs boson, h. In the case of a Higgsino-like neutralino NLSP, $\widetilde{\chi}_1^0$, direct decay of $\widetilde{\chi}_1^0$ to the Goldstino can yield a Higgs boson, $\widetilde{\chi}_1^0 \to h\widetilde{G}$. The unique low scale supersymmetry breaking signatures can then be used as a method to tag for events which contain a Higgs boson.

The existence of the Goldstino clearly presents many unique experimental challenges and opportunities, many of which have been overlooked in the past. This report contains a nearly comprehensive compendium of the relevant signatures which can be probed at Run II.

The overall scale of SUSY breaking, which is so crucial in determining the experimental signatures, can tell us much about the manner in which SUSY is broken. Weakly-coupled spontaneous supersymmetry breaking that occurs directly in the visible MSSM sector leads to an unacceptable superpartner mass spectrum, with some of the superpartners very light. Supersymmetry must therefore be broken in some other sector of nature, generally referred to as the SUSY breaking sector. This spontaneous breaking may result as the consequence of non-perturbative gauge dynamics, but might also be the result of non-supersymmetric boundary conditions on an internal space, or result geometrically from a non-BPS ground state of extended branes on which the MSSM degrees of freedom reside. Regardless of the ultimate source, a messenger sector must couple the SUSY breaking sector to the MSSM visible sector superpartners. The messenger sector is then said to "transmit" SUSY breaking to the visible sector. The MSSM visible sector superpartner masses, $\widetilde{m}$, are related to the intrinsic SUSY breaking scale $\sqrt{F}$, and the messenger sector mass scale, M_m, by

$$\widetilde{m} \propto \frac{F}{M_m}. \tag{1.4}$$

The messenger interactions must be at least as strong as gravity, implying an upper limit on the messenger scale of $M_m \lesssim M_p$. The limit in which the messenger interactions are of gravitational strength, $M_m \sim M_P$, is generally referred to as high-scale or gravity-mediated SUSY breaking. In this case the intrinsic SUSY breaking scale is the intermediate scale $\sqrt{F} \sim 10^{11}$ GeV. In principle, however, the messenger scale can be anywhere between just above the electroweak scale up to the Planck scale. A messenger scale significantly below the Planck scale, $M_m \ll M_P$, is generally referred to as low-scale SUSY breaking. Note that with low-scale SUSY breaking, the gravitino mass eq. (1.1) is well below the MSSM superpartner masses and electroweak scale eq. (1.4); $m_{\widetilde{G}} \ll \widetilde{m}$ for $M_m \ll M_p$. So with low-scale SUSY breaking the gravitino is naturally the LSP, and NLSP superpartner of an MSSM particle is unstable to decay to the Goldstino as discussed above.

If the messenger scale is in fact well below the Planck scale, it is likely that the usual $SU(3)_C \times SU(2)_L \times U(1)_Y$ Standard Model gauge interactions play some role in the messenger sector [3,4]. This is because the structure of supersymmetric gauge theories dictates that gauginos couple at the renormalizable level only through gauge interactions. If the MSSM scalars, including the Higgs bosons which determine the electroweak scale, received mass predominantly from non-gauge (and therefore non-renormalizable and hence suppressed) interactions, the gauginos would be unacceptably light. It is therefore natural within low-scale SUSY breaking, to consider theories of gauge-mediated SUSY breaking (GMSB) [8–10]. In general, GMSB arises if some massive fields which couple to the SUSY breaking sector, and therefore have a non-supersymmetric mass spectrum, also transform under the Standard Model gauge groups. These heavy fields are referred to as messengers, with the messenger masses determining the messenger scale M_m.

In GMSB theories the MSSM squarks, sleptons, and gauginos obtain mass radiatively from gauge interactions with the massive messengers. Since the messenger interactions are the usual gauge interactions, the superpartners generally acquire a mass in proportion to associated gauge coupling squared or equivalently fine structure constant

$$\widetilde{m} \sim \frac{\alpha_a}{4\pi}\frac{F}{M_m} \tag{1.5}$$

where M_m is the characteristic messenger mass, and $\alpha_1, \alpha_2 \alpha_3$ are the fine structure constants for the $U(1)_Y$, $SU(2)_L$, and $SU(3)_C$ gauge interactions. The precise definition of the minimal model of gauge-mediation (MGM) is given in Appendix A1. The dependence of the fine structure constants generally leads to a hierarchy between the masses of the strongly interacting squarks and gluino, $\widetilde{Q}$ and $\widetilde{g}$, which couple to $SU(3)_C$, the Wino and left handed sleptons, $\widetilde{W}$ and $\widetilde{\ell}_L$, which couple to $SU(2)_L$, and the Bino and right handed sleptons, $\widetilde{B}$ and $\widetilde{\ell}_R$, which couple to $U(1)_Y$. The minimal expectation for the mass ordering of the superpartners with GMSB is then $m_{\widetilde{Q}}, m_{\widetilde{g}} \gg m_{\widetilde{W}}, m_{\widetilde{\ell}_L} > m_{\widetilde{B}}, m_{\widetilde{\ell}_R}$. Based on this mass ordering, either the Bino or right handed slepton, $\widetilde{B}$ and $\widetilde{\ell}_R$, are natural candidates within GMSB for the NLSP, which is crucial in determining the

phenomenology. However, it is worth noting that this mass ordering is only representative of the minimal expectations for GMSB. The structure and representations of the messengers as well as their couplings to the SUSY breaking sector need not be universal. Almost any mass ordering can in fact be obtained from sufficiently general models of GMSB [4,11,12]. So it is important when considering phenomenological signatures not to focus too closely on any one particular class of underlying model.

Gauge-mediated supersymmetry breaking, even as an effective phenomenological theory of SUSY breaking, is by itself incomplete. The MSSM Higgs sector possesses certain global symmetries in the supersymmetric limit which must be broken in order to obtain acceptable electroweak symmetry breaking without the appearance of an unacceptable Peccei-Quinn axion or very light Higgsino. These symmetries, however, commute with the gauge interactions at leading order, and are not broken at this order by gauge couplings with the messenger fields. Additional interactions between the Higgs and messenger sectors are therefore required, beyond the minimal gauge interactions [10]. The existence of these additional interactions has the possible phenomenological consequence of making the relative gaugino and Higgsino mixtures of the neutralinos uncertain [4], as described in Appendix A2i.

Perhaps the most appealing theoretical feature of GMSB is the natural lack of SUSY contributions to lepton flavor or quark flavor violating processes such as $\mu \to e\gamma$ decay, $K \leftrightarrow \bar{K}$ oscillations, or $b \to s\gamma$ decay. This arises because the leading contributions to visible sector soft SUSY breaking involving the squark and slepton superpartners depend only on gauge couplings. All soft SUSY-breaking parameters are then automatically flavor independent or aligned with the quark or lepton Yukawa couplings. Because of decoupling, this is generally possible if the messenger scale is well below the flavor scale at which the standard model Yukawa couplings are determined. But with high-scale SUSY breaking arising from Planck scale operators no separation of the messenger and flavor scales is possible and it is difficult to enforce a symmetry in the high energy theory that can prevent flavor violation in the visible sector soft SUSY breaking parameters. Even with GMSB, however, if the messenger scale is not too far below the flavor scale, sub-leading flavor violating effects can persist. In particular, this presents the possibility of observing small lepton flavor violation with NLSP sleptons [13].

In order to assess discovery reaches for a collider experiment it is useful to introduce the notion of a Model Line (rather than a model point) in which dimensionless parameters and ratios of the dimensionful model parameters are fixed, but with the overall superpartner mass scale varying. This allows a discovery reach to be deduced along a Model Line for a given type of representative model in terms of the overall superpartner mass scale, or more conveniently in terms of the mass of a given superpartner. Since with low-scale SUSY breaking it is likely that gauge-mediation plays some role in transmitting SUSY breaking to the visible sector, it is reasonable to employ the MGM to define some of the Model Lines. Representative Model Lines for each type of NLSP were developed for the Run II workshop, and the results presented in this report are based on these Model Lines. The NLSP decay length can be varied at each point on the Model Line by varying the SUSY breaking scale, holding the other ratios of parameters fixed. The phenomenological importance of the parameters which determine the Model Lines are described in Section II, and the specific parameters of the individual Model Lines are presented in subsequent sections.

The results of the Low-Scale Supersymmetry Breaking Working Group for the SUSY-Higgs Run II workshop are presented in the remainder of this report. Section III contains a summary of the object identification and acceptances employed for the studies presented in this report. Separate studies were undertaken by the CDF and DØ detector collaborations, and by independent groups referred to as ISAJET studies, and PYTHIA-SHW studies for convenience. The remaining sections present results organized by the various scenarios for the NLSP. Sections IV through VIII contain results for Bino-like neutralino NLSP, Higgsino-like neutralino NLSP, stau NLSP, slepton co-NLSP, and squark NLSP respectively. The types of triggers, cuts, and analysis required to probe each NLSP scenario are detailed, as well as Run II discovery reaches along the defined Model Lines. When applicable the cases of prompt NLSP decay, macroscopic NLSP decay, and NLSP decay well outside the detector are each considered. The CDF, DØ, ISAJET, and PYTHIA-SHW studies are complementary in the sense that they are often based on different event selection criteria, and are presented separately within each section. Section IX discusses the signatures associated with other NLSP scenarios. Section X presents results for direct Goldstino pair production. The Appendices contain the precise definition of the MGM, phenomenological implications of variations of the MGM, decay rates for MSSM particles to the Goldstino, a list of the Model Lines studied, a short glossary of acronyms peculiar to our analyses, and an estimate of the charge exchange length for massive strongly interacting particles in matter.

Contributions from the large number of participants in the working group are dispersed throughout the report. The CDF studies include contributions from W. Bokhari, A. Connolly, R. Culbertson, R. Demina,

G. Grim, R. Thurman-Keup, D. Stuart, B. Tannenbaum and Ming-Jer Wang. The DØ studies were carried out by J. Qian, S. Chopra, D. Cutts, and G. Landsberg. The ISAJET studies were carried out by H. Baer, P. Mercadante, X. Tata, and Y. Wang, who presented these and related studies in [14]. The PYTHIA-SHW studies were carried out by K. Matchev and S. Thomas. The work on prompt squark decay was contributed by C.-L. Chou and M. Peskin, and on sbaryon and mesino signals by U. Sarid and S. Thomas. Additional work on Bino-like neutralino NLSP, stau NLSP, and slepton co-NLSPs was contributed at the workshop meetings by B. Dutta, D. Muller, and S. Nandi and has also been reported on together with related studies in [15] and [16]. The appendices and introductory material in each section were prepared by S. Martin and S. Thomas.

II MODEL LINES FOR RUN II STUDIES AND MINIMAL GAUGE MEDIATION

Since gauge mediation is likely to play some role in low-scale SUSY breaking it is reasonable to employ the minimal model of gauge mediation (MGM) to define representative Model Lines for the studies presented in this report. This provides a well-defined framework to assess discovery reach and to study specific signatures for each possible type of NLSP. Any specific model is special in some way. However, the Model Lines developed for this working group were chosen to be as representative as possible. Most of the important features of each Model Line depend only the NLSP and superpartner mass orderings which determine the cascade decays. In most cases the specific cascades are not important, so the results of the studies presented in this report should be fairly robust.

The MGM is the simplest phenomenological model of gauge mediated SUSY breaking (GMSB). This model is useful for phenomenological studies since any given model is specified in terms of six parameters

$$\Lambda \ , \ N \ , \ M_m \ , \ \tan\beta \ , \ \mathrm{sgn}(\mu) \ , \ C_G \tag{2.1}$$

defined below. In addition, either a Bino-like neutralino NLSP, stau NLSP, or slepton co-NLSP naturally arise a functions of the model parameters, allowing these possibilities to be covered within the MGM.

The MGM assumes N generations of messenger fields in the $\mathbf{5}\oplus\overline{\mathbf{5}} \in SU(5) \supset SU(3)_C \times SU(2)_L \times U(1)_Y$. The messengers have an overall supersymmetric mass M_m, with the scalar and fermion split by a SUSY breaking auxiliary order parameter F_S with units of [mass]^2. The MSSM gaugino masses arise from one-loop coupling to the messengers,

$$M_a = k_a N \Lambda \, \frac{\alpha_a}{4\pi} \tag{2.2}$$

where

$$\Lambda = F_S / M_m \tag{2.3}$$

is the effective visible sector SUSY breaking parameter, and $a = 1, 2, 3$ for the Bino, Wino, and gluino respectively, and $k_1 = \frac{5}{3}$, $k_2 = k_3 = 1$. The MSSM scalar masses arise from two-loop coupling to the messengers

$$m_\phi^2 = 2N\Lambda^2 \left[\frac{5}{3} \left(\frac{Y}{2}\right)^2 \left(\frac{\alpha_1}{4\pi}\right)^2 + C_2 \left(\frac{\alpha_2}{4\pi}\right)^2 + C_3 \left(\frac{\alpha_3}{4\pi}\right)^2 \right] \tag{2.4}$$

where Y is the ordinary weak hypercharge normalized as $Q = T_3 + \frac{1}{2}Y$, $C_2 = \frac{3}{4}$ for weak isodoublet scalars and zero for weak isosinglets, and $C_3 = \frac{4}{3}$ for squarks and zero for other scalars. The gaugino masses eq. (2.2) which arise at one loop, and the scalar masses eq. (2.4) which arise at two loops are each specific realizations of the estimate eq. (1.5) for GMSB. Note that the gaugino masses scale like N while the scalar masses scale like $\sqrt{N}$.

The MSSM superpartner masses (2.2) and (2.4) are evolved from the messenger scale to the electroweak scale by renormalization group evolution. This is the only way in which the messenger scale M_m directly enters, so the MSSM parameters only depend weakly (logarithmically) on M_m. The constraint of electroweak symmetry breaking with the known Z boson mass is imposed on the electroweak scale parameters. These constraints may be determined in terms of the ratio of Higgs expectation values, $\tan\beta = \langle H_u^0 \rangle / \langle H_d^0 \rangle$, and $\mathrm{sgn}(\mu)$ where

μ is supersymmetric Higgs and Higgsino mass parameter. A Bino-like neutralino or slepton is generally the NLSP. Many groups have developed computer code to calculate electroweak scale MSSM parameters in terms of the MGM parameters, including the ISAJET code in versions 7.34 and later [17].

The effective SUSY breaking order parameter F_S felt by the messengers may not coincide with the ultimate underlying SUSY breaking order parameter F which determines the Goldstino coupling. To account for this a dimensionless factor $C_G \gtrsim 1$ may be introduced relating F and F_S by

$$F = C_G F_S \tag{2.5}$$

With all other MGM parameters fixed, C_G may be used to control the NLSP decay length.

The phenomenological meaning and importance of the MGM parameters can be summarized as follows:

- Λ: This effective visible sector SUSY breaking parameter sets the overall mass scale for all the MSSM superpartners. For electroweak scale superpartners $\Lambda \sim \mathcal{O}(100 \text{ TeV})/\sqrt{N}$. To first approximation, all of the MSSM superpartner masses scale linearly with Λ.

- N: The gaugino masses scale like the number of messenger generations, N, while the squark and slepton masses scale like $\sqrt{N}$. For low values of N a Bino-like neutralino, $\widetilde{\chi}_1^0$, is the NLSP, while for larger values a right-handed slepton, $\widetilde{\ell}_R$, is the NLSP.

- M_m: The messenger scale enters as the scale at which the boundary conditions for renormalization group evolution of the MSSM parameters are imposed. The electroweak scale and all of the sparticle masses depend only on the logarithm of M_m. The lower limit $M_m > \Lambda$ is required in order to avoid color and charge breaking in the messenger sector, and $M_m \lesssim 10^{16}$ GeV to satisfy the defining criterion for low-scale SUSY breaking.

- $\tan\beta$: The ratio of the MSSM Higgs vacuum expectation values is in a range $1.5 \lesssim \tan\beta \lesssim 60$. The lower limit leads to a light CP-even Higgs scalar, which is presently being confronted at LEP. Large values of $\tan\beta$ yield a $\widetilde{\tau}$ slepton which is significantly lighter than the other sleptons.

- sgn(μ): The sign of Higgs and Higgsino supersymmetric mass parameter μ appears in the chargino and neutralino mass matrices. For a Higgsino-like neutralino $\widetilde{\chi}_1^0$ NLSP with low to moderate values of $\tan\beta$, sgn(μ) is crucial in determining the relative strength of the $\widetilde{\chi}_1^0$ coupling to Higgs and Z bosons through the Goldstino. Our convention for the sign of μ follows that of [18] and [19]. (In general, one could allow μ to have a complex phase once the other parameters are fixed to be real. However, in general this would require CP violation and we will not consider it here.)

- C_G: The ratio of the messenger sector SUSY breaking order parameter to the intrinsic SUSY breaking order parameter controls the coupling to the Goldstino. The NLSP decay length scales like C_G^2.

For each Model Line, Λ is varied with the other parameters or ratios held fixed. Since the superpartner masses scale nearly linearly with Λ, it is straightforward and natural to find a discovery or exclusion reach just by varying Λ. However, since the scale Λ does not appear directly in any relevant process accessible at an accelerator, it is best to quote the discovery reach in terms of physical masses such as the NLSP mass or the mass of the superpartner which has the largest production cross-section (typically the lightest chargino).

The parameters for MGM Model Lines studied in the Run II workshop for a Bino-like neutralino NLSP, stau NLSP, and slepton co-NLSP are given in Sections IV, VI and VII respectively. The parameters for the Higgsino-like Neutralino NLSP Model Lines studied are given in Section V. These two Model Lines are modified MGM Lines with fixed ratios of μ/M_1 in order to ensure that the NLSP $\widetilde{\chi}_1^0$ has a sizeable Higgsino component. This is equivalent to modifying the Higgs scalar soft masses at the messenger scale to be different from the left-handed slepton masses. In the MGM these fields have the same gauge quantum numbers and are degenerate at the messenger scale. Since a squark NLSP is likely to have the largest SUSY production cross section, the squark NLSP Model Line studied in Section VIII is simply defined to be a single squark with varying mass. For each Model Line, the Goldstino decay constant parameter C_G is a free parameter, and can be varied in order to adjust the NLSP decay length.

III OBJECT IDENTIFICATION AND ACCEPTANCES

The identification and acceptance of objects within events generated for the results presented in this report differ slightly for the CDF, DØ, and ISAJET studies. This section presents some information on how objects such as electrons, muons, taus, photons, jets, b-jets, etc. are identified and accepted. Some differences in identification and acceptance between Run I and Run II are also discussed. In addition, the general procedures are indicated for how signal efficiencies are derived for the present studies.

A 2 TeV Tevatron center-of-mass energy is assumed throughout. All event generators used in the studies presented in this report employ leading order tree-level cross sections for signal processes. Inclusion of next to leading order QCD K-factor corrections can increase production cross sections for electroweak states by 15-20% [20]. This can have an important impact on the interpretation of any observed signal. However, because the cross section is a rapidly falling function of superpartner mass, these K-factor corrections would only increase the discovery reach in mass for signals originating from chargino or slepton production by roughly 5 GeV.

A CDF study object identification and acceptance parameters

Both current limits on low-scale SUSY breaking based on Run I data and projections of sensitivities for Run II are presented as part of the CDF contribution to the working group. Although some Run I results are based on the PYTHIA event generator, most results, including all Run II projections, are based on the ISAJET event generator. The efficiencies for Run I analysis were found with the standard full CDF Monte Carlo detector simulation. However, at the time of this study, a full Run II Monte Carlo was not available so the efficiencies for the Run II projections are estimated using the highly–parameterized SHW Monte Carlo [21], developed for the SUSY-Higgs Run II workshop. The SHW object identification cuts and efficiencies are employed. These are based on Run I experience with corrections for detector changes in Run II.

High-p_T electron identification begins with clusters of energy in the electromagnetic calorimeters. A track is required to be found in the tracking chambers with a p_T consistent with the cluster E_T. The cluster is required to be isolated from other energy in the calorimeter. Typically, for high-E_T electrons, the additional E_T in a cone of radius $\mathcal{R} \equiv \sqrt{(\Delta\phi)^2 + (\Delta\eta)^2} = 0.4$ around the electron cluster is required to be less than 10% of the cluster's energy. However, a cut requiring less than 2 GeV in the cone is used for the low-p_T electrons in the trilepton analysis. Triggers for electrons over 20 GeV are on the order of 97% efficient.

Photons are found as electrons with no tracks pointing to them. Without the track, the trigger has more background and it is necessary to require that the photon (with $23 < E_T < 50$ GeV, $|\eta| < 1.0$) is isolated in the trigger, passes a tight fiducial cut (clusters are far from calorimeter cracks), and has a cluster in the shower max detector, the combination of which is not very efficient. Above 50 GeV, there is no isolation or shower max requirement and the trigger is much more efficient.

In Run II, we expect to use looser fiducial cuts for electrons and photons. A new, more sophisticated and efficient isolation trigger will be installed and fiducial cuts are expected to be loosened. The Central Outer Tracker (COT) will provide tracking coverage for $|\eta| < 1$, similar to Run I. However the Intermediate Silicon Layers (ISL) will provide new tracking coverage out to $|\eta| < 2$ in Run II. Run I studies indicate the $1 < |\eta| < 2$ region has signal–to–noise comparable to the central region so with the additional tracking coverage, it is expected to be nearly equal to the central region. Therefore all electrons and photons with $|\eta| < 2$ are included in Run II projections. A fiducial cut efficiency of approximately 90% and a identification cut efficiency of approximately 85% are expected for Run II.

Muons are identified by matching tracks in the central tracker to tracks in the muon chambers, which are outside steel shielding. In Run I, the coverage was broken up between a central region, a central extension and a forward region with significant gaps in between. In Run II, the far forward region will be removed but the central region coverage is greatly expanded. Overall, muon coverage in CDF will be increased by approximately 15%. In the region $|\eta| < 0.6$ we will have 100% coverage, for $0.6 < |\eta| < 1.0$, 95% coverage, and for $1.0 < |\eta| < 1.5$, 75% coverage. For muons that are contained in the muon chambers, the identification efficiency is expected to be approximately 90%. The ISL again provides tracking at larger η, making these regions similar to the central region.

The τ lepton is identified as an e or μ in its leptonic decays. They can also be identified in their hadronic decays when there are one or three tracks in a narrow cone. These tracks are also required to be isolated from other tracks and the corresponding energy cluster to be thin, consistent with a low-mass object. For τ's

passing E_T and η cuts, the identification efficiency is approximately 55%. In Run I, it was possible to identify τ's with $|\eta| < 1$ and it should be possible to extend the coverage for τ identification to larger $|\eta|$ by using the ISL. In projections for this report, it will not be assumed that this can be done.

In Run I in CDF, jets were clustered using a cone algorithm. The cone has a radius of 0.4, 0.7 or 1.0 in $\eta - \phi$ space; the smaller radii being used in to separate jets in a busier environment. In Run II there are likely to be other algorithms available, including improved energy measurement due to analyzing tracks in the jet. Jet identification is approximately 100% efficient, apart from the 10-15% energy resolution.

The tagging of jets as heavy flavor (b or c quarks) will improve significantly in Run II. The Silicon Vertex Detector (SVX) coverage of the long interaction region ($\sigma = 30$ cm) will go from 65% in Run I to 90% in Run II. Overall, the probability for tagging one of the two b jets in top events will go from 40% to 65%. In addition the new SVX will be double-sided, improving background rejection. The ISL will also be able to contribute to tagging, with somewhat worse signal–to–noise compared to the SVX.

The listing of identifiable objects here is not complete. Of course there is missing E_T, the only object that might be measured more poorly in Run II (due to additional interactions in an event), but even this may be compensated by improved understanding. Unless noted otherwise, the total momentum of the generated non-interacting particles (usually the $\widetilde{G}$ and possibly neutrinos) is employed as the missing E_T for the signal samples. This is adequate since the signal events have such large missing E_T that the resolution smearing doesn't significantly affect the efficiency estimate.

A heavy charged particle may be identified through its dE/dx and/or its time of flight. Objects which decay to jets, leptons and even photons, close to the interaction vertex or far from it can also be identified. Charged objects that decay in flight leaving a "kink" in a track can also be found. The detector has good coverage with powerful, versatile devices, leaving us limited by the amount of time the collaboration can put into analysis.

In all cases, backgrounds are projected from Run I data or very conservative background assumptions are made. Using data for the projections correctly includes all sources of "physics" background (Standard Model sources which yield the same signature as the SUSY model) and "detector" backgrounds (mismeasurements and misidentifications) which are very difficult to model thoroughly. Unless there are obvious improvements or degradations, using Run I data is a conservative assumption. The main degradation will come from multiple vertices in events, but that is balanced by a detector improved in almost all respects. It is also balanced by the enormous experience gained in Run I, which should be matched by similar innovation and improvement in Run II. The history of the accelerator is to exceed projections in delivered luminosity and the history of the collaborations is to exceed projected sensitivities.

B DØ study object identification and acceptance parameters

All DØ studies described in this report, except those extrapolated from Run I analysis, are carried out at the particle level using ISAJET [17]. Due to a large number of Monte Carlo events generated, no detector simulation is done for supersymmetry signals.

Leptons, $\ell = e, \mu$, and photons, γ, are 'reconstructed' from the generated particle list by requiring them to have transverse energy, E_T, or momentum, p_T, greater than 5 GeV and to be within the pseudorapidity ranges:

e: $|\eta| < 1.1$ or $1.5 < |\eta| < 2.0$;

μ: $|\eta| < 1.7$;

γ: $|\eta| < 1.1$ or $1.5 < |\eta| < 2.0$.

These fiducial ranges are dictated by the coverages of the electromagnetic calorimeter and the central tracker of the DØ detector. Furthermore, the leptons and photons must be isolated. Additional energy in a cone with a radius $\mathcal{R} \equiv \sqrt{(\Delta\phi)^2 + (\Delta\eta)^2} = 0.5$ in $\eta - \phi$ space around the lepton/photon is required to be less than 20% of its energy.

Jets are reconstructed using a cone algorithm with a radius $\mathcal{R} = 0.5$ in $\eta - \phi$ space and are required to have $E_T^j > 20$ GeV and $|\eta^j| < 2.0$. All particles except neutrinos, the lightest supersymmetric particles (LSP), and the identified leptons and photons are used in the jet reconstruction. The transverse momentum imbalance ($\not{E}_T$) is defined to be the total transverse energy of neutrinos and the LSPs.

Energies or momenta of leptons, photons and jets of Monte Carlo events are taken from their particle level values without any detector effect. Smearing of energies or momenta of leptons, photons and jets according

to their expected resolution typically changes signal efficiencies by less than 10% relatively and therefore has negligible effect on the study.

The reconstruction efficiencies are assumed to be 90% for leptons and photons. For the purpose of background estimations, the probability for a jet to be misidentified as a lepton or a photon are assumed to be $\mathcal{P}(j \to \ell) = 10^{-4}$ and $\mathcal{P}(j \to \gamma) = 10^{-4}$ respectively. The probability for an electron to be misidentified as a photon is also assumed to be $\mathcal{P}(e \to \gamma) = 10^{-4}$. These probabilities are slightly smaller than those obtained in Run I. For comparison, the typical misidentification probabilities determined in Run I are $\mathcal{P}(j \to e) = 5 \times 10^{-4}$, $\mathcal{P}(j \to \gamma) = 7 \times 10^{-4}$, and $\mathcal{P}(e \to \gamma) = 4 \times 10^{-3}$. With a new magnetic central tracking system, the improved misidentification rates given above should be achievable in Run II.

In Run I, tagging of b-jets was limited to the use of soft muons in DØ. Secondary vertex tagging of b-jets will be a powerful addition in Run II. For the studies described below, a tagging efficiency of 60% is assumed for those b-jets with $E_T > 20$ GeV and $|\eta| < 2.0$. The probability $\mathcal{P}(j \to b)$ for a light-quark or gluon jet to be tagged as a b-jet is assumed to be 10^{-3}. These numbers are optimistic extrapolations of what CDF achieved in Run I.

Heavy stable charged particles can be identified [22,23] using the expected large ionization energy losses, dE/dx, in the silicon detector, fiber tracker, preshower detectors and calorimeter. Based on Ref. [22], a generic dE/dx cut is introduced with an efficiency of 68% for heavy stable charged particles and a rejection factor of 10 for the minimum ionization particles (MIP). Note that the efficiency for identifying at least one such particle in events with two heavy stable charged particles is 90%.

With the addition of preshower detectors, DØ will be able to reconstruct the distance of the closest approach (DCA) of a photon with a resolution ~ 1.5 cm [22]. Here the DCA is defined as the distance between the primary event vertex and the reconstructed photon direction. Thereby it will enable identification of photons produced at secondary vertices. In the following, a photon is called displaced if its DCA is greater than 5.0 cm and is denoted by γ'. The further assumption is made that the probability for a photon produced at the primary vertex to have the measured DCA> 5 cm is $\mathcal{P}(\gamma \to \gamma') = 2 \times 10^{-3}$ (about 3σ).

All final states studied have large E_T (p_T) leptons/photons with or without large $\not{E}_T$. A minimum p_T of 50 GeV of the hard scattering is applied for all signal processes. Triggering on these events is not expected to pose any problem. Nevertheless, a 90% trigger efficiency is assume for all the final states.

In order to find the reach in mass scale for a given supersymmetric signature, a significance for the signal must be defined. The significance $N_s/\delta N_b$ is defined as the ratio between the number of expected signal events, N_s, and the error, δN_b, on the estimated number of background events. Here a 20% systematic uncertainty is assumed for all estimated observable background cross sections. Therefore,

$$\delta N_b = \sqrt{\mathcal{L} \cdot \sigma_b + (0.2 \cdot \mathcal{L} \cdot \sigma_b)^2} \tag{3.1}$$

The sensitivity is characterized using the minimum signal cross section σ_{dis} for a 5 standard deviation (5σ) discovery:

$$\frac{N_s}{\delta N_b} = \frac{\mathcal{L} \cdot \sigma_{dis} \cdot \epsilon}{\delta N_b} = 5 \tag{3.2}$$

where ϵ is the efficiency for the signal. The minimum observable signal cross section σ_{obs} defined as $\sigma_{dis} \cdot \epsilon$ for the discovery is therefore independent of signal processes. The σ_{obs} as a function of $\mathcal{L}$ for several different values of σ_b are shown in Fig. 3. It decreases dramatically as $\mathcal{L}$ increases for small $\mathcal{L}$ values and flattens out for large $\mathcal{L}$ values. Clearly, the sensitivity can be improved for large $\mathcal{L}$ values by tightening the cuts to reduce backgrounds further.

C ISAJET study object identification and acceptance parameters

Signals for the ISAJET studies presented in this report are generated with ISAJET [17]. A bug in the program which resulted in an underestimate of the chargino production cross section has also been corrected. To model the experimental conditions at the Tevatron, the toy calorimeter package ISAPLT is interfaced with ISAJET. Calorimetry coverage of $-4 \leq \eta \leq 4$ is assumed with a cell size given by $\Delta\eta \times \Delta\phi = 0.1 \times 0.087$. The hadronic (electromagnetic) calorimeter resolution is taken to be $0.7/\sqrt{E}$ ($0.15/\sqrt{E}$). Jets are defined as hadronic clusters with $E_T > 15$ GeV within a cone of $\Delta R = \sqrt{\Delta\eta^2 + \Delta\phi^2} = 0.7$ with $|\eta_j| \leq 3.5$. Muons and electrons with $E_T > 7$ GeV and $|\eta_\ell| < 2.5$ are considered to be isolated if the scalar sum of electromagnetic

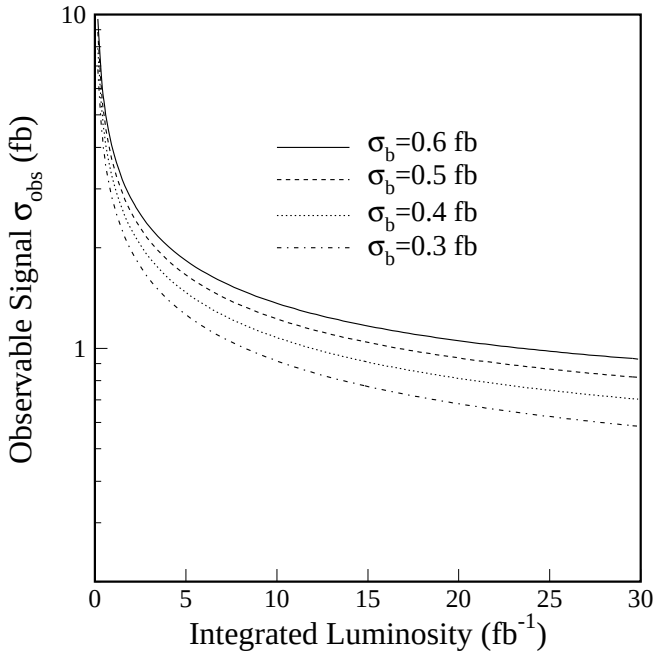

FIGURE 3. The minimum observable signal cross section σ_{obs} for a 5σ discovery as a function of integrated luminosity for four different values of background cross sections.

and hadronic E_T (not including the lepton, of course) in a cone with $\Delta R = 0.4$ about the lepton is smaller than max(2 GeV, $\frac{1}{4}E_T(\ell)$). Isolated leptons are also required to be separated from one another by $\Delta R \geq 0.3$. Photons are identified within $|\eta_\gamma| < 1$ if $E_T > 15$ GeV, and are considered to be isolated if the additional E_T within a cone of $\Delta R = 0.3$ about the photon is less than 4 GeV. τ leptons are identified as narrow jets with just one or three charged prongs with $p_T > 2$ GeV within 10° of the jet axis and no other charged tracks in a 30° cone about this axis. The invariant mass of these tracks is required to be $\leq m_\tau$ and the net charge of the three prongs required to be ± 1. QCD jets with $E_T = 15(\geq 50)$ GeV are misidentified as taus with a probability of 0.5% (0.1%) with a linear interpolation in between.

D PYTHIA-SHW study object identification and acceptance parameters

Signal and background rates for the PYTHIA-SHW studies presented in this report were generated with the PYTHIA [24] option of the SUSY-Higgs Workshop (SHW) v.2.2 detector simulation package [25–27] developed for the SUSY-Higgs Run II workshop. The definition of SHW v.2.2 objects is given in the SHW description in the SUSY-Higgs workshop report [21]. The following modifications in the SHW–TAUOLA package are made for the results presented in this report: (1) TAUOLA is modified to account for the correct (on average) polarization of tau leptons coming from decays of supersymmetric particles. (2) The tracking coverage is extended to $|\eta| < 2.0$, which increases the electron and muon acceptance, as is expected in Run II [28]. For muons with $1.5 < |\eta| < 2.0$, the same fiducial efficiency as for $1.0 < |\eta| < 1.5$ is applied. (3) The existing electron isolation requirement is retained and a muon isolation requirement $I < 2$ GeV is added, where I is the total transverse energy contained in a cone of size $\Delta R = \sqrt{\Delta\phi^2 + \Delta\eta^2} = 0.4$ around the muon. (4) The jet cluster E_T cut is increased to 15 GeV and the jet energy is corrected for muons. A simple electron/photon rejection cut of $E_{em}/E_{had} < 10$ is also added to the jet reconstruction algorithm, where E_{em} (E_{had}) is the cluster energy from the electromagnetic (hadronic) calorimeter. (5) The calorimeter $\not{E}_T$ is corrected for muons. The addition of the muon isolation cut and the jet E_{em}/E_{had} cut allows the occasional ambiguity between jet and muon objects in SHW v. 2.2 to be uniquely resolved.

IV BINO-LIKE NEUTRALINO NLSP

Neutralinos are in general mixtures of the gauginos and Higgsinos. Since the gauginos are superpartners of the gauge bosons, a gaugino-like neutralino NLSP decays to the Goldstino predominantly by emission of a γ or Z boson. In many models of supersymmetry breaking, including the MGM, the gaugino masses are related by gaugino mass unification relations, $M_1 \simeq 0.5\, M_2$, which imply that a gaugino-like neutralino NLSP is mostly Bino, the superpartner of the $U(1)_Y$ hypercharge gauge boson. Since the projection of the hypercharge gauge boson is larger in the photon than in the Z boson and because of the more favorable kinematics, a Bino-like neutralino NLSP decays to the Goldstino predominantly by emission of a photon:

$$\widetilde{\chi}_1^0 \to \gamma \widetilde{G}\,. \tag{4.1}$$

Supersymmetric particles are produced in pairs, with all cascades passing through the NLSP. For a Bino-like neutralino NLSP which decays by eq. (4.1), all supersymmetric final states include two hard photons, large missing energy carried off by the Goldstinos, and possibly other hard partons from cascade decays to the NLSP, $\gamma\gamma X \not{E}_T$. If the supersymmetry breaking scale $\sqrt{F}$ is smaller than a few 100 TeV, the decay length eq. (1.3) for the decay eq. (4.1) is short enough that the two hard photons appear to originate from the interaction point. In this case the photons are said to be prompt. However, for $\sqrt{F}$ between a few 100 and a few 1000 TeV, the decay eq. (4.1) can take place over a macroscopic distance, but within the detector. In this case the photons are said to be non-prompt or displaced, with a finite distance of closed approach (DCA) to the interaction point. For $\sqrt{F}$ greater than a few 1000 TeV, the decays eq. (4.1) take place outside the detector. In this case $\widetilde{\chi}_1^0$ is essentially stable on the scale of the experiment and escapes as missing energy. The resulting signatures are then qualitatively similar to traditional SUSY missing energy signatures with a stable $\widetilde{\chi}_1^0$, and will not be considered further in this report. The experimental signatures that are unique to a Bino-like neutralino NLSP with low scale supersymmetry breaking are therefore:

$$\begin{array}{llll}
\bullet\ \text{Prompt decays} & \widetilde{\chi}_1^0 \to \gamma\widetilde{G} & : \ \gamma\gamma X \not{E}_T\,, & X = \text{leptons and jets} \\
\bullet\ \text{Macroscopic decays} & \widetilde{\chi}_1^0 \to \gamma\widetilde{G} & : \ \gamma\gamma X \not{E}_T\,, & X = \text{leptons and jets} \\
 & & \quad \text{Displaced photons} &
\end{array} \tag{4.2}$$

Observation of either of these signatures would yield interesting information about the superpartners and supersymmetry breaking. The final state $\gamma\gamma X \not{E}_T$, interpreted as arising from decay to Goldstino pairs, would immediately imply that the supersymmetry breaking scale is low. A large branching ratio for $\widetilde{\chi}_1^0 \to \gamma\widetilde{G}$ would imply the NLSP is mostly Bino. Finally, with displaced photons, the decay length distribution would yield the neutralino life time, and give an essentially model independent measure of the SUSY breaking scale.

For the quantitative studies presented below, a Model Line within the MGM is defined in which the NLSP is Bino-like with nearly 100% branching ratio $\widetilde{\chi}_1^0 \to \gamma\widetilde{G}$. The fixed parameters that define the Model Line are:

$$\text{Bino} - \text{like Neutralino NLSP Model Line}: \qquad N = 1,\ \frac{M_m}{\Lambda} = 2,\ \tan\beta = 2.5,\ \mu > 0, \tag{4.3}$$

with the overall superpartner mass scale defined by Λ, which is allowed to vary. The mass spectrum of the phenomenologically important superpartners and the lightest CP-even Higgs boson h^0, is shown in Figure 4 as a function of Λ in the range 60-160 TeV. Over the entire model line $\widetilde{\chi}_1^0$ is the NLSP, and the mass ordering of the superpartner spectrum is $m_{\widetilde{\chi}_1^0} < m_{\widetilde{\ell}_R} < m_{\widetilde{\chi}_2^0, \widetilde{\chi}_1^\pm}$. The left-handed sleptons, the mostly-Higgsino neutralino and chargino states, the squarks, and the heavy Higgs bosons, are all too heavy to be produced at the Tevatron. The lightest neutralino, $\widetilde{\chi}_1^0$, is mostly $U(1)_Y$ Bino, while $\widetilde{\chi}_2^0$ and $\widetilde{\chi}_1^\pm$ are mostly $SU(2)_L$ Wino, and nearly degenerate. The light right-handed sleptons, $\widetilde{e}_R$ and $\widetilde{\mu}_R$, are effectively degenerate with $\widetilde{\tau}_1$ which is mostly $\widetilde{\tau}_R$ with a small $\widetilde{\tau}_L$ component from left-right mixing. The Higgs mass varies very slowly along the model line, due mainly to the varying virtual effects of the massive stop squarks.

The total SUSY cross sections for the light states are shown in Fig. 5. The largest cross sections are for $\widetilde{\chi}_1^+\widetilde{\chi}_1^-$ and $\widetilde{\chi}_1^\pm\widetilde{\chi}_2^0$ production. These arise predominantly in the S-wave through off-shell γ^*, Z^*, and W^* couplings to the $SU(2)_L$ Wino components. Even though the right-handed sleptons are lighter, $\widetilde{\ell}_R^+\widetilde{\ell}_R^-$ production cross sections are smaller because of P-wave suppression and smaller $U(1)_Y$ hypercharge coupling. Since the two

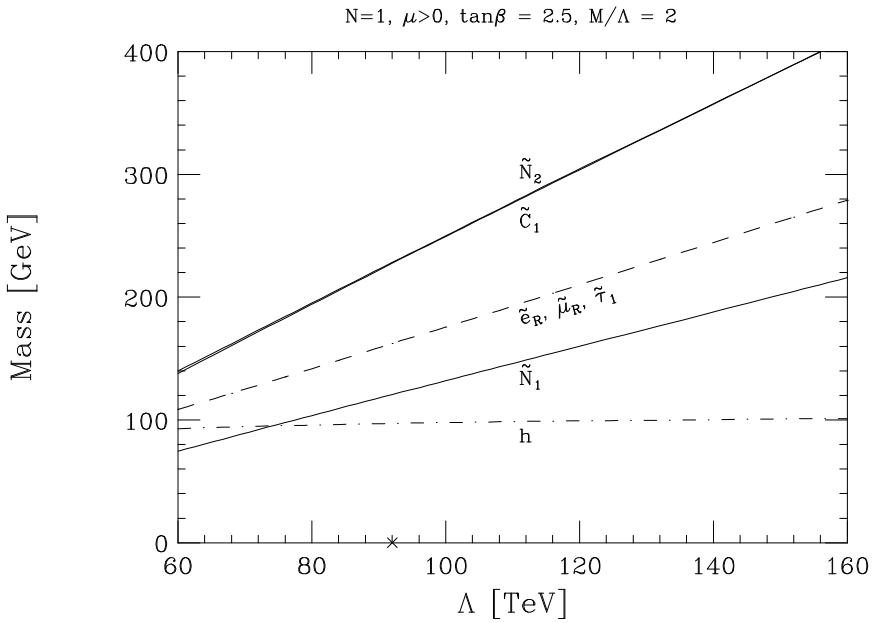

FIGURE 4. The masses of the lightest neutralinos, charginos, sleptons, and lightest CP-even Higgs boson as a function of the overall scale Λ along the Bino-Like Neutralino NLSP Model Line.

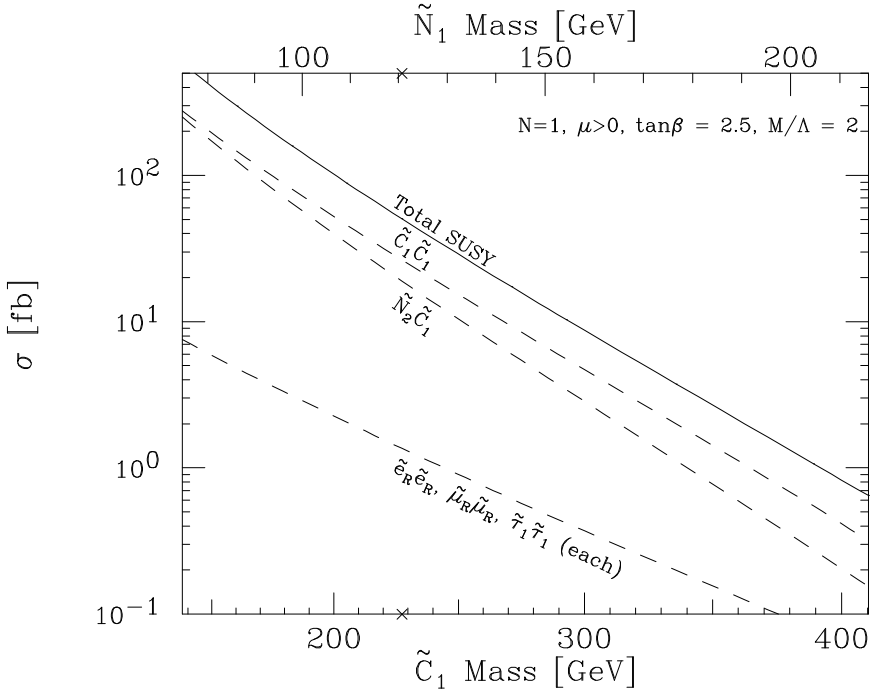

FIGURE 5. The most significant supersymmetric total production cross-sections in $p\overline{p}$ collisions with $\sqrt{s} = 2$ TeV, as a function of $m_{\tilde{\chi}_1^\pm}$ and $m_{\tilde{\chi}_1^0}$ along the Bino-like Neutralino NLSP Model Line.

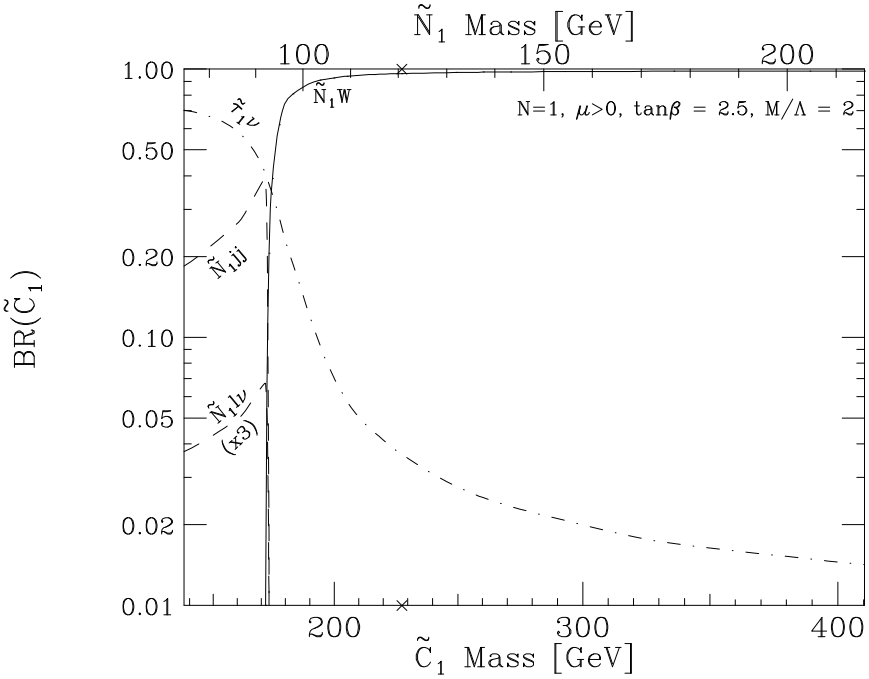

FIGURE 6. Important branching ratios for $\widetilde{\chi}_1^{\pm}$ decay as a function of $m_{\widetilde{\chi}_1^{\pm}}$ and $m_{\widetilde{\chi}_1^0}$ along the Bino-like Neutralino NLSP Model Line.

largest production cross-sections both involve the chargino, $m_{\widetilde{\chi}_1^{\pm}}$ is probably the best figure of merit for the discovery reach along this Model Line.

The specific final states which arise from $\widetilde{\chi}_1^+\widetilde{\chi}_1^-$ and $\widetilde{\chi}_1^{\pm}\widetilde{\chi}_2^0$ production depend on the $\widetilde{\chi}_1^{\pm}$ and $\widetilde{\chi}_2^0$ decay modes which give rise to various possible cascades to the NLSP $\widetilde{\chi}_1^0$. The $\widetilde{\chi}_1^{\pm}$ and $\widetilde{\chi}_2^0$ branching ratios are shown in Figs. 6 and 7 as a function of mass. Since $\widetilde{\chi}_1^{\pm}$ and $\widetilde{\chi}_2^0$ are highly Wino-like, the dominant decay modes are dictated primarily by which states with $SU(2)_L$ quantum numbers are open, and therefore depend on the overall superpartner mass scale. This leads to three regions along the model line which have qualitatively different cascades and final states. In the low mass region, $m_{\widetilde{\chi}_1^{\pm}} \lesssim 175$ GeV, only three-body decays are open. For intermediate masses, 175 GeV $\lesssim m_{\widetilde{\chi}_1^{\pm}} \lesssim 205$ GeV, the two-body mode $\widetilde{\chi}_1^{\pm} \to W^{\pm}\widetilde{\chi}_1^0$ is open and dominates. And for larger masses, $m_{\widetilde{\chi}_1^{\pm}} \gtrsim 205$ GeV, the two-body mode $\widetilde{\chi}_2^0 \to h\widetilde{\chi}_1^0$ is open and dominates. The dominance of the Higgs mode if kinematically open is generic if the lightest two neutralinos are gaugino-like, since the Higgs coupling is only singly suppressed by the small gaugino-Higgsino mixing, while other two body modes, such as $\widetilde{\chi}_2^0 \to Z\widetilde{\chi}_1^0$, are doubly suppressed in this mixing. This presents the interesting possibility of obtaining Higgs bosons from supersymmetric cascades, and is discussed further in subsection IV C.

A representative spectrum and decay chains with some branching ratios are shown in Fig. 8 for $\Lambda = 100$ TeV. For internal comparisons between different studies and detailed Monte Carlo studies, a reference Model Point on the model line is defined by $\Lambda = 90$ TeV, corresponding to $m_{\widetilde{\chi}_1^{\pm}} = 225$ GeV. The reference Model Point is indicated by an $\times$ in Figs. (4) through (7).

A Prompt Decays to Photons

Prompt decays $\widetilde{\chi}_1^0 \to \gamma\widetilde{G}$ give rise to spectacular events with two hard photons and significant missing energy. A search for $\gamma\gamma X\not{E}_T$ events provides a very sensitive discovery reach for SUSY in this channel for a number of reasons. The $\gamma\gamma$ branching ratio is nearly 100%, which gives a large advantage over other channels which require, for example, leptonic decay of W and/or Z. There is essentially no standard model background to $\gamma\gamma X\not{E}_T$, although there is significant background from jets faking photons or mismeasured $\not{E}_T$. An inclusive search for $\gamma\gamma X\not{E}_T$, independent of X, is possible. So the specific form of cascade decays do not affect the discovery reach which depends mainly on the production cross section. Finally, the detectors have a relatively

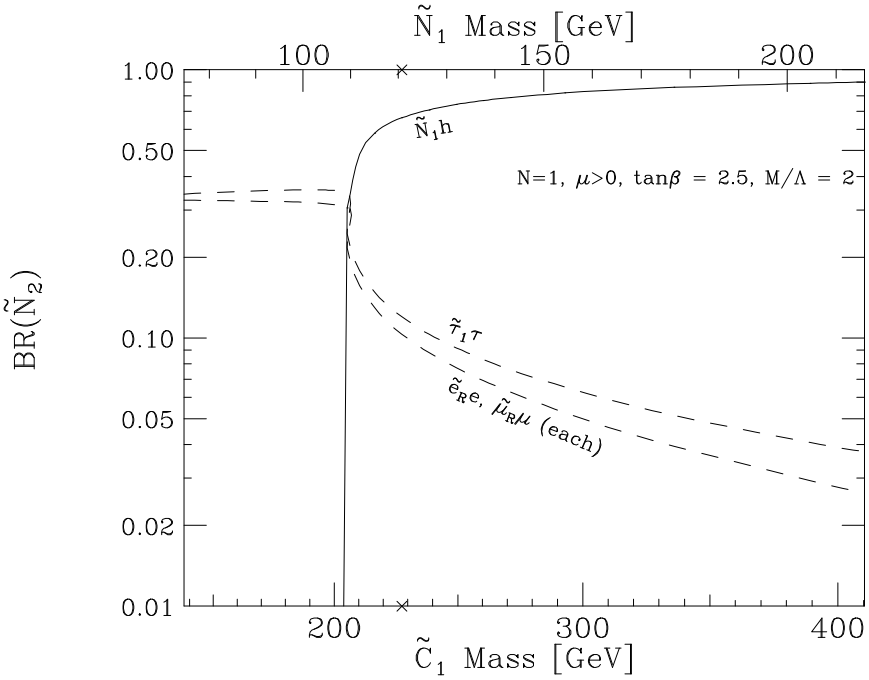

FIGURE 7. Important branching ratios for $\tilde{\chi}_2^0$ decay as a function of $m_{\tilde{\chi}_1^\pm}$ and $m_{\tilde{\chi}_1^0}$ along the Bino-like Neutralino NLSP Model Line.

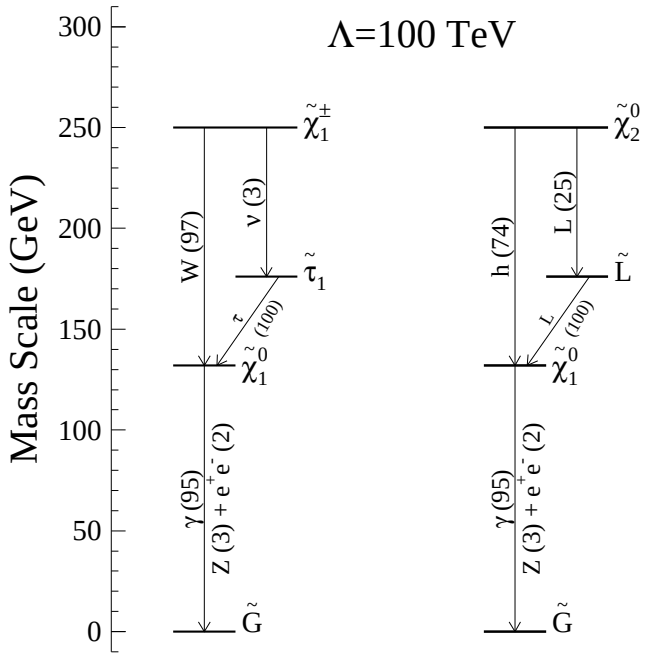

FIGURE 8. Superpartner spectrum and important cascade decays for the Bino-like Neutralino NLSP Model Line with $\Lambda = 100$ TeV. Branching ratio percentages are shown in parentheses.

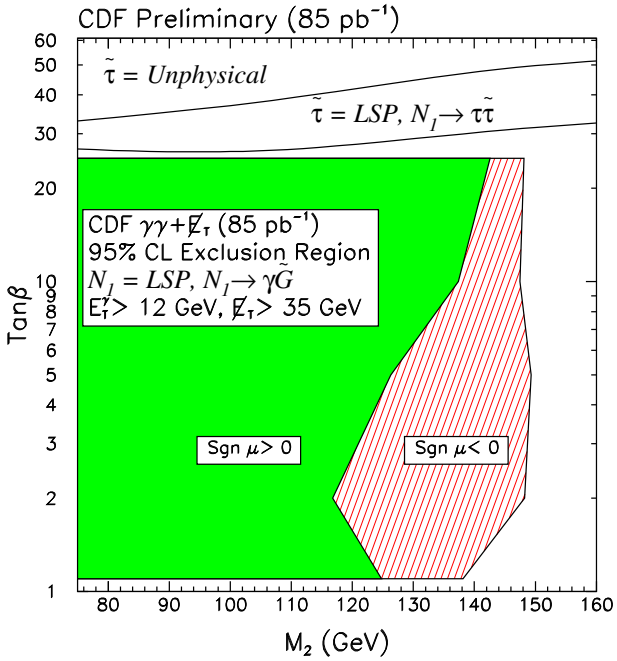

FIGURE 9. Limits on the MGM as a function of $\tan\beta$ and the Wino mass, M_2, with $N = 1$ and $M/\Lambda = 3$ from $\gamma\gamma X\not{E}_T$ CDF Run I data.

large coverage and detection efficiency for photons. CDF and DØ have searched for this mode in Run I, and a brief review of those results is included below. Improvements in triggering, coverage, efficiency, and the projected Run II sensitivity in this channel are also presented.

1 CDF study of promptly-decaying Bino-like NLSP

CDF searched for the signature of two photons and $\not{E}_T$ in Run I and reported no excess of events beyond the one unusual candidate event mentioned below [29]. The search utilizes 85 pb^{-1} of data and requires two central ($|\eta| < 1$) photons with $E_T > 12$ GeV and 35 GeV of $\not{E}_T$. Photons are separated from electrons and jets by requiring the EM clusters to be isolated in the calorimeter and isolated from tracks in the central tracking chamber. The sample comes from two triggers: a high-threshold diphoton trigger with loose requirements and a low-threshold trigger with tighter fiducial and isolation requirements. Events that have both photons with $|\eta| < 1$ and over the E_T threshold, and come on the high-threshold trigger have a per–photon acceptance of 87% and an efficiency of 84%. However the corresponding numbers for the low-threshold trigger are 73% and 68% due to the tighter trigger requirements. The fraction of diphoton events which actually contain two photons as opposed to jets faking photons, is low, 15%.

A model for the $\not{E}_T$ distribution in these events is derived from $Z \rightarrow ee$ events which have a similar topology and should have no true $\not{E}_T$. The $\not{E}_T$ is measured as a function of the event scalar ΣE_T, excluding the EM clusters. This function is then applied to the diphoton sample to produce an expected $\not{E}_T$ distribution which agrees well with the observed distribution. Above $\not{E}_T$ of 35 GeV, only 0.5 events are expected and only one event survives, the $ee\gamma\gamma\not{E}_T$ candidate event. This event contains two photons, a well-measured electron, a second, unreliably identified, electron candidate, and $\not{E}_T$. The event, which has an estimated standard model background many orders of magnitude less than one, is analyzed and discussed elsewhere [29]. As a candidate for low scale supersymmetry breaking, the electrons would come from cascade decays of $\tilde{\chi}$'s or sleptons and the photons and $\not{E}_T$ would come from the $\tilde{\chi}_1^0 \rightarrow \gamma\tilde{G}$ decay. To set limits, the MGM is employed with parameters $N = 1$, $M/\Lambda = 3$ with $\tan\beta$, sign(μ), and Λ varied (similar to the Model Line eq. (4.3)). The resulting excluded region is shown in Fig. 9.

In Run II, many proposed signatures will be investigated. Techniques are required which cover as many theoretical model possibilities as feasible in a simple way. One such technique is to investigate a baseline

signature (such as $\gamma\gamma$) and look for other objects in those events. The Run I $\gamma\gamma$ search includes not only the search with $\not\!\!E_T$ but also with 4 or more jets, b-quark jets, electrons, muons, and hadronically decaying τ's [29]. The results are shown in Table 2 - no excesses are found. Note that this technique requires a sophisticated set of tools from the collaboration to calculate instrumental backgrounds and an equally sophisticated set of simulations from theorists for physics backgrounds.

TABLE 2. Summary of the results from searches for identifiable objects in events with two photons with $E_T > 12$ GeV in the Run Ib CDF data.

Event Selection	Events Observed	Background Estimate
$\not\!\!E_T > 35$ GeV, $\lvert\Delta\phi_{\not\!\!E_T - jet}\rvert > 10°$	1	0.5 ± 0.1
$N_{jet} > 4$, $E_T > 10$ GeV, $\lvert\eta\rvert < 1.0$	2	1.6 ± 0.4
b-tag, $E_T > 25$ GeV, $\lvert\eta\rvert < 2.0$	2	1.3 ± 0.7
γ, $E_T > 10$ GeV, $\lvert\eta\rvert < 1.0$	0	0.1 ± 0.1
Central e or μ, $E_T > 25$ GeV	3	0.3 ± 0.1
τ, $E_T > 25$ GeV, $\lvert\eta\rvert < 1.2$	1	0.2 ± 0.1

To project the sensitivity in Run II, the signal efficiency and backgrounds must be estimated. To do this the Model Line eq. (4.3) and various approximations for estimating the efficiency are employed. First, in Run II the plug region of the CDF calorimeter will have very similar properties to the central region in Run I. The addition of the ISL tracking silicon detector makes isolation cuts for plug clusters very similar to the central region. Since no detailed simulation is available, it is assumed that the plug region will have the same efficiency and background as the central. This is also justified by preliminary studies of the plug in Run I which show that the plug is almost as effective as the central region even using the VTX (a vertex detector which doesn't measure p_T) instead of the ISL. The region $|\eta| < 2$ will therefore be assumed to be available in Run II. For the model points investigated here, this improves the efficiency by 60%.

Trigger isolation cuts will be made much more efficient and it is assumed that the fiducial cuts on the low-threshold trigger will be loosened. This means the Run I high-threshold acceptance and efficiency for all of the projected Run II data may be used, with an improvement in efficiency of a few percent (most events will pass the high-threshold trigger anyway). Since the expected $\not\!\!E_T$ is large, the resolution on the $\not\!\!E_T$ is not expected to have much of an effect on the efficiency, and the Monte Carlo generated $\not\!\!E_T$ is used for the event's total $\not\!\!E_T$.

To estimate backgrounds, note that the main backgrounds are QCD with either one real photon and one jet faking a photon or two fake photons. The Run II projection will be based on the Run I measured background distribution with a correction for the increase in the center–of–mass energy from 1.8 TeV to 2 TeV. QCD Monte Carlo indicates that the dijet cross section above a threshold E_T cut typically increases by 20%, so this factor is included in the background estimate. The E_T distribution also tends to increase an average of 5% and this effect is included as well. To make the projection, these factors are applied to the measured photon E_T spectrum. These factors are then also applied to the measured ΣE_T distribution, along with the conversion between ΣE_T and $\not\!\!E_T$, to arrive at the projected $\not\!\!E_T$ distribution.

With a background and signal distribution, a new set of cuts can be optimized (with the constraint that the projected background is not to be reduced far below 1 event). The Run I analysis optimized to 12 GeV photon E_T and 35 GeV $\not\!\!E_T$. Here the projected Run II data optimizes at $E_T > 14$ GeV and $\not\!\!E_T > 40$ GeV.

With 2 fb^{-1}, 1 background event and 20% systematics, we can expect to exclude more than 4 signal events. For a 5σ discovery about 17 events would be required. Table 3 summarizes the sensitivity along the Model Line (4.3). Figure 10 shows that the reach for CDF alone is approximately a $\widetilde{\chi}_1^{\pm}$ mass of 320 GeV for a limit or 250 GeV for a discovery. With 10 fb^{-1}, and no further optimization, these masses are estimated to be are 370 and 310 GeV, and with 30 fb^{-1}, 390 and 330 GeV.

TABLE 3. Projected limits and discovery potential for $\gamma\gamma X \not{E}_T$ events along the Bino-like Neutralino NLSP Model Line with 2 fb^{-1} in the CDF study.

Λ (TeV)	92	110	128	157
$m_{\tilde{\chi}_1^\pm}$ (GeV)	225	275	325	403
$m_{\tilde{\chi}_1^0}$ (GeV)	121	146	171	212
$\sigma\times$BR (fb)	46	14.0	4.0	0.60
Total $A\cdot\epsilon$ (%)	41	44	45	46
Signal events	38	12	3.6	0.55
95% C.L. limit (fb)	4.9	4.5	4.4	4.3
5σ discovery (fb)	21.0	19.0	19.0	19.0

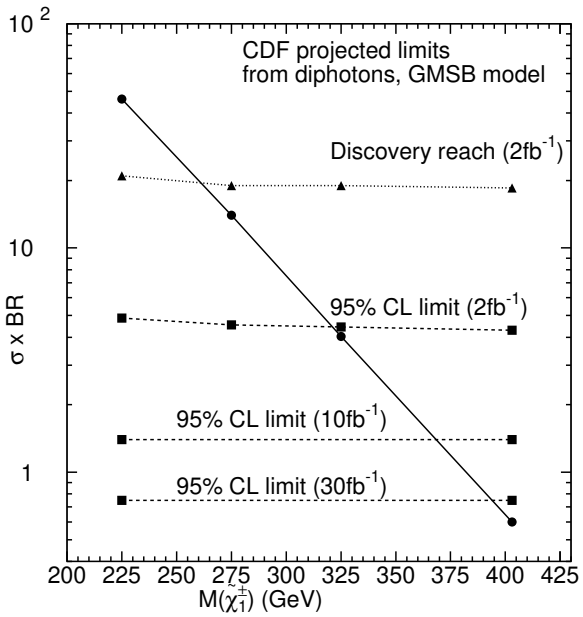

FIGURE 10. Projected CDF limits on the total SUSY cross section for the Bino-like Neutralino NLSP Model Line from the $\gamma\gamma X \not{E}_T$ Run II analysis. The total SUSY cross section in fb as a function of the $\tilde{\chi}_1^\pm$ mass is also indicated.

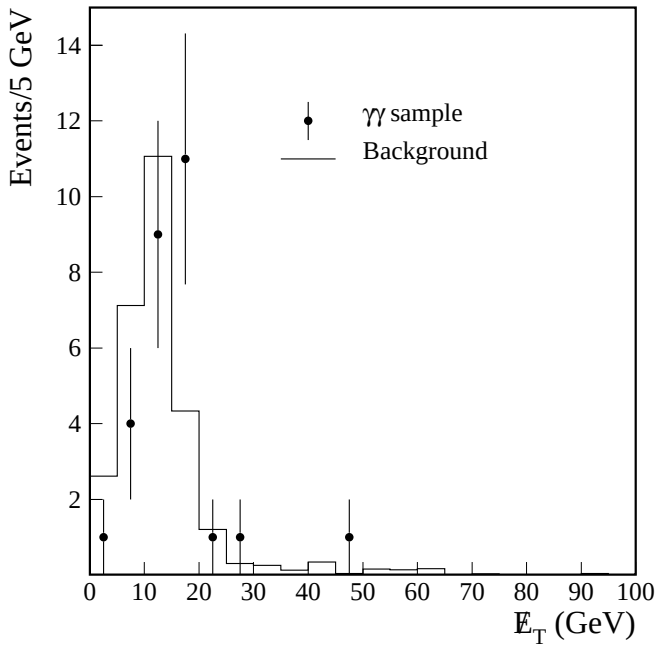

FIGURE 11. The $\not{E}_T$ distributions of the $\gamma\gamma$ and background samples for DØ in Run I. The number of events with $\not{E}_T < 20$ GeV in the background sample is normalized to that in the $\gamma\gamma$ sample. Note that there is a 14 GeV $\not{E}_T$ requirement in the trigger. The $\not{E}_T$ values plotted here are calculated off-line and therefore may differ from their values at the trigger level.

2 DØ study of promptly-decaying Bino-Like NLSP

Motivated by supersymmetric models with low scale supersymmetry breaking with a Goldstino, the DØ Collaboration reported a search [30] in Run I for di-photon events with large $\not{E}_T$ ($\gamma\gamma X\not{E}_T$ events) from a data sample with an integrated luminosity of 106.3 ± 5.6 pb^{-1}. The $\gamma\gamma X\not{E}_T$ events were selected by requiring two identified photons, one with $E_T^\gamma > 20$ GeV and the other with $E_T^\gamma > 12$ GeV, each within pseudorapidity $|\eta^\gamma| < 1.1$ or $1.5 < |\eta^\gamma| < 2.0$, and a $\not{E}_T$ greater than 25 GeV. Two events satisfied all requirements.

The principal backgrounds were multijet, direct photon, $W + \gamma$, $W +$ jets, $Z \to ee$, and $Z \to \tau\tau \to ee$ events from Standard Model processes with misidentified photons and/or mismeasured $\not{E}_T$. The numbers of estimated background events were 2.1 ± 0.9 from $\not{E}_T$ mismeasurement (QCD) and 0.2 ± 0.1 from misidentified photons (fakes). This led to an observed background cross section of 20 fb from QCD and of 2 fb from fakes in Run I. The $\not{E}_T$ distributions before the $\not{E}_T$ cut for both candidates and background events are shown in Fig. 11. Note that events with large $\not{E}_T$ are rare.

Since the backgrounds are dominated by the $\not{E}_T$ mismeasurement, they can be significantly reduced by raising the $\not{E}_T$ cut. Therefore, the following selection criteria are used for the Run II studies:

1) At least two photons with $E_T^\gamma > 20$ GeV;

2) $\not{E}_T > 50$ GeV.

The backgrounds with this set of selection criteria are expected to be significantly reduced by the increased cutoffs on $\not{E}_T$ and photon E_T and by the improved photon identification. The total observable background cross section in Run II is estimated to be $\sigma_b = 0.4(\text{QCD}) + 0.2(\text{fakes}) = 0.6$ fb assuming reduction factors of 5 from the raised $\not{E}_T$ cutoff, 4 from the improved $\mathcal{P}(j \to \gamma)$, 3 from the higher photon E_T requirement, and 10 from the decreased $\mathcal{P}(e \to \gamma)$ fake probability.

If the $\widetilde{\chi}_1^0 \to \gamma\widetilde{G}$ decays are prompt, $\gamma\gamma X\not{E}_T$ events are expected. The distributions of photon E_T and event $\not{E}_T$ for $\Lambda = 80, 140$ TeV, corresponding to $m_{\widetilde{\chi}_1^\pm} = 194, 357$ GeV, are shown in Fig. 12 for Run II. These events typically have high E_T photons together with large transverse momentum imbalances, and therefore can be selected using the $\gamma\gamma X\not{E}_T$ criteria discussed above. Table 4 shows the detection efficiencies, significances, along

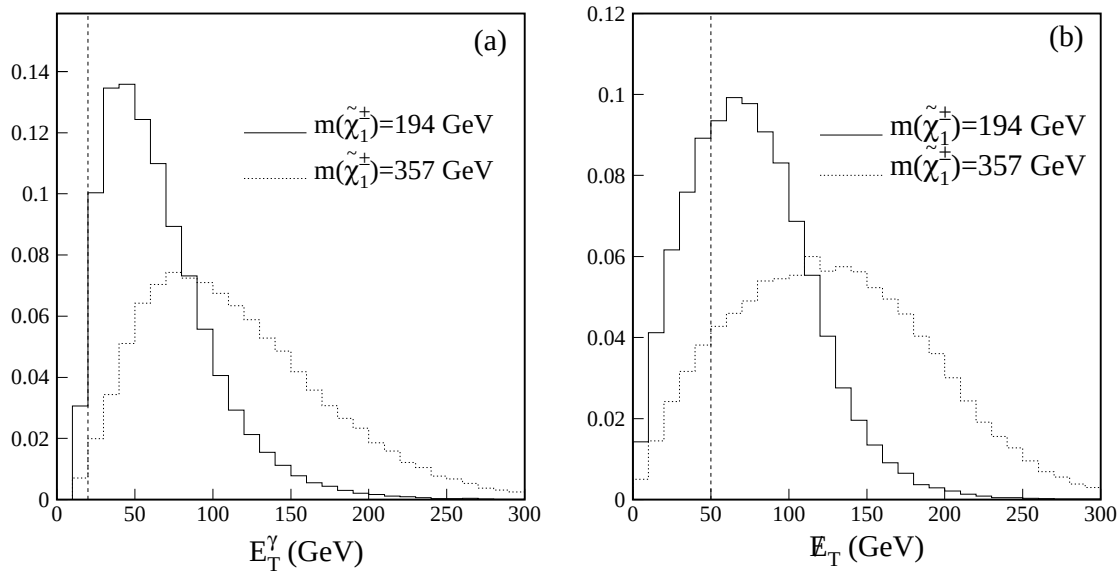

FIGURE 12. Distributions of (a) photon E_T and (b) event $\not{E}_T$ for Λ = 80, 140 TeV ($m_{\tilde{\chi}_1^{\pm}}$ = 194, 357 GeV) for the Bino-like Neutralino NLSP Model Line with prompt decay in the DØ study. The vertical dashed lines indicate the cutoffs. All distributions are normalized to have unit area.

with the total theoretical SUSY cross sections, and chargino and neutralino masses for different values of Λ along the Bino-like Neutralino Model Line. Figure 13 compares the 5σ discovery cross sections σ_{dis} with the theoretical SUSY cross sections for two different values of $\mathcal{L}$ as functions of the chargino mass $m_{\tilde{\chi}_1^{\pm}}$. The discovery reach in chargino mass with $\mathcal{L}$=2, 30 fb^{-1} is 290, 340 GeV respectively.

TABLE 4. The supersymmetry cross section (σ_{th}), $\tilde{\chi}_1^{\pm}$ and $\tilde{\chi}_1^0$ masses, detection efficiency of the $\gamma\gamma X\not{E}_T$ selection, and significances for different values of Λ along the Bino-like Neutralino NLSP Model Line in the DØ study. The relative statistical error on the efficiency is typically 2%. The observable background cross section is assumed to be 0.6 fb with a 20% systematic uncertainty.

Λ (TeV)	60	80	100	120	140	160
$m_{\tilde{\chi}_1^{\pm}}$ (GeV)	138	194	249	304	357	410
$m_{\tilde{\chi}_1^0}$ (GeV)	75	104	132	160	188	216
σ_{th} (fb)	464	105	27	7.7	2.2	0.7
ϵ (%)	16.1	24.3	28.2	30.1	30.6	30.2
$N_s/\delta N_b$ (2 fb^{-1})	136	46	14	4.2	1.2	0.4
$N_s/\delta N_b$ (30 fb^{-1})	400	137	41	12	3.6	1.1

3 ISAJET Studies of Bino-like NLSP

Tevatron signals for the MGM Bino-like Neutralino Model Line parameters eq. (4.3) have been simulated using ISAJET [17]. This is an extension of a previous study [31] of hadron collider signatures of the MGM with a Bino like NLSP. This analysis has been repeated for acceptances and cuts more appropriate to Run II.

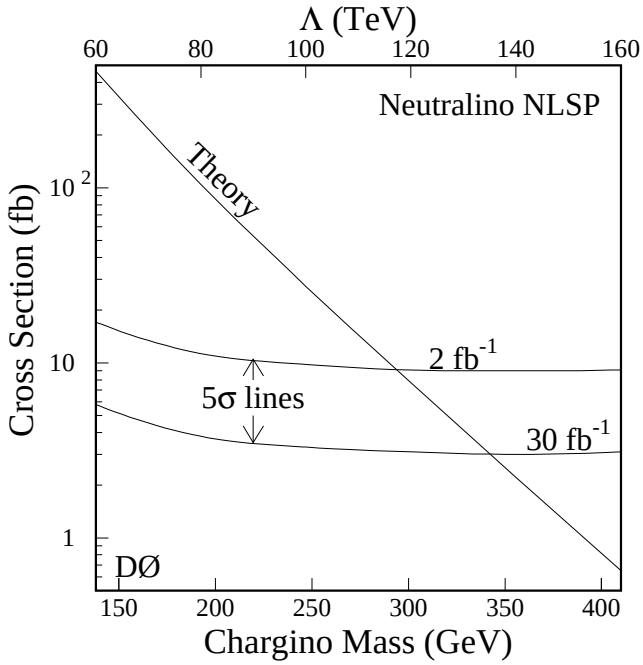

FIGURE 13. The 5σ discovery cross section curves as functions of the chargino mass along with the SUSY cross sections for the Bino-like Neutralino Model Line in the DØ studies. The two curves correspond to integrated luminosities of 2 and 30 fb^{-1}.

A bug in the program which resulted in an underestimate of the chargino production cross section has also been corrected.

The ISAJET simulations are used to classify the supersymmetric signal events primarily by the number of isolated photons — events with < 2 photons arise when one or more of the photons is outside the geometric acceptance, has too low an E_T, or happens to be close to hadrons. The signal events are separated further into clean and jetty events and classified by the number of isolated leptons (e and μ). In addition to the acceptance cuts described above, an additional global requirement of $\not{E}_T > 40$ GeV is imposed, which together with the presence of jets, leptons or photons may also serve as a trigger for these events.

Before describing the results of the computation it is useful to consider non-supersymmetric Standard Model backgrounds to the signal events. The backgrounds are expected to be smallest in the two photon channel, which will be the main focus for the purpose of assessing the reach. A detailed estimate of the background has not been attempted because the recent analysis by the DØ collaboration [32], searching for charginos and neutralinos in the GMSB framework, points out that the major portion of the background arises from mismeasurement of QCD jets and for yet higher values of $\not{E}_T$ from misidentification of jets/leptons as photons. In other words, this background is largely instrumental, and hence rather detector-dependent. From Fig. 1 of Ref. [32], the inclusive $\gamma\gamma X\not{E}_T > 40$ GeV (60 GeV) background level (for $E_T(\gamma_1, \gamma_2) > (20$ GeV, 12 GeV)) is estimated to correspond to ~ 0.9 (0.1) event in the DØ data sample of ~ 100 pb^{-1}. The background from jet mismeasurement, of course, falls steeply with $\not{E}_T$. The inclusive $\gamma\gamma X\not{E}_T$ background is also sensitive to the minimum E_T of the photon.

Changing the photon and $\not{E}_T$ requirements alter the SUSY signal. To assess this, the signal distributions of (a) $E_T(\gamma_2)$, the transverse energy of the softer photon in two photon events, and (b) $\not{E}_T$ in $\gamma\gamma + \not{E}_T$ events that pass the above cuts, are shown in Fig. 14 for three values of $m_{\tilde{\chi}_1^\pm}$. The following features are worth noting.

- For $m_{\tilde{\chi}_1^\pm} \simeq 250$ GeV corresponding to $\Lambda \simeq 100$ TeV (which is within the Run II reach), reducing the $E_T(\gamma)$ cut does not increase the signal. In fact, it may be possible to further harden this cut to reduce the residual backgrounds. Although not shown explicitly here, it has been checked that increasing the cut on the hard photon to $E_T(\gamma_1) > 40$ GeV results in very little loss of signal for $m_{\tilde{\chi}_1^\pm} > 250$ GeV or $\Lambda \gtrsim 100$ TeV.

- In view of the discussion of Standard Model backgrounds, it is clear that requiring $\not{E}_T > 60$ GeV greatly

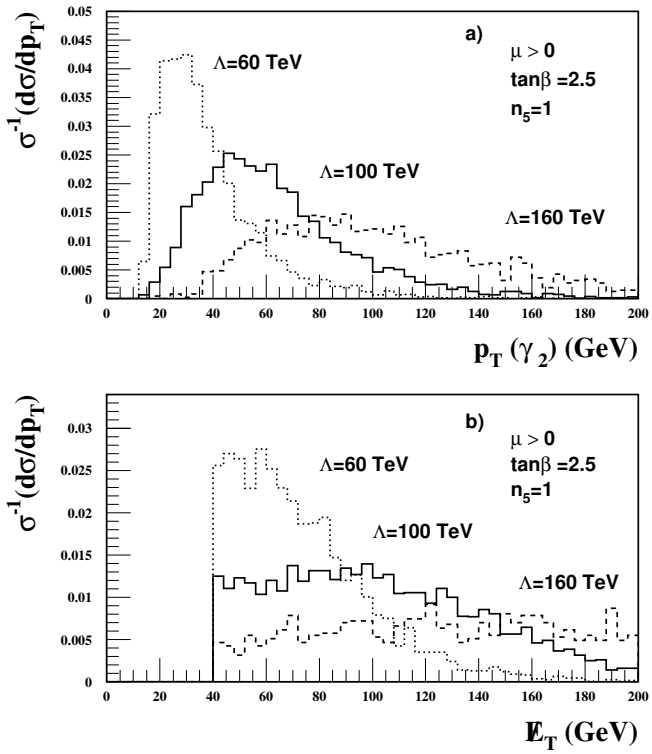

FIGURE 14. a) Transverse energy distributions for the softer photon, and b) missing energy distributions for the inclusive mode $\gamma\gamma X \not{E}_T$ after cuts along the Bino-like Neutralino Model Line in the ISAJET study. Results are shown for $\Lambda = 60, 100, 160$ TeV corresponding to $m_{\tilde{\chi}_1^\pm} = 135, 250, 410$ GeV.

reduces the background with modest loss of signal. Indeed, it may be possible to reduce the background to negligible levels by optimizing the cuts on the photon and on $\not{E}_T$.

The results of the computation of various topological cross sections for a 2 TeV $p\bar{p}$ collider after cuts are shown in Fig. 15 for (a) 0 photon, (b) one photon, and (c) two photon events. For this figure a cut of $\not{E}_T > 60$ GeV has been employed. As mentioned, this reduces the cross section by just a small amount, especially for the larger $\tilde{\chi}_1^\pm$ masses in this figure. The lines with the crosses correspond to events with at least one jet, while those without correspond to events free of jet activity. The solid, dashed, dotted and dashed-dotted lines correspond to 0,1,2 and ≥ 3 lepton events, respectively. Finally, the heavy solid line represents the sum of all the topologies, *i.e.* the inclusive SUSY cross section after cuts. Some features are worth noting:

- The signal cross sections in 1γ and 2γ channels after cuts are comparable. Since the background in the 2γ channel is considerably smaller (recall that a significant portion of the background arises from fake photons), the maximum reach is obtained in this channel.
- Events with at least one jet dominate clean events, irrespective of the number of photons.
- Over much of the Model Line sparticle production is dominated by $\tilde{\chi}_1^\pm \tilde{\chi}_1^\pm$ and $\tilde{\chi}_1^\pm \tilde{\chi}_2^0$ processes – squarks and gluinos are generally too heavy to be produced. The event topologies are thus qualitatively determined by chargino and neutralino decay patterns.

A conservative estimate of the reach may be obtained by assuming an inclusive $\gamma\gamma X \not{E}_T \geq 60$ GeV background level of 0.1 event per 100 pb^{-1}; *i.e.* assuming a background effective cross section of 1 fb. This corresponds to a "5σ reach" for the signal cross section of 3.5 fb (1 fb) for an integrated luminosity of 2 fb^{-1} (25 fb^{-1}) at the Tevatron Run II (TeV33). This translates to a reach in chargino mass of $m_{\tilde{\chi}_1^\pm} \leq 280(330)$ GeV or equivalently to $\Lambda \leq 110(130)$ TeV at Run II (TeV33). As mentioned above, it may be possible to further reduce the background by hardening the $E_T(\gamma)$ and $\not{E}_T$ requirements with only modest loss of signal. The

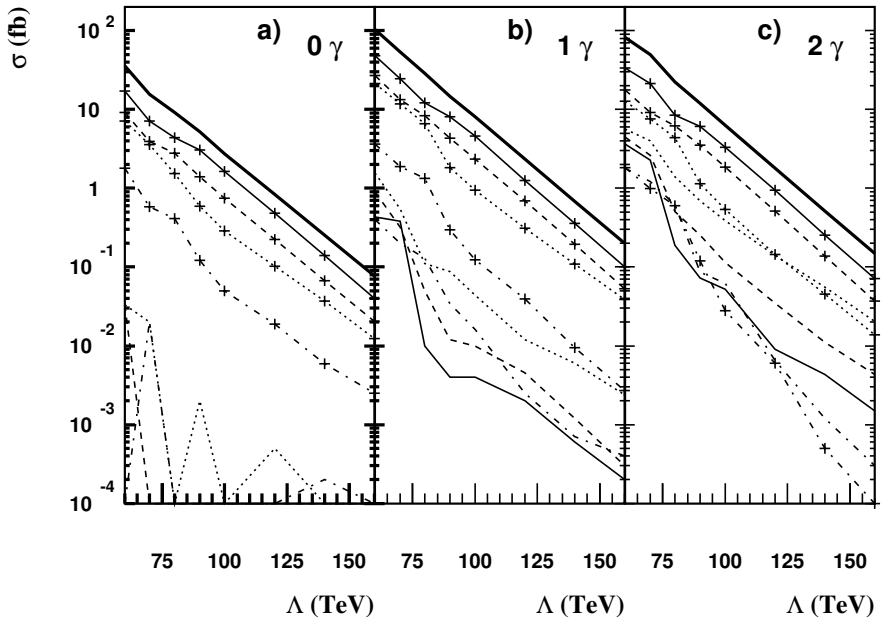

FIGURE 15. Inclusive topological cross sections for a) $0\gamma X \not\!\!E_T$, b) $\gamma X \not\!\!E_T$, and c) $\gamma\gamma X \not\!\!E_T$ after cuts along the Bino-like Neutralino Model Line as a function of Λ in the ISAJET study. The heavy solid lines are the totals. The solid, dash, dot, and dot-dash lines with crosses are for events with at least one jet and with 0,1,2,3 leptons respectively. The solid, dash, dot, and dot-dash lines without crosses are likewise for events with no jets and with 0,1,2,3 leptons respectively.

background may also be reduced if jet/lepton misidentification as a photon is considerably smaller than in Run I [32]. Optimistically assuming that the reach is given by the 5 (10) event level in Run II (TeV33), leads to the conclusion that the experiments may probe chargino masses as high as $m_{\widetilde{\chi}_1^\pm} < 300(375)$ GeV corresponding to $\Lambda \lesssim 118(145)$ TeV.

B Non-prompt Decays and Photon Pointing

The decay rate for $\widetilde{\chi}_1^0 \to \gamma\widetilde{G}$ depends on the supersymmetry breaking scale, and may take place over a macroscopic distance, as given in eq. (1.3) and illustrated in Fig. 2. Since the $\widetilde{\chi}_1^0$ are not ultra-relativistic, the decay photons are roughly uniformly distributed in solid angle in the lab frame. Decay over a macroscopic distance, but within the detector volume, therefore gives a displaced photon with finite impact parameter or finite distance of closest approach (DCA) to the beam axis. The calorimeters have multiple layers of position measurements which allow some degree of photon pointing by determining the line along which the EM shower develops. It is therefore possible to identify a displaced photon arising from a secondary vertex, and possibly to determine the decay length by using time-of-flight information [33]. A measurement of the decay length distribution would yield an essentially model independent measure of the supersymmetry breaking scale.

1 CDF study of Displaced Photons

CDF has some power to resolve a photon shower that doesn't point back to the interaction region. The calorimeter has a preradiator that measures in the $r-\phi$ direction with a resolution of 2.5 cm and a shower max detector with a resolution of about 0.6 cm and 16 cm lever arm between them. A finite $\widetilde{\chi}_1^0$ lifetime could be detected as a broadening of the distribution of $\Delta\phi$ between these $r-\phi$ measurements. The resulting lifetime measurement is best if $\widetilde{\chi}_1^0$ has a lifetime of about 1 ns where the uncertainty would be about 3 ns/$\sqrt{N_\gamma}$ and is susceptible to systematics. This resolution can be characterized as about 10 times worse than DØ's, completely due to the difference in resolution of the preradiators.

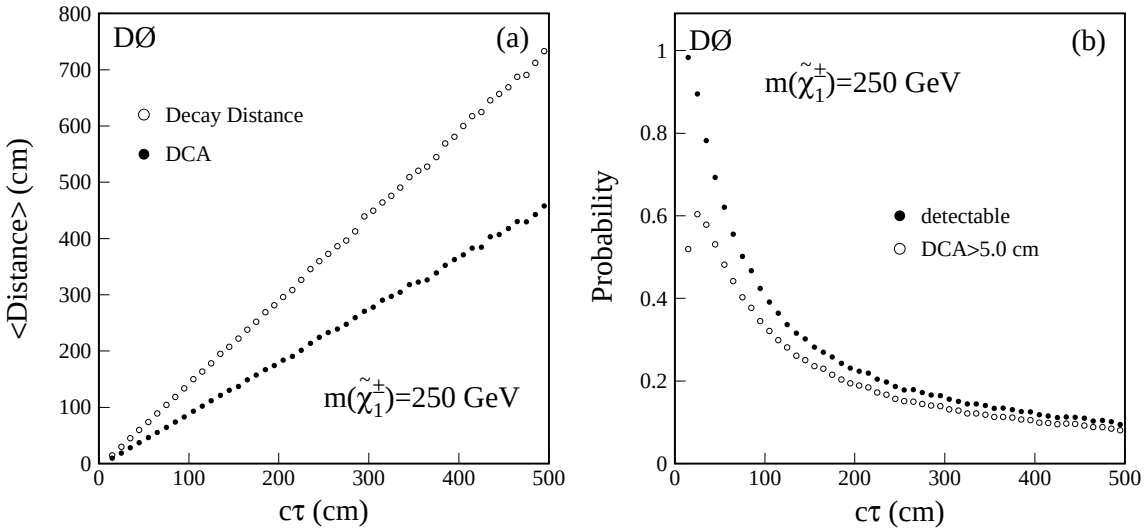

FIGURE 16. (a) Average lab frame decay distance and photon DCA as a function of the proper decay distance $c\tau(\widetilde{\chi}_1^0 \to \gamma\widetilde{G})$ in cm. (b) The probability that a displaced photon appears within the tracking volume, defined by $r < 50$ cm and $|z| < 120$ cm, and the probability that such a photon has a DCA> 5 cm as functions of $c\tau(\widetilde{\chi}_1^0 \to \gamma\widetilde{G})$ in cm. In both plots $m_{\tilde{\chi}_1^{\pm}} \simeq 250$ GeV and $m_{\tilde{\chi}_1^0} \simeq 130$ GeV corresponding to $\Lambda = 100$ TeV on the Bino-like Neutralino NLSP Model Line in the DØ study.

There are also other ways in which a finite $\widetilde{\chi}_1^0$ lifetime could be measured. If there were many signal events the one-photon excess to the two-photon excess could be compared to derive a probability of decay outside the detector and therefore a lifetime. Also with enough statistics, the 10% of diphoton events with one or both photons converting could be studied. The conversion could be reconstructed in the silicon systems or central trackers and the impact parameters and lifetime accurately measured.

2 DØ study of Displaced Photons

If a non-prompt $\widetilde{\chi}_1^0 \to \gamma\widetilde{G}$ decay occurs inside the tracking volume of the DØ detector, the photon is expected to traverse standard electromagnetic detectors (the preshower detectors and the electromagnetic calorimeter). It can, therefore, be identified. However, if the decay occurs outside the tracking detector, the photon identification is problematic. For this study, the photon is assumed to be identifiable if it is produced inside a cylinder defined by the DØ tracking volume, $r < 50$ cm and $|z| < 120$ cm, and is lost if it is produced outside the cylinder. Figure 16(a) shows the average decay distance and photon distance of closest approach as functions of the proper decay length, $c\tau(\widetilde{\chi}_1^0 \to \gamma\widetilde{G})$, for $\Lambda = 100$ TeV corresponding to $m_{\widetilde{\chi}_1^{\pm}} \simeq 250$ GeV and $m_{\tilde{\chi}_1^0} \simeq 130$ GeV. Due to its heavy mass, the Lorentz boost for the $\tilde{\chi}_1^0$ is typically small, $\gamma \sim 1.5$. The probabilities that a photon is identifiable within the tracking volume as defined above, and that the identifiable photon has DCA> 5 cm as functions of the $\tilde{\chi}_1^0$ proper decay distance $c\tau(\widetilde{\chi}_1^0 \to \gamma\widetilde{G})$ are shown in Fig. 16(b), again for $\Lambda = 100$ TeV. Photons with DCA> 5 cm could be identified as displaced. Distributions for other superpartner masses are similar.

Displaced photon events with secondary vertices are in principle very dramatic. However, tagging on displaced photons alone is unlikely to sufficiently reduce backgrounds from cosmic rays or mismeasurements. So some other characteristic must be employed to tag these events. Figure 17 shows jet multiplicity and E_T distributions for $m_{\widetilde{\chi}_1^{\pm}} = 194, 357$ GeV corresponding to $\Lambda = 80, 140$ TeV on the Bino-like Neutralino NLSP model line. Most of the events have large E_T jets. Events are therefore selected with displaced photons accompanied by jets and large $\not{E}_T$:

1) At least one displaced photon with $E_T^{\gamma'} > 20$ GeV;

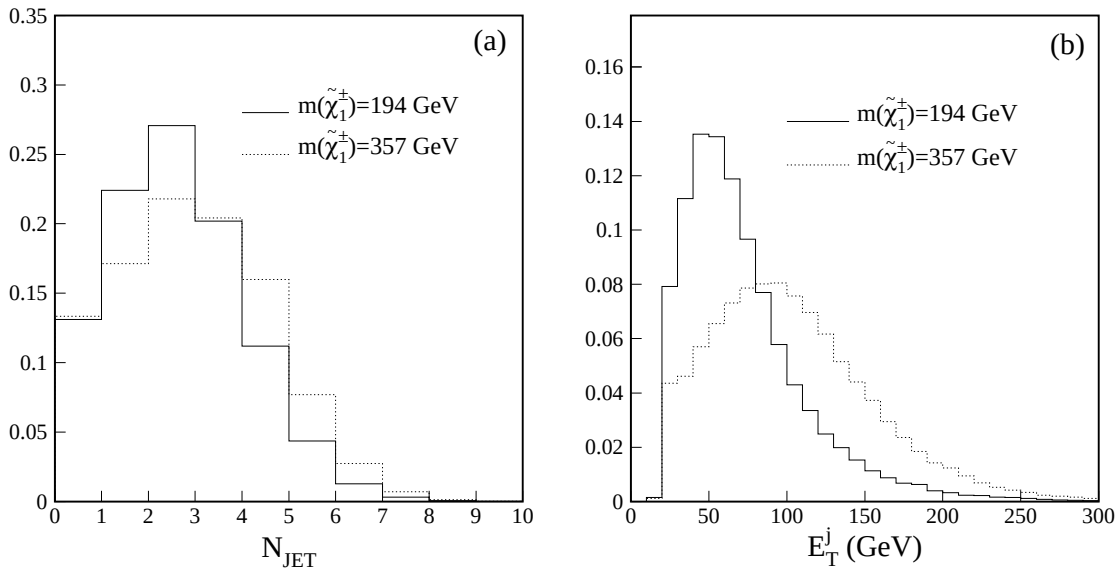

FIGURE 17. Distributions of (a) jet multiplicity and (b) jet E_T for $m_{\tilde{\chi}_1^{\pm}} = 194$, 357 GeV, corresponding to $\Lambda = 80$, 140 TeV on the Bino-like Neutralino NLSP Model Line in the DØ study. All distributions are normalized to have unit area.

2) At least two jets with $E_T^j > 20$ GeV;

3) $\not\!\!E_T > 50$ GeV.

This gives a $\gamma' jj\not\!\!E_T$ sample, where γ' indicates a displaced photon. The dominant backgrounds are the same as those for $\gamma jj\not\!\!E_T$ events, namely QCD direct photon and multijet events or W events with an electron misidentified as photon, with mismeasured $\not\!\!E_T$ and a real or fake photon, with in this case a vertex-pointing photon being misidentified as a displaced photon. Using $\mathcal{P}(\gamma \to \gamma') = 2 \times 10^{-3}$ (about 3σ), the observable background cross section from QCD and W events is estimated to be 0.6 fb. The detection efficiencies and the expected significances of the $\gamma' jj\not\!\!E_T$ selection for $c\tau(\tilde{\chi}_1^0 \to \gamma\tilde{G}) = 50$ cm are tabulated in Table 5 as an example. The estimated 5σ discovery reaches in chargino mass and Λ are shown in Fig. 18 as a function of $c\tau(\tilde{\chi}_1^0 \to \gamma\tilde{G})$ along with those expected from the $\gamma\gamma X\not\!\!E_T$ analysis. As expected, the $\gamma\gamma X\not\!\!E_T$ analysis has a stronger dependence on the decay length than the $\gamma' jj\not\!\!E_T$ analysis. Further discussion of the photon pointing capabilities of DØ is given in the Beyond the MSSM Subgroup report [34].

C Associated Higgs Production from Supersymmetric Cascades

An inclusive search for $\gamma\gamma X\not\!\!E_T$ is very efficient in identifying a Bino-like Neutralino NLSP which decays to the Goldstino by emission of a photon. The precise nature of the extra partons, X, would provide information about the superpartner mass orderings and couplings. As discussed at the beginning of this section, if the two lightest neutralinos, $\tilde{\chi}_1^0$ and $\tilde{\chi}_2^0$, are gaugino-like, the second lightest neutralino decays predominantly to the lightest one by emission of a Higgs boson, $\tilde{\chi}_2^0 \to h\tilde{\chi}_1^0$, when this mode is open. This presents the exciting possibility of obtaining a sample of Higgs bosons in $\gamma\gamma X\not\!\!E_T$ events. In this case SUSY could be used to tag Higgs events. Identification of the Higgs boson in the mode $h \to b\bar{b}$ would require b-tag(s) of the resulting jets and observation of a peak in the di-jet invariant mass distribution. This possibility of using SUSY to tag for Higgs bosons has the great advantage over Standard Model Higgs channels of being rate-limited rather than background-limited.

1 CDF study of Associated Higgs production in SUSY events

For the Bino-like Neutralino Model Line, $\tilde{\chi}_1^{\pm}\tilde{\chi}_2^0$ pair production with the dominant decays $\tilde{\chi}_1^{\pm} \to W^{\pm}\tilde{\chi}_1^0$ with $\tilde{\chi}_2^0 \to h\tilde{\chi}_1^0$ and $h \to b\bar{b}$ gives the final states $\gamma\gamma bbjj\not\!\!E_T$ and $\gamma\gamma bbl\not\!\!E_T$. Requiring an SVX b-tag leaves no

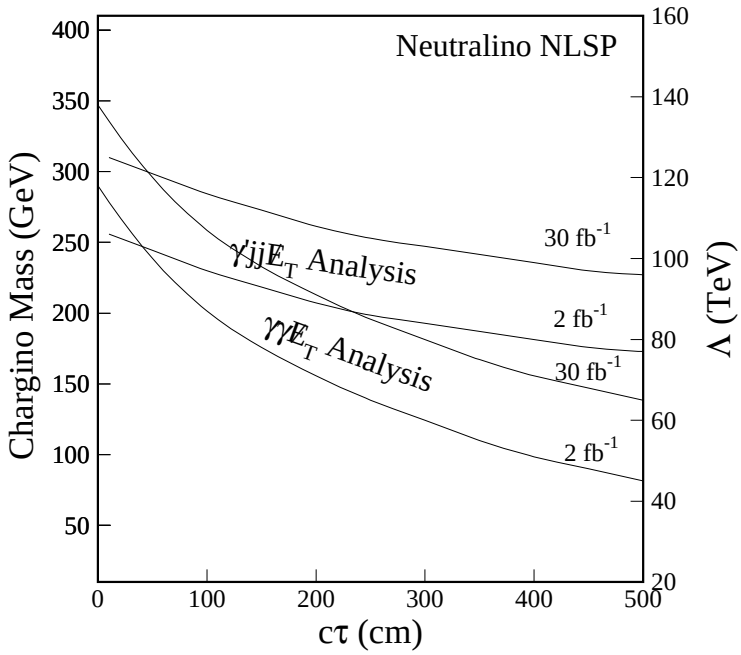

FIGURE 18. The 5σ discovery reaches of the $\gamma' jj\not{E}_T$ and the $\gamma\gamma X\not{E}_T$ analysis in chargino mass in GeV and Λ in TeV as a function $c\tau(\widetilde{\chi}_1^0 \to \gamma\widetilde{G})$ in cm for $\mathcal{L}$=2, 30 fb^{-1} on the Bino-like Neutralino NLSP Model Line in the DØ study.

TABLE 5. The detection efficiency of the $\gamma' jj\not{E}_T$ selection, and the significances for different values of Λ on the Bino-like Neutralino NLSP Model Line with displaced photons $c\tau(\widetilde{\chi}_1^0 \to \gamma\widetilde{G}) = 50$ cm in the DØ study. The relative statistical error on the efficiency is typically 2%. The observable background cross section is assumed to be 0.6 fb with a 20% systematic uncertainty.

Λ (TeV)	60	80	100	120	140	160
$m_{\tilde{\chi}_1^\pm}$ (GeV)	138	194	249	304	357	410
$m_{\tilde{\chi}_1^0}$ (GeV)	75	104	132	160	188	216
σ_{th} (fb)	464	105	27	7.7	2.2	0.7
ϵ (%)	11.2	23.6	31.1	33.3	33.2	32.1
$N_s/\delta N_b$ (2 fb^{-1})	93	44	15	4.6	1.3	0.4
$N_s/\delta N_b$ (30 fb^{-1})	278	133	45	14	3.9	1.2

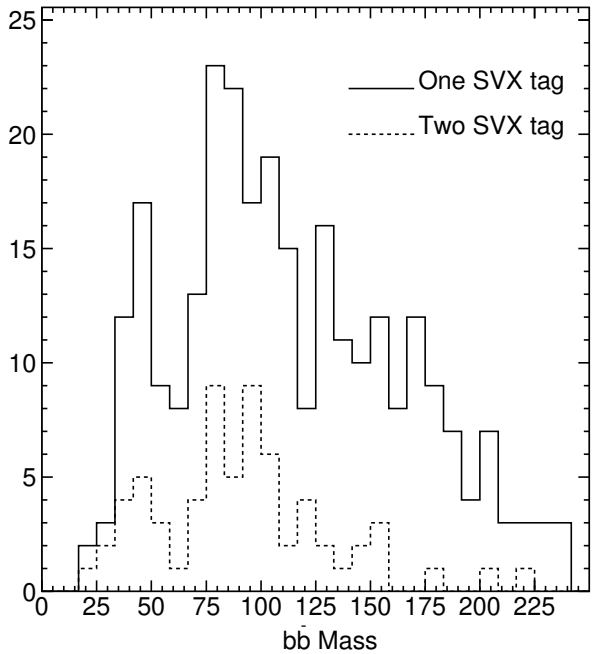

FIGURE 19. The $b\bar{b}$ invariant mass distribution in $\gamma\gamma X \not{E}_T$ events for the reference Model Point on the Bino-like Neutralino NLSP Model Line, corresponding to $m_{\widetilde{\chi}_1^\pm} = 225$ GeV, $m_h = 97$ GeV in the CDF study with 40 fb^{-1}. Essentially no Standard Model background is expected, and the background here is combinatoric. In this crude analysis, a peak in the distribution is apparent – a more sophisticated analysis would increase the signal to noise.

Standard Model background. At the reference Model Point on the Model Line, with a $\widetilde{\chi}_1^\pm$ mass of 225 GeV, about 15 events with at least one b-tag and three events with two b-tags are expected in 2 fb^{-1}. The $b\bar{b}$ invariant mass with one and two SVX b-tags is shown in Fig. 19 for the reference Model Point. Because of the large jet multiplicity (c.f. Fig. 17) the combinatoric background within a SUSY event is significant. However, a broad peak can be seen in this simple analysis, and a stronger Higgs signal would be apparent with a more sophisticated analysis.

V HIGGSINO-LIKE NEUTRALINO NLSP

Neutralinos are in general mixtures of both gaugino and Higgsino eigenstates. A general NLSP neutralino can therefore decay to the Goldstino by emission of either a Higgs boson, Z boson, or photon

$$\widetilde{\chi}_1^0 \to (h, Z, \gamma)\ \widetilde{G} \tag{5.1}$$

Pair production of superpartners which cascade decay to a general NLSP neutralino then gives rise to the di-boson final states $(hh, h\gamma, hZ, Z\gamma, ZZ, \gamma\gamma)X\not{E}_T$, where X represents additional partons from the cascade decays [3,35,36]. Di-boson signatures which include Higgs and Z bosons and $\not{E}_T$ are quite novel discovery modes for SUSY at the Tevatron. In conventional SUSY signatures, in which the lightest neutralino, $\widetilde{\chi}_1^0$, is assumed to escape the detector without decay to the Goldstino, the mass splittings between supersymmetric particles required in order for h or Z to arise in a cascade decay typically imply the superpartners are too heavy to be produced in sufficient numbers at the Tevatron. For this reason events with reconstructed Z bosons are in fact generally rejected in present SUSY searches. However, since the Goldstino is essentially massless, sufficient phase space is available for the $\widetilde{\chi}_1^0 \to h\widetilde{G}$ and $\widetilde{\chi}_1^0 \to Z\widetilde{G}$ modes. The Higgs final states also present the exciting possibility of discovering and studying the Higgs boson in association with supersymmetry.

If the supersymmetry breaking scale $\sqrt{F}$ is smaller than a few 100 TeV, the decay length (1.3) for the decays (5.1) is short enough that the decay products appear to originate from the interaction point. For the photon mode $\widetilde{\chi}_1^0 \to \gamma\widetilde{G}$ the photon is then prompt, while for $\widetilde{\chi}_1^0 \to h\widetilde{G}$ with $h \to b\bar{b}$ or $\widetilde{\chi}_1^0 \to Z\widetilde{G}$ with $Z \to \ell\ell, jj$, the

final state partons are prompt with invariant masses associated to the parent Higgs or Z boson. However, for $\sqrt{F}$ between a few 100 and a few 1000 TeV, the decays (5.1) can take place over a macroscopic distance, but within the detector. In this case the di-bosons are non-prompt or displaced. For displaced decays $\widetilde{\chi}_1^0 \to h\widetilde{G}$ with $h \to bb$ or $\widetilde{\chi}_1^0 \to Z\widetilde{G}$ with $Z \to \ell\ell, jj$ secondary vertices arise, again with decay product invariant masses which can be associated to the parent Higgs or Z boson. For the hadronic decay modes, especially $h, Z \to b\bar{b}$, Standard Model backgrounds from heavy quark production with displaced secondary vertices are possible, but may be controlled by use of invariant mass and angular distributions. For $\sqrt{F}$ greater than a few 1000 TeV, the decays eq. (5.1) take place outside the detector. The resulting signatures are then qualitatively similar to traditional SUSY missing energy signatures with a stable $\widetilde{\chi}_1^0$. The experimental signatures for a general neutralino NLSP with low scale supersymmetry breaking are therefore:

- Prompt decays $\quad \widetilde{\chi}_1^0 \to (h, Z, \gamma)\widetilde{G} \;:\; (hh, h\gamma, hZ, Z\gamma, ZZ, \gamma\gamma)X\not{E}_T, \quad X =$ leptons and jets
- Macroscopic decays $\quad \widetilde{\chi}_1^0 \to (h, Z, \gamma)\widetilde{G} \;:\; (hh, h\gamma, hZ, Z\gamma, ZZ, \gamma\gamma)X\not{E}_T, \quad X =$ leptons and jets (5.2)
  Displaced photons, $b\bar{b}$ pairs, or $\ell^+\ell^-$ pairs

All the possible final state signatures for a general neutralino NLSP with observable decay to the Goldstino are given in Table 6, including the heavy boson decays $h \to b\bar{b}$ and $Z \to \ell^+\ell^-, \nu\bar{\nu}, jj$. Observation of any of these signatures would yield interesting information about the $\widetilde{\chi}_1^0$ composition, and would imply the SUSY breaking scale is low. Observation of a displaced h or Z decay would be very dramatic. A measure of the decay length distribution would give an indirect measure of the SUSY breaking scale. Certain of the di-boson final states could be an interesting source of Higgs bosons.

TABLE 6. Final state signatures for a general Higgsino-gaugino neutralino NLSP with observable decay to the Goldstino, $\widetilde{\chi}_1^0 \to (h, Z, \gamma)\widetilde{G}$. Partons resulting from a common h or Z parent, with the associated invariant mass, are grouped together. $X \equiv$ additional partons from cascade decays to the $\widetilde{\chi}_1^0$ NLSP.

	γ	$h \to b\bar{b}$	$Z \to \ell^+\ell^-$	$Z \to \nu\bar{\nu}$	$Z \to jj$
γ	$\gamma\gamma X\not{E}_T$	$\gamma(b\bar{b})_h X\not{E}_T$	$\gamma(\ell^+\ell^-)_Z X\not{E}_T$	$\gamma X\not{E}_T$	$\gamma(jj)_Z X\not{E}_T$
$h \to b\bar{b}$		$(b\bar{b})_h(b\bar{b})_h X\not{E}_T$	$(b\bar{b})_h(\ell^+\ell^-)_Z X\not{E}_T$	$(b\bar{b})_h X\not{E}_T$	$(b\bar{b})_h(jj)_Z X\not{E}_T$
$Z \to l^+l^-$			$(\ell^+\ell^-)_Z(\ell^+\ell^-)_Z X\not{E}_T$	$(\ell^+\ell^-)_Z X\not{E}_T$	$(\ell^+\ell^-)_Z(jj)_Z X\not{E}_T$
$Z \to \nu\bar{\nu}$				$X\not{E}_T$	$(jj)_Z X\not{E}_T$
$Z \to jj$					$(jj)_Z(jj)_Z X\not{E}_T$

The branching ratios $\mathrm{Br}(\tilde{\chi}_1^0 \to \tilde{G} + (\gamma, h, Z))$ are determined by the relative Higgsino and gaugino content of $\widetilde{\chi}_1^0$. The general expressions for the decay widths are given in Appendix B. The Higgsino-gaugino content dependence is illustrated in Fig. 20 as a function of the neutralino mixing angle $\tan^{-1}(\mu/M_1)$ for $\tan\beta = 3$ and 40 with fixed $\tilde{\chi}_1^0$ mass, where μ and M_1 are the Higgsino and Bino mass parameters respectively. For definiteness the Higgs decoupling limit in which decays to the heavy scalar and pseudoscalar Higgs bosons, H and A, are kinematically blocked is employed throughout. For $|\tan^{-1}(\mu/M_1)|$ large, $\widetilde{\chi}_1^0$ is gaugino-like and $\widetilde{\chi}_1^0 \to \gamma\widetilde{G}$ dominates, while for $|\tan^{-1}(\mu/M_1)|$ small, $\widetilde{\chi}_1^0$ is Higgsino-like and $\widetilde{\chi}_1^0 \to h\widetilde{G}$ and $\widetilde{\chi}_1^0 \to Z\widetilde{G}$ are important. The dependence of the branching ratios on $\mathrm{sgn}(\mu)$ and $\tan\beta$ apparent in Fig. 20 can be understood in terms of the $\widetilde{\chi}_1^0$ quantum numbers and couplings [37]. For small $\tan\beta$ a Higgsino-like $\widetilde{\chi}_1^0$ is predominantly an $SU(2)_L$ triplet(singlet) for $\mathrm{sgn}(\mu) = +(-)$, and couples to the Goldstino predominantly through the Z (Higgs) boson. For larger $\tan\beta$ a Higgsino-like $\widetilde{\chi}_1^0$ is equal mixtures of $SU(2)_L$ triplet and singlet and couples through the Goldstino with equal strength to the Z and Higgs bosons.

Because of the large range of possibilities for combinations of $\widetilde{\chi}_1^0$ NLSP branching ratios illustrated in Fig. 20, and the many associated possible final states listed in Table 6, two Higgsino-like Neutralino NLSP Model Lines are defined for the Run II workshop. The first Model Line is defined such that the branching ratios in each mode $\widetilde{\chi}_1^0 \to (h, Z, \gamma)\widetilde{G}$ are roughly of the same order for a $\widetilde{\chi}_1^0$ mass in the range 150-200 GeV. This is realized for the fixed MGM parameters

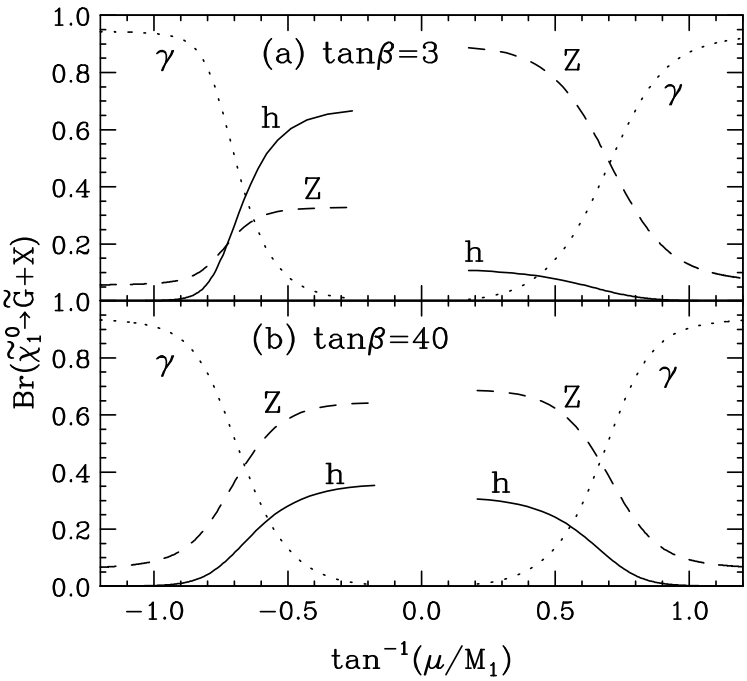

FIGURE 20. Branching ratios of the lightest neutralino to the Goldstino, $\mathrm{Br}(\widetilde{\chi}_1^0 \to \tilde{G} + (\gamma, h, Z))$, as a function of the neutralino mixing angle $\tan^{-1}(\mu/M_1)$, for a fixed mass $m_{\widetilde{\chi}_1^0} = 160$ GeV and $m_h = 105$ GeV for (a) $\tan\beta = 3$ and (b) $\tan\beta = 40$.

$$\text{Higgsino} - \text{like Neutralino NLSP Model Line I}: \qquad N = 2,\ \frac{M_m}{\Lambda} = 3,\ \tan\beta = 3,\ \mu = -\frac{3}{4}\, M_1 \tag{5.3}$$

with the overall superpartner mass scale defined by Λ varying. The ratio $\mu/M_1 = -3/4$ fixes the neutralino Higgsino-gaugino mixing angle $\tan^{-1}(\mu/M_1) \simeq -0.64$ along Model Line I. This is a modification of the usual relation implied by electroweak symmetry breaking with minimal MGM boundary conditions for the Higgs soft masses at the messenger scale. As described in Appendix A2i, modification of the Higgs soft masses may in fact arise from additional interactions between the Higgs and messenger sectors which are required in any realistic model. Because all the $\widetilde{\chi}_1^0 \to (\gamma, h, Z)\widetilde{G}$ branching ratios are of the same order, the Higgsino-like Neutralino NLSP Model Line I is useful for study of the di-boson final states $hhX\not{E}_T$, $\gamma hX\not{E}_T$, $\gamma ZX\not{E}_T$, and $hZX\not{E}_T$.

The second Model Line is defined such that the $\widetilde{\chi}_1^0 \to Z\widetilde{G}$ mode dominates. This occurs for a Higgsino-like $\widetilde{\chi}_1^0$ with low $\tan\beta$ and $\mu > 0$. The MGM Model Line fixed parameters are

$$\text{Higgsino} - \text{like Neutralino NLSP Model Line II}: \qquad N = 2,\ \frac{M_m}{\Lambda} = 3,\ \tan\beta = 3,\ \mu = \frac{1}{3}\, M_1 \tag{5.4}$$

with the overall superpartner mass scale defined by Λ varying. The ratio $\mu/M_1 = 1/3$ fixes the neutralino Higgsino-gaugino mixing angle $\tan^{-1}(\mu/M_1) \simeq 0.32$ along Model Line II, and again is a modification of the usual MGM relation. Because of the dominant $\widetilde{\chi}_1^0 \to Z\widetilde{G}$ decay mode, the Higgsino-like Neutralino NLSP Model Line II is most useful for study of the many interesting signatures associated with the $ZZX\not{E}_T$ and $\gamma ZX\not{E}_T$ final states.

For both the Higgsino-like Neutralino NLSP Model Line I and Model Line II, the two lightest neutralinos, $\widetilde{\chi}_1^0$ and $\widetilde{\chi}_2^0$, and the lightest chargino, $\widetilde{\chi}_1^\pm$, are all Higgsino-like and approximately degenerate. The masses of the lightest neutralinos, chargino, right-handed sleptons, and lightest CP-even Higgs boson as a function of the overall scale Λ along Model Line I are shown in Fig. 21. The superpartner mass spectrum along Model Line II is similar. Even though the right-handed sleptons are not much heavier than the Higgsino-like neutralinos and chargino, the $\widetilde{\ell}_R^+\widetilde{\ell}_R^-$ s-channel production cross section through γ^* and Z^* is relatively small because of P-wave suppression and pure $U(1)_Y$ hypercharge coupling. In contrast, the s-channel production cross sections

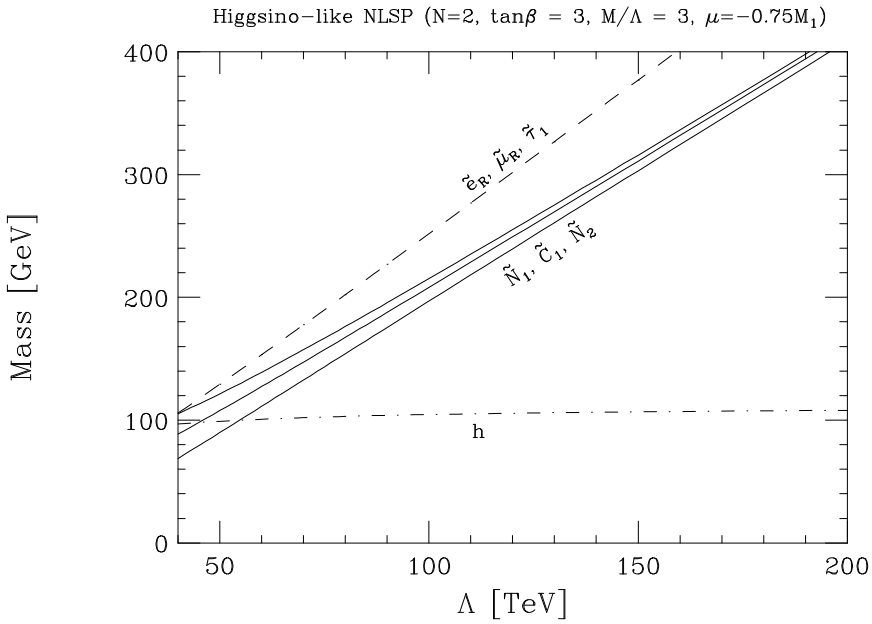

FIGURE 21. Masses in the lightest neutralinos, chargino, sleptons, and CP-even Higgs boson as a function of the overall scale Λ along the Higgsino-like Neutralino NLSP Model Line I.

for $\widetilde{\chi}_1^+\widetilde{\chi}_1^-$, $\widetilde{\chi}_1^\pm\widetilde{\chi}_i^0$, and $\widetilde{\chi}_i^0\widetilde{\chi}_j^0$ for $i,j=1,2$ through γ^*, Z^* and W^* are S-wave through $SU(2)_L$ couplings. The total SUSY production cross section turns out to be almost entirely from these Higgsino-like states on both Model Line I and Model Line II. So the Higgsino-like Neutralino Model Lines are effectively determined only by the μ parameter or equivalently the $\widetilde{\chi}_1^0$ or $\widetilde{\chi}_1^\pm$ mass, the ratio μ/M_1 or equivalently the neutralino mixing angle, and the Higgs and Z boson masses. Note in Fig. 21 that the splitting between the Higgsino-like states is small compared to the overall mass scale. So the additional partons X from cascade decays $\widetilde{\chi}_2^0 \to X\widetilde{\chi}_1^0$ and $\widetilde{\chi}_1^\pm \to X\widetilde{\chi}_1^0$ may not be particularly useful at the trigger level, but might be useful in disentangling the general magnitude of the mass splittings if a signal in one of the di-boson channels were established.

In addition to the Higgsino-gaugino content discussed above, the $\widetilde{\chi}_1^0 \to (h,Z,\gamma)\widetilde{G}$ branching ratios also depend on the $\widetilde{\chi}_1^0$ mass through the phase space available to the h and Z modes which suffer a β^4 velocity suppression near threshold [38,4,39]. So even a Higgsino-like $\widetilde{\chi}_1^0$ decays predominantly by $\widetilde{\chi}_1^0 \to \gamma\widetilde{G}$ for masses not too far above the h and Z masses. The mass dependence of the branching ratios is illustrated for Model Line I in Fig. 22 in which the total SUSY cross section times branching ratio into the di-boson final states is given as a function of the $\widetilde{\chi}_1^0$ mass. The hh and hZ di-boson modes dominate for very large masses, while the $\gamma\gamma$ mode dominates for smaller masses. However, because of the strong phase space suppression near threshold there is a transition region which extends over a significant range of mass between these limits in which the mixed di-boson mode γh is important. This mode is particularly useful for masses in the transition region since the photon is quite hard. The existence of a transition region in mass in which the γh mixed di-boson mode is significant is generic for Higgsino-like neutralino NLSP with mostly $SU(2)_L$ singlet quantum numbers (low to moderate $\tan\beta$ with $\mu < 0$ or large $\tan\beta$ with either sign of μ). The major model dependence is the extent of this transition region in $\widetilde{\chi}_1^0$ mass.

The mass dependence of the $\widetilde{\chi}_1^0$ branching ratios is illustrated for Model Line II in Fig. 23 in which the total SUSY cross section times branching ratio into the di-boson final states is given as a function of the $\widetilde{\chi}_1^0$ mass. The ZZ mode dominates for moderate to large mass, while the $\gamma\gamma$ mode dominates for very small mass. The γZ mixed di-boson mode is important in a transition region of mass between these limits. The existence of this transition region in mass is generic for a Higgsino-like neutralino NLSP with mostly $SU(2)_L$ triplet quantum numbers (low to moderate $\tan\beta$ with $\mu > 0$), but the extent of the transition region is model dependent. Because of the dominance of the neutralino coupling to the Z boson through the Goldstino on Model Line II, the γZ mixed mode is important in a relatively narrow transition region of masses.

For comparisons and detailed study of the di-boson final states which contain Higgs bosons, a reference Model Point is defined on Model Line I by $\Lambda = 80$ TeV corresponding to $m_{\widetilde{\chi}_1^0} = 154$ GeV, $m_{\widetilde{\chi}_1^\pm} = 167$ GeV, and $m_h = 104$ GeV.

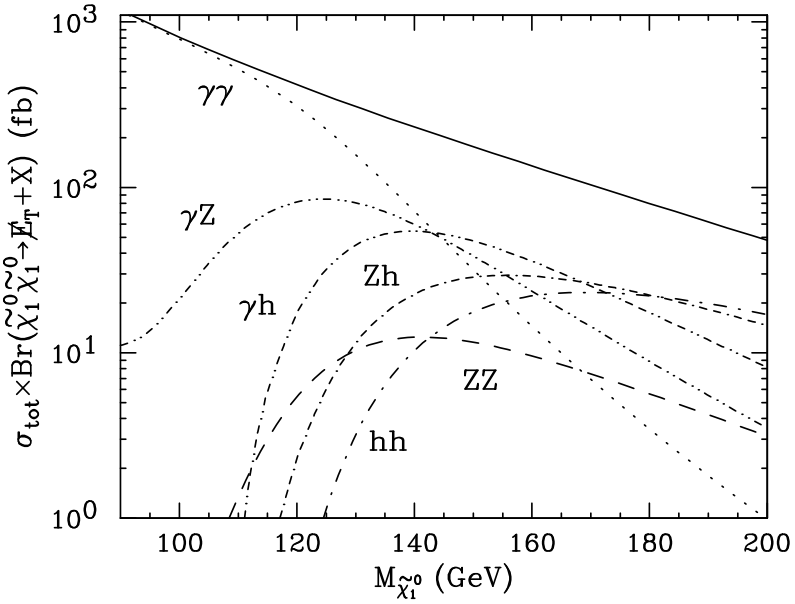

FIGURE 22. Total SUSY production cross section times branching ratios into various di-boson final states in $p\bar{p}$ collisions with $\sqrt{s} = 2$ TeV, as a function of the $\tilde{\chi}_1^0$ mass along the Higgsino-like Neutralino NLSP Model Line I with a fixed ratio $\mu/M_1 = -3/4$. The solid line indicates the total SUSY production cross section.

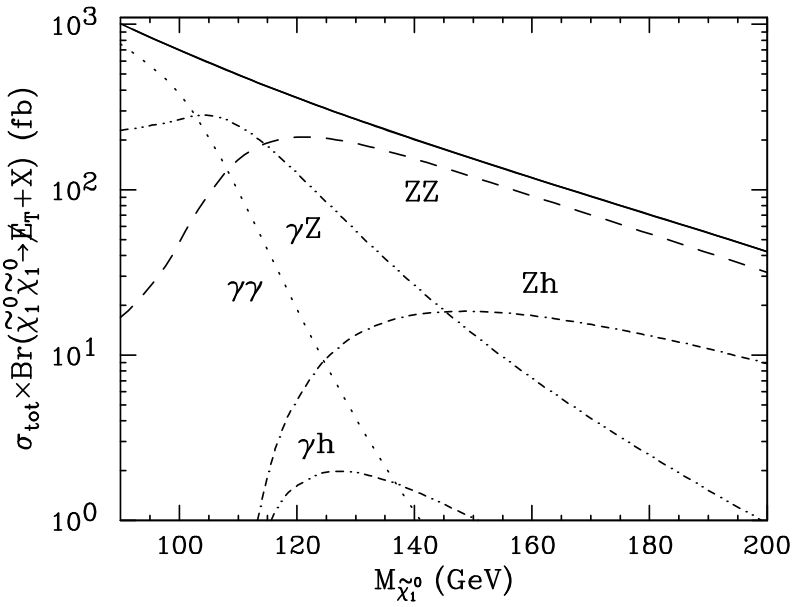

FIGURE 23. Total SUSY production cross section times branching ratios into various di-boson final states in $p\bar{p}$ collisions with $\sqrt{s} = 2$ TeV, as a function of the $\tilde{\chi}_1^0$ mass along the Higgsino-like Neutralino NLSP Model Line II with a fixed ratio $\mu/M_1 = 1/3$. The solid line indicates the total SUSY production cross section.

A Prompt Decays to Higgs Bosons, Z Bosons, and Photons

Prompt decays $\widetilde{\chi}_1^0 \to (h, Z, \gamma)\widetilde{G}$ in various combinations for each $\widetilde{\chi}_1^0$ yield the large number of signatures listed in Table 6, all with $\not\!\!E_T$. Channels with tagged b-jets from Higgs decay, with a photon, or with a reconstructed leptonic Z boson are particularly useful, although hadronic channels may also be observable.

1 CDF study of Higgsino-like Neutralino NLSP

CDF has investigated the Higgsino-like Neutralino Model Line I in both the $\gamma b X \not\!\!E_T$ and $b\bar{b}X\not\!\!E_T$ channels arising from the γh and hh di-boson modes. The $\gamma b X \not\!\!E_T$ channel has been studied in Run I and the same data has been used to set limits on several models, including Model Line I [40]. The data is based on a single isolated, central photon trigger with a threshold of 23 GeV. Off-line, an isolated, central ($|\eta| < 1$) photon is required with $E_T > 25$ GeV. A standard SVX b–tag of a jet is required with corrected $E_T > 30$ GeV and $|\eta| < 2$ and the event must have 40 GeV of $\not\!\!E_T$. Two events survive all cuts while no reliable background prediction can be calculated. More than 7 events of anomalous production are excluded – Table 7 and Fig. 24 show the resulting limits.

TABLE 7. Efficiencies and limits in the $\gamma b X \not\!\!E_T$ channel for the Higgsino-like Neutralino NLSP Model Line I from CDF in Run I with 85 pb^{-1} of integrated luminosity. Efficiencies do not include branching ratios.

Λ (TeV)	60.9	70.3	81.0	89.5
$m_{\tilde{\chi}_1^\pm}$ (GeV)	130	147	170	186
$m_{\tilde{\chi}_1^0}$ (GeV)	113	132	156	174
$A \cdot \epsilon$(%)	20.9	5.7	6.4	8.7
BR (%)	3	20	23	18
$\sigma_{th} \times BR$ (fb)	10.0	40.2	23.0	11.0
$\sigma_{95\%\ lim} \times BR$ (fb)	400	1450	1300	950

Projected limits in the $\gamma b X \not\!\!E_T$ channel may also be obtained for Run II. To estimate the background, the Run I histograms of photon E_T and $\not\!\!E_T$ are scaled up in energy by 5% and the overall normalization is increased by a factor of 1.2 to correct for the increase to 2 TeV and for the 2 fb^{-1} of integrated luminosity. Comparing the signal and background photon E_T and $\not\!\!E_T$ distributions it is found that the $\not\!\!E_T$ distribution shows the greater discrimination power. So the $\not\!\!E_T$ cut is increased to 60 GeV where the one event background level can be maintained.

For the efficiency in Run II, the full efficiency of the Run I analysis is used as a starting point. The b–tagging coverage improvement in Run II is assumed to contribute a factor of 1.6 to the efficiency due to the increase in the length of the SVX detector. The improved photon coverage contributes another factor of 1.6 due to improvements in the trigger isolation and fiducial efficiency, and increasing the coverage from $|\eta| < 1$ to $|\eta| < 2$. The projected Run II limits are presented in Table 8 and Figure 25. This mixed di-boson signature requires that one neutralino NLSP decays by $\widetilde{\chi}_1^0 \to \gamma\widetilde{G}$ while the other decays by $\widetilde{\chi}_1^0 \to h\widetilde{G}$. This mixed mode is only significant in the transition region of $\widetilde{\chi}_1^0$ mass, as discussed above, and is less useful for very large masses. The CDF Run II exclusion reach will be up to approximately 180 GeV, while a 5σ discovery may or may not be possible. For larger luminosities, the signal and background may be scaled without optimizing the analysis cuts again. As shown in Figure 25 a sensitivity up to a $\widetilde{\chi}_1^\pm$ mass of 250 GeV for 10 fb^{-1} and 280 GeV for 30 fb^{-1} are expected.

The Higgsino-like Neutralino NLSP Model Line I can also have be probed with a $b\bar{b}X\not\!\!E_T$ selection. An analysis of this channel may be borrowed from a SUGRA analysis which uses this channel to search for sbottom squark pair production, $\tilde{b}\tilde{b}$, with each sbottom decaying by $\tilde{b} \to b\widetilde{\chi}_1^0$ and with the $\widetilde{\chi}_1^0$ escaping the

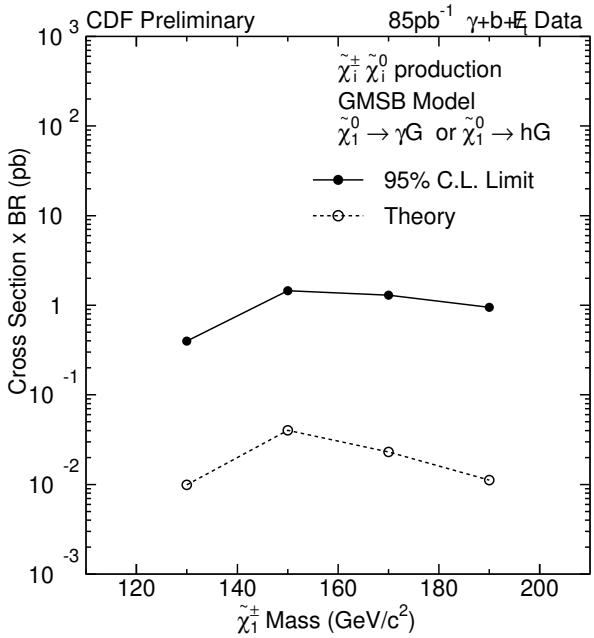

FIGURE 24. CDF Run I limits with 85 pb^{-1} of integrated luminosity on the total SUSY cross section times branching ratio in the $\gamma bX\not\!\!E_T$ channel along the Higgsino-like Neutralino Model Line I as a function of chargino mass.

TABLE 8. Summary of the Monte Carlo points used to investigate the projected limits in the $\gamma bX\not\!\!E_T$ channel for the Higgsino-like Neutralino NLSP Model Line I for CDF in Run II with 2 fb^{-1} of integrated luminosity. Efficiencies do not include branching ratios.

Λ (TeV)	60.9	70.3	81.0	89.5	110	134
$m_{\tilde{\chi}_1^{\pm}}$ (GeV)	130	147	170	186	236	284
$m_{\tilde{\chi}_1^0}$ (GeV)	113	132	156	174	226	275
BR(%)	3	20	23	18	11	6
$\sigma\times$BR (fb)	14.0	54.0	30.0	15.0	2.3	0.4
$A\cdot\epsilon$ (%)	50	14	16	22	30	35
$\sigma\times$BR 95% C.L. limit (fb)	4.0	14.0	13.0	9.1	6.7	5.7

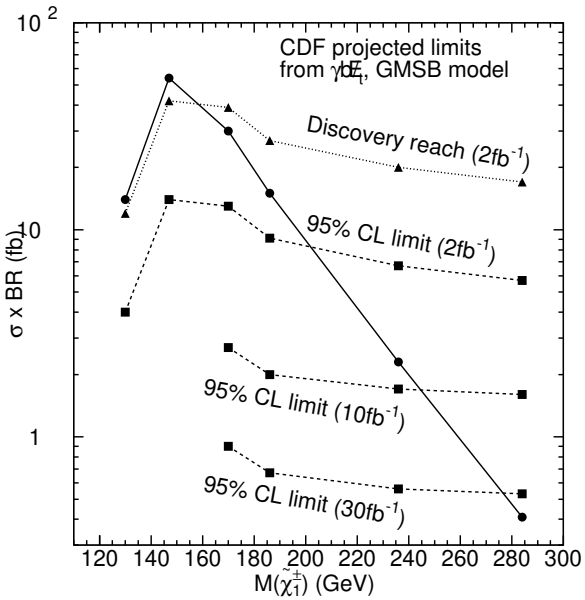

FIGURE 25. CDF projected Run II limits on the total SUSY cross section times branching ratio in the $\gamma b X \not\!\!E_T$ channel along the Higgsino-like Neutralino Model Line I as a function of chargino mass. The solid line is the theoretical expectation from the Higgsino-like Neutralino NLSP Model Line I.

detector as missing energy [7]. In that analysis, several options for the final cuts are offered which may be evaluated for Model Line I. The requirements placed on the events are: two jets with $E_T > 20$ and 30 GeV, one jet with $|\eta| < 1$, $\not\!\!E_T > 50$ GeV, the jets must not be correlated with the $\not\!\!E_T$, the jets must not be back–to–back, and one jet must have a standard SVX b–tag. These are the same as the basic SUGRA analysis cuts with the exception of the requirement of no isolated leptons in the event (to reject W's). At this point the efficiency of additional cuts can be checked and compared to the background prediction, as shown in Table 9. The no–leptons requirement is not a large loss in efficiency, requiring 2 or 3 jets is a clear loss, and either the sample with one tag or with two tags may be used. For the present analysis the sample with two tags will be employed.

TABLE 9. Summary of the CDF optimization for the Monte Carlo cuts for the $b\bar{b}X\not\!\!E_T$ channel for the Higgsino-like Neutralino NLSP Model Line I at the point with $m_{\tilde{\chi}_1^\pm} = 187$ GeV. The efficiency for "w/o lepton removal" is obtained without requiring the absence of central or plug isolated leptons (no corresponding background estimate was given in [7]).

Cuts	ϵ(%)	background (fb)	Signal/$\sqrt{\text{background}}$
basic, w/o lepton removal	59	-	-
basic	48	356	2.5
basic, $n_{jet} \leq 3$	2.6	172	0.2
basic, 2 b–tags	18	50	2.5

In Run II with 2 fb^{-1} of integrated luminosity, assuming statistical uncertainties dominate, a limit of approximately 20 events is expected or a discovery sensitivity to 50 events or more. These limits translate to cross section limits as indicated in Table 10 and Fig. 26. For larger luminosities, the signal and backgrounds are scaled with the results shown in Fig. 26.

Although it is clear from this estimate that there is not a great deal of sensitivity, this channel has a large

TABLE 10. Results for CDF projected Run II limits on the Higgsino-like Neutralino NLSP Model Line I in the $b\bar{b}X\not{E}_T$ channel with 2 fb^{-1} of integrated luminosity. Cross sections include branching ratios.

Λ (TeV)	60.9	70.3	81.0	89.5	110	134
$m_{\tilde{\chi}_1^\pm}$ (GeV)	130	147	170	186	236	284
$m_{\tilde{\chi}_1^0}$ (GeV)	113	132	156	174	226	275
BR(%)	3	32	58	70	81	84
$\sigma\times$BR (fb)	14	86	77	60	17	6
$A\cdot\epsilon$ (%)	33	10	12	18	25	29
$\sigma\times$BR 95% C.L. limit (fb)	30	100	83	56	40	34

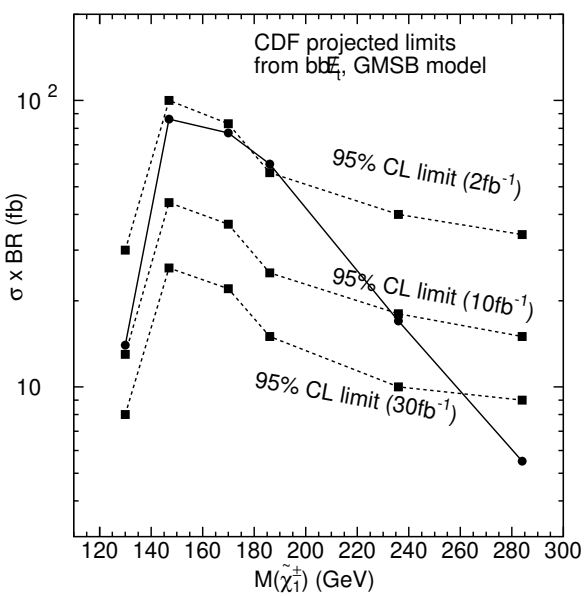

FIGURE 26. CDF Projected Run II limits on the total SUSY cross section times branching ratio in the $bbX\not{E}_T$ channel along the Higgsino-like Neutralino Model Line I as a function of chargino mass. The solid line is the theoretical expectation.

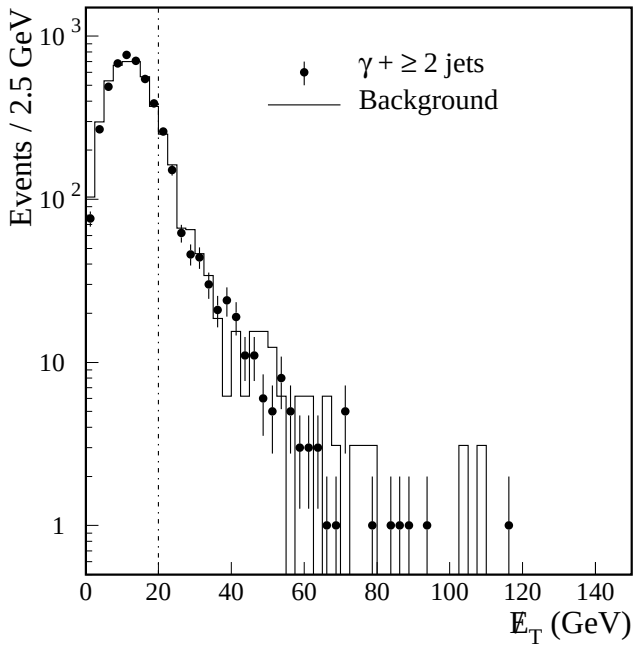

FIGURE 27. The DØ Run I $\not\!\!E_T$ distributions of γjj and background events. The number of events in the background is normalized to the γjj sample for $\not\!\!E_T < 20$ GeV, the region left of the dot-dashed line.

potential for more optimization for the parameters of Model Line I. For example, in a significant fraction of events, one of the NLSP neutralinos decays by $\widetilde{\chi}_1^0 \to Z\widetilde{G}$ in which the Z boson could be found as leptons or a second dijet peak. In addition, there are jets and leptons in the cascade decays and the $\not\!\!E_T$ and jet cuts are not optimized.

2 DØ study of Higgsino-like Neutralino NLSP

The DØ collaboration has investigated the Higgsino-like Neutralino Model Line I in the $\gamma bj\not\!\!E_T$ channel arising from the γh di-boson mode. In Run I a similar $\gamma jj\not\!\!E_T$ search [41] for single-photon events with at least two jets and large $\not\!\!E_T$ was carried out. The $\gamma jj\not\!\!E_T$ events were selected by requiring at least one identified photon with $E_T^\gamma > 20$ GeV and within pseudorapidity ranges $|\eta^\gamma| < 1.1$ or $1.5 < |\eta^\gamma| < 2.0$, two or more jets having $E_T^j > 20$ GeV and $|\eta^j| < 2.0$, and $\not\!\!E_T > 25$ GeV. A total of 318 events were selected from a data sample corresponding to an integrated luminosity of 99.4 ± 5.4 pb^{-1}.

The principal backgrounds were found to be QCD direct photon and multijet events, where there was mismeasured $\not\!\!E_T$ and a real or fake photon. The number of events from this source was estimated to be 315 ± 30. Other backgrounds such as those from W with electrons misidentified as photons were found to be small, contributing 5 ± 1 events. This led to an observed background cross section of 3200 fb from the $\not\!\!E_T$ mismeasurement and of 50 fb from the fakes. The $\not\!\!E_T$ distribution before the $\not\!\!E_T > 25$ GeV cut is shown in Fig. 27. The backgrounds can be significantly reduced by raising the requirement on $\not\!\!E_T$, as is apparent in Fig. 27.

Events with a high E_T photon, b-jets and large $\not\!\!E_T$ are expected in several new physics models, including the Higgsino-like Neutralino NLSP Model Line I. These events, referred to as $\gamma bj\not\!\!E_T$, are in many ways similar to the $\gamma jj\not\!\!E_T$ events and thereby can be selected similarly:

1) At least one photon with $E_T^\gamma > 20$ GeV;

2) At least two jets with $E_T^j > 20$ GeV;

3) At least one jet is tagged as a b-quark jet with $E_T^b > 20$ GeV;

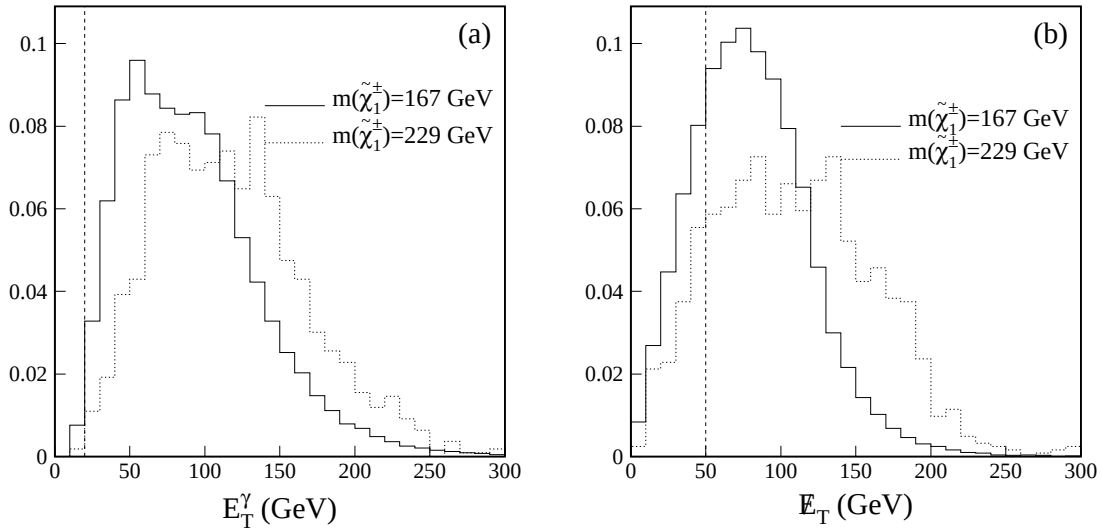

FIGURE 28. The SUSY photon E_T (a) and event $\not{E}_T$ (b) distributions for the Higgsino-like Neutralino NLSP Model Line I with $\Lambda = 80,\ 110$ TeV corresponding to $m_{\tilde{\chi}_1^\pm} = 167,\ 229$ GeV, in the DØ study. All distributions are normalized to have unit area.

4) $\not{E}_T > 50$ GeV;

5) No leptons with $E_T^\ell > 20$ GeV.

The backgrounds from the QCD multijet events with real or misidentified photons and from the W events with electrons faking photons are estimated to be 0.63 fb, assuming background reduction factors of 5 from the raised $\not{E}_T$ requirement, 2 from the improved photon identification and using the assumed value of $\mathcal{P}(j \to b) = 10^{-3}$. The dominant background sources are expected to be $\gamma b\bar{b}$ and $\gamma t\bar{t}$ events. These background sources cannot be reduced by the tagging of b-jets. However, the $\gamma b\bar{b}$ contribution is expected to be small due to the large $\not{E}_T$ requirement. Monte Carlo studies show that it is negligible. The $\gamma t\bar{t}$ with $t\bar{t} \to W^+W^-b\bar{b}$ contribution is reduced by the requirements 4) and 5) and is estimated using the cross section of Ref. [42]. A total of 0.9 fb observable background cross section is assumed.

The SUSY events for Model Line I in the $\gamma bj\not{E}_T$ channel are characterized by high E_T photons and large $\not{E}_T$ as shown in the Fig. 28 for $\Lambda = 80, 110$ TeV, corresponding to $m_{\tilde{\chi}_1^\pm} = 167, 229$ GeV and $m_{\tilde{\chi}_1^0} = 154, 218$ GeV respectively. These events can be selected using the $\gamma bj\not{E}_T$ selection criteria discussed above. The detection efficiencies and $N_s/\delta N_b$ significances are shown in Table 11 for different values of Λ along Model Line I. Most of the events selected are due to the γh di-boson mode with $h \to b\bar{b}$. However, a non-negligible fraction of the events are actually due to the γZ di-boson mode with $Z \to b\bar{b}$. The Run II discovery reach in Λ and $m_{\tilde{\chi}_1^\pm}$ along Model Line I is shown in Fig. 29 for integrated luminosities of $\mathcal{L}$=2,30 fb^{-1}.

3 ISAJET studies of Higgsino-like Neutralino NLSP

The hh di-boson mode along the Higgsino-like Neutralino NLSP Model Line I with $h \to b\bar{b}$ leads to the $bbbbX\not{E}_T$ channel. Signals in this channel with multiple tagged b-jet plus $\not{E}_T$ events, and perhaps other jets, leptons, and possibly photons in the case that one of the neutralinos decays as $\tilde{\chi}_1^0 \to \gamma\tilde{G}$, have been simulated using ISAJET [17].

The dominant Standard Model background to multi-b events presumably comes from $t\bar{t}$ production and is shown in Table 12, where the signal cross section for Model Line I with $\Lambda = 100$ TeV, corresponding to $m_{\tilde{\chi}_1^\pm} = 208$ GeV and $m_{\tilde{\chi}_1^0} = 197$ GeV, is also shown. For events with one or two tagged b-jets, the $t\bar{t}$ backgrounds come when the b-jets from t decay are tagged; *i.e.* the rate for events where other jets are mis-tagged as b-jets is just a few percent. This is also true for signal events. On the other hand, in the $bbbX\not{E}_T$

TABLE 11. The $\tilde{\chi}_1^{\pm}$, $\tilde{\chi}_1^0$ and h masses, theoretical SUSY cross section, $\tilde{\chi}_1^0$ decay branching ratios, detection efficiency of the $\gamma bj\not{E}_T$ selection, and significances for different values of Λ along the Higgsino-like Neutralino Model Line I in the DØ study. The relative statistical error on the efficiency is typically 4%. The background cross section is assumed to be 0.9 fb with a 20% systematic error.

Λ (TeV)	80	90	100	110	120
$m_{\tilde{\chi}_1^{\pm}}$ (GeV)	167	188	208	229	249
$m_{\tilde{\chi}_1^0}$ (GeV)	154	176	197	218	239
m_h (GeV)	103	104	105	105	106
σ_{th} (fb)	118	69	41	24	15
$\mathrm{Br}(\tilde{\chi}_1^0 \to \gamma\tilde{G})$	0.38	0.21	0.15	0.10	0.08
$\mathrm{Br}(\tilde{\chi}_1^0 \to h\tilde{G})$	0.38	0.52	0.59	0.63	0.66
ϵ (%)	8.0	6.8	5.4	4.3	3.6
$N_s/\delta N_b$ (2 fb^{-1})	13	6.7	3.2	1.5	0.8
$N_s/\delta N_b$ (30 fb^{-1})	38	19	8.9	4.1	2.2

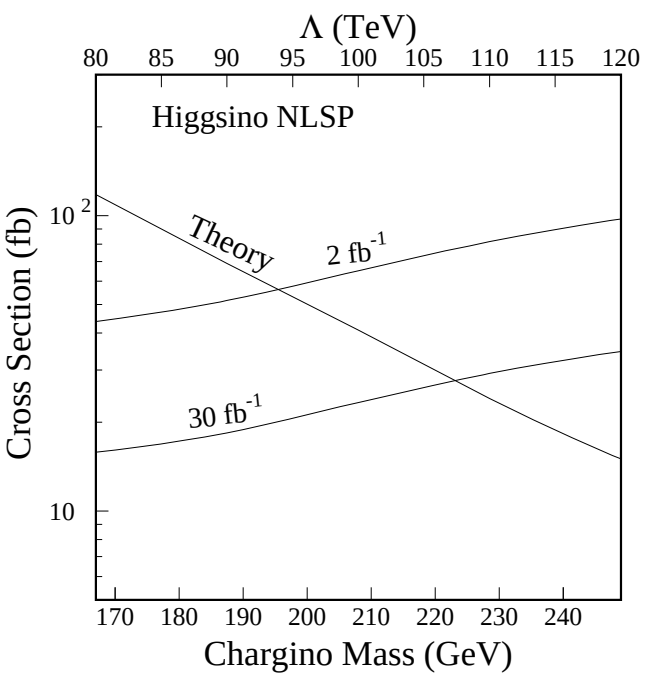

FIGURE 29. The 5σ discovery cross section curves as functions of Λ and the $\tilde{\chi}_1^{\pm}$ mass along the Higgsino-like Neutralino NLSP Model Line I in the DØ study along with the theoretical cross section.

channel at least one of the tagged b-jets in the $t\bar{t}$ background has to come from a c or light quark or gluon jet that is misidentified as a b-jet, or from an additional b produced by QCD radiation. This is not, however, the case for signal events which contain up to four b-jets. In each of the last two columns of Table 12 where the top background and the SUSY signal are shown, two numbers are presented: the first of these is the cross section when all the tagged jets come from real b's, while the second number in parenthesis is the cross section including c and light quark or gluon jets that are mistagged as b, with the assumed probabilities $\mathcal{P}(c \to b) = 5\%$ and $\mathcal{P}(q, g \to b) = 0.2\%$. Indeed it can be see that the bulk of the $bbbX\not{E}_T$ background is reducible and comes from mistagging jets, whereas the signal is essentially all from real b-jets.

TABLE 12. The background cross section in fb for multiple tagged b-jets plus lepton plus $\not{E}_T$ events from $t\bar{t}$ production after basic cuts and triggers in the ISAJET study. Also shown are the corresponding SUSY signal cross sections for the Higgsino-like Neutralino NLSP Model Line I with $\Lambda = 100$ TeV corresponding to $m_{\widetilde{\chi}_1^\pm} = 208$ GeV and $m_{\widetilde{\chi}_1^0} = 197$ GeV. The numbers in parenthesis for the $bbbX\not{E}_T$ channel include events from charm or light quark jets faking a b-jet. Whereas this fake rate dominates the background in the $3b$ channel, it is negligible in the $bX\not{E}_T$ and $bbX\not{E}_T$ channels.

	$bX\not{E}_T$		$bbX\not{E}_T$		$bbbX\not{E}_T$	
	$t\bar{t}$	SUSY	$t\bar{t}$	SUSY	$t\bar{t}$	SUSY
0ℓ	508	11.6	221	7.5	1.2 (8.1)	2.6 (2.7)
1ℓ	812	1.2	345	0.57	1.5 (9.3)	0.11 (0.11)
2ℓ	132	0.49	56	0.31	0.13 (0.31)	0.04 (0.05)
3ℓ	0.22	0.03	0	0.04	0 (0)	0 (0)

It is clear from Table 12 that the best signal to background ratio is obtained in the $bbbX\not{E}_T$ channel for events with $\geq 3b$-jets. Our detailed analysis shows that although the signal cross section is rather small, $bbbX\not{E}_T$ channel with a lepton veto (since top events with large $\not{E}_T$ typically contain leptons) offers the best hope for identifying the signal above Standard Model backgrounds. The signal is seen to be of similar magnitude as the background for $\Lambda = 100$ TeV on Model Line I, corresponding to $m_{\widetilde{\chi}_1^\pm} = 208$ GeV, a point beyond reach via the $\gamma\gamma$ channel. To further enhance the signal relative to the background the additional cuts are imposed,

- $\not{E}_T \geq 60$ GeV, and
- 60 GeV $\leq m_{bb} \leq 140$ GeV for at least one pair of tagged b-jets in the event.

The first of these reduces the signal from 2.7 fb to 2.1 fb while the background is cut by more than half to 3.4 fb. The mass cut was motivated by the fact that for Model Line I, at least one pair of tagged b's comes via $h \to bb$ decay, with $m_h \sim 100$ GeV, while the b's from top decay form a continuum. However, this cut leads to only a marginal improvement in the statistical significance and the signal to background ratio. This may be traced to the fact that, because of top event kinematics, one b-pair is likely to fall in the 'Higgs mass window'. Reducing this window to 100 ± 20 GeV leads to a slightly improved S/B but leads to too much loss of signal to improve the significance.

The signal cross section via the $bbbX\not{E}_T$ channel after the basic cuts as well as the additional $\not{E}_T$ and m_{bb} cuts introduced above is shown by the solid curve labeled $h \to bb$ in Fig. 30. For small $\widetilde{\chi}_1^0$ masses, the signal is small because of the reduction in the branching ratio $\widetilde{\chi}_1^0 \to h\widetilde{G}$ apparent in Fig. 22. The corresponding dashed lines show the minimum cross section for a signal to be observable at the 3σ level at Run II with an integrated luminosity of 2 fb^{-1} and 30 fb^{-1}. For Run II with 2 fb^{-1} there could just barely be an observable signal in the $bbbX\not{E}_T$ channel for the parameters of Model Line I. With 30 fb^{-1} of integrated luminosity, the signal exceeds the 3σ level for 75 TeV $\leq \Lambda \leq$ 120 TeV, corresponding to a $\widetilde{\chi}_1^0$ mass of up to 240 GeV, and significantly extends the reach obtained along Model Line I with, for example, the $\gamma\gamma X\not{E}_T$ channel. Furthermore there appears to be no window between the upper limit of the $\gamma\gamma X\not{E}_T$ channel and the lower limit of the $bbbX\not{E}_T$ channel. A few points are worth noting.

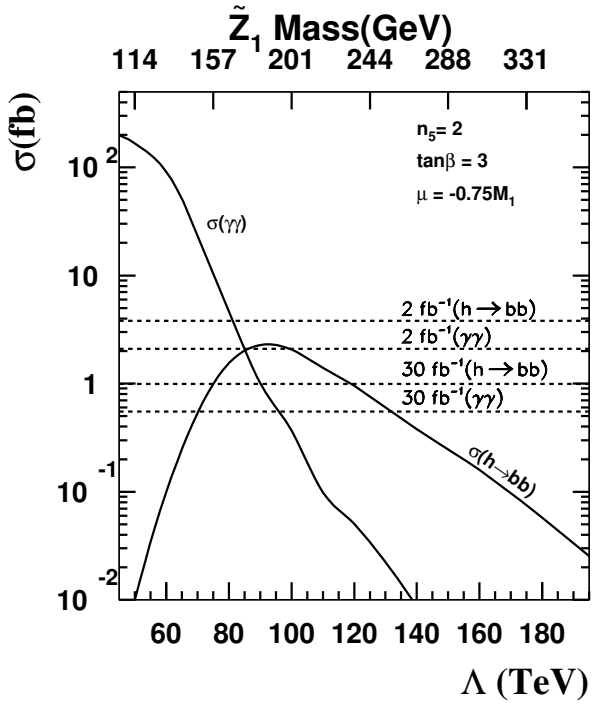

FIGURE 30. SUSY signal cross sections for the Higgsino-like Neutralino Model Line I in the $\gamma\gamma X \not{E}_T$ channel (labeled $\sigma(\gamma\gamma)$, and $bbbX\not{E}_T$ channel after all ISAJET study cuts described in the text. The dashed horizontal lines denote the minimum cross section for 3σ observation in Run II with an integrated luminosity of 2 fb^{-1} and 30 fb^{-1}.

1. Since the background dominantly comes from events where a c or light quark or gluon jet is mis-tagged as a b-jet, the reach via the $bbbX\not{E}_T$ channel is very sensitive to the assumptions about the b mis-tag rate. Indeed, if the mis-tag rate is twice as big as assumed here, there will be no reach in this channel at Run II.

2. The $bbbX\not{E}_T$ signal starts to become observable for $m_{\tilde{\chi}_1^0} \sim 140$ GeV where the branching ratio for $\tilde{\chi}_1^0 \to h\tilde{G}$ becomes comparable to that for $\tilde{\chi}_1^0 \to \gamma\tilde{G}$. The $\tilde{\chi}_1^0$ mass for which $\tilde{\chi}_1^0 \to h\tilde{G}$ becomes dominant depends on m_h, which in turn is sensitive to $\tan\beta$.

The $bbbX\not{E}_T$ channel provides a promising probe of the Higgsino-like Neutralino Model Line I at Run II, and is rapidly helped by increasing luminosity and by reducing the background from mis-tagged charm (light quark or gluon jets to below 5% (0.2%).

Despite the fact that the top background alone is 50 to several hundred times larger than the SUSY signal in all relevant one and two tagged b plus multilepton channels in Table 12, we have examined whether it is possible to separate the signal from the background. Attention was focused on the $2b+0\ell$ signal which has the best S/B ratio, and required in addition that $\not{E}_T \geq 60$ GeV (which reduces the background by almost 50% with about a 20% loss of signal) and further 60 GeV $\leq m_{bb} \leq$ 140 GeV (which reduces the background by another factor of half with a loss of 25% of the signal). Several other distributions were also studied including, jet multiplicity, θ_{bb}, $\delta\phi(bb)$ but none of these proved useful to enhance the signal over the top background. The signal is below the 5σ discovery level over essentially the entire Model Line I; only for $m_{\tilde{\chi}_1^0} \sim 155 \pm 10$ GeV does the signal cross section exceed the 5σ level of 7.7 fb. Moreover the S/B ratio never exceeds about 15% which falls below our detectability criterion $S/B \geq 20\%$. While it is possible to improve the S/B ratio via additional cuts, these typically degrade the statistical significance of the signal.

4 PYTHIA-SHW studies of Higgsino-like Neutralino NLSP

The Z boson decay mode of a general neutralino NLSP, $\widetilde{\chi}_1^0 \to Z\widetilde{G}$, leads to the possibility of di-boson modes which have one or two Z bosons. The existence of Z boson(s) arising from decay to the Goldstino gives many possible final state signatures, depending on the Z boson decay mode, $Z \to \ell\ell, jj, \nu\nu$. The possible di-boson final state signatures which include at least one Z boson were listed in the last three rows and columns of Table 6. The sensitivity of Run II to signatures associated with the γZ mode for Model Line I and the ZZ mode for Model Line II have been estimated based on some Run I analysis of similar final states. The signatures associated with this have been analyzed using the PYTHIA [24] option of the SHW detector simulation package [25–27].

For the parameters of Model Line I the $\gamma Z \not{E}_T$ di-boson mode dominates the total cross section in the transition region of masses as discussed at the beginning of Section V, and illustrated in Fig. 22. Leptonic decay of the Z provides the cleanest final state, $\gamma \ell^+ \ell^- \not{E}_T$, which is similar to existing Run I studies of Standard Model $Z\gamma$ production without $\not{E}_T$ [43,44]. For a Higgsino-like neutralino NLSP search, however, an additional large p_T cut, made possible by decay to the Goldstinos, as well as a more stringent photon E_T cut should reduce the backgrounds to a negligible level. In order to isolate a leptonically decaying Z boson, a hard photon, and missing energy, the following cuts are applied

1. At least one photon with $p_T > 25$ GeV and $|\eta| < 2.0$.

2. Two opposite-charge, same flavor leptons with $p_T > (15, 10)$ GeV, $|\eta| < 2.0$ and invariant mass $|m_{\ell\ell} - M_Z| < 10$ GeV.

3. $\not{E}_T > 25$ GeV.

Backgrounds necessarily include a fake lepton, fake photon, or energy mismeasurement. The probabilities for misidentifying an electron or jet as a photon are conservatively assumed to be $\mathcal{P}(e \to \gamma) = 10^{-3}$ and $\mathcal{P}(j \to \gamma) = 10^{-3}$. The probability for jet energy mismeasurement to be greater than or equal to E_0 is taken to be

$$\mathcal{P}(j \to \not{E}_T > E_0) = \exp(1.86 - 0.3E_0/\mathrm{GeV}) \tag{5.5}$$

valid for $E_0 > 20$ GeV [45]. For the missing energy cut of 25 GeV given above this corresponds to $\mathcal{P}(j \to \not{E}_T > 25\ \mathrm{GeV}) \simeq 0.0036$. The main backgrounds are from $WWj \to \ell\ell j \not{E}_T$ with the jet faking a photon, $t\bar{t}j \to \ell\ell b\bar{b}j\not{E}_T$ with the jet faking a photon, $Zjj \to \ell\ell jj$ with one jet faking $\not{E}_T$ and the other faking a photon, and $Z\gamma j$ with the jet faking $\not{E}_T$. Other potential backgrounds from $Z \to \ell\ell\tau\tau$ with an electron from $\tau \to e\not{E}_T$ decay misidentified as a photon, $WZ \to e\ell\ell$ with the electron misidentified as a photon, are significantly smaller. Continuum $\gamma\ell\ell j$ with the jet faking $\not{E}_T$ is very efficiently reduced to negligible levels by the invariant mass cut given above, while $ZZj \to \tau\tau j \to \ell\ell j\not{E}_T$ with the jet faking a photon is also reduced to negligible levels by the combination of invariant mass and $\not{E}_T$ cuts. The total expected background from all these sources to the $\gamma\ell\ell\not{E}_T$ final state with the cuts given is found to be 0.06 fb. For the parameters of Model Line II with a $\widetilde{\chi}_1^0$ mass of 130 GeV, the acceptance times efficiency for the signal in the $\gamma\ell\ell\not{E}_T$ channel with the above cuts (not including $\mathrm{Br}(Z \to \ell\ell) \simeq 0.07$) is found to be 0.39. Using this along with the background quoted above, the reach for a 3σ observation with 2 (30) fb^{-1} of integrated luminosity should be 155 (220) GeV for the $\widetilde{\chi}_1^0$ mass along Model Line I, and 130 (165) GeV along Model Line II. The reach is better along Model Line I since the $\widetilde{\chi}_1^0 \to \gamma\widetilde{G}$ and $\widetilde{\chi}_1^0 \to Z\widetilde{G}$ modes are comparable in the relevant mass range, while for Model Line II $\widetilde{\chi}_1^0 \to Z\widetilde{G}$ dominates above the narrow transition region of mass.

Invisible decay of the Z gives rise to the signature $\gamma\not{E}_T$. This channel has been studied in Run I as a probe for anomalous γZ couplings with $Z \to \nu\nu$ [46,47]. The largest background in Run I was from single W production with $W \to e\nu$ and the electron misidentified as a photon. This background can be substantially reduced by raising the photon E_T and $\not{E}_T$ cuts beyond the Jacobian peak for $W \to \ell\nu$ [45]. This may be accomplished with the cuts

1. One photon with $p_T > 50$ GeV and $|\eta| < 2.0$.

2. $\not{E}_T > 50$ GeV.

Monte Carlo simulation indicates that only roughly 1% of $W \to e\nu$ decays have both an electron with $p_T > 50$ GeV and $\not{E}_T > 50$ GeV. With a total cross section $\sigma(p\bar{p} \to W) \simeq 6$ nb, a misidentification rate $\mathcal{P}(e \to \gamma) = 10^{-3}$, branching ratio $\mathrm{Br}(W \to e\nu) \simeq 11\%$, and assuming a photon acceptance of 0.8, this gives a $\gamma\not{E}_T$ background from this source of 5 fb after cuts. Additional backgrounds arise from γj and jj with one jet faking a photon *and* in each case the remaining jet energy mismeasured to be below the minimum pedestal. The Run I $\gamma\not{E}_T$ analysis [46,47] estimated < 45 fb from this source with a $\not{E}_T$ cut of 35 GeV. Raising the $\not{E}_T$ cut to 50 GeV given above should reduce this background to an insignificant level. A final source for background is muon bremsstrahlung from cosmic or beam halo muons. With the combination of larger $\not{E}_T$ cut, improved photon pointing, and for cosmic rays a larger signal to noise implied by larger instantaneous luminosity, it should be possible to reduce the background from this source, estimated to be 135 fb after cuts in the Run I $\gamma\not{E}_T$ analysis [46,47], by a factor of roughly 30 [45]. The total $\gamma\not{E}_T$ background with the above cuts is therefore estimated to be of order 10 fb. Note that with data, it should be possible to accurately characterize the $\gamma\not{E}_T$ backgrounds from these sources, as was the case in Run I. With the cuts given above the acceptance time efficiency for the signal in the $\gamma\not{E}_T$ channel (not including $\mathrm{Br}(Z \to \nu\nu) \simeq 0.20$) is found to be 0.5. With the estimated background given above, the reach for a 3σ observation with 2 (30) fb^{-1} of integrated luminosity should be 135 (165) GeV for the $\widetilde{\chi}_1^0$ mass along Model Line I, and 130 (145) GeV along Model Line II.

Hadronic decay of the Z in the $\gamma Z\not{E}_T$ mode gives rise to the signature $\gamma jj\not{E}_T$. Backgrounds are similar to those of the $\gamma\not{E}_T$ channel. The $\gamma jj\not{E}_T$ channel has been studied in Run I in order to place limits on squark and gluino masses in very specific supersymmetric models [48]. Further background suppressions not included in the Run I study are possible with acoplanarity, sphericity and invariant dijet mass cuts to reconstruct the Z boson, and a lepton veto. Although a detailed study has not been attempted, the total background is expected to be smaller than for the $\gamma\not{E}_T$ channel, due to the presence of two additional hard partons. Given the significant Z hadronic branching ratio, the $\gamma jj\not{E}_T$ channel should therefore provide somewhat better reach than the $\gamma\ell^+\ell^-\not{E}_T$ or $\gamma\not{E}_T$ channels in Run II.

For the parameters of Model Line II the $ZZ\not{E}_T$ di-boson mode dominates at larger $\tilde{\chi}_1^0$ mass as discussed at the beginning of Section V, and illustrated in Fig. 23. Leptonic decay of each Z boson gives rise to the spectacular signature $\ell^+\ell^-\ell'^+\ell'^-\not{E}_T$, with the lepton pairs reconstructing the Z mass (in one choice of pairing for $\ell = \ell'$). This gold plated channel is expected to be essentially background free, but suffers from small leptonic branching ratio. Because of this Run II with even 30 fb^{-1} of integrated luminosity will not be sensitive to the parameters of Model Line I in this channel. For Model Line II however, with the dominant $\widetilde{\chi}_1^0 \to Z\widetilde{G}$ decay mode, the reach for a 3σ observation with 30 fb^{-1} of integrated luminosity should approach 170 GeV for the $\widetilde{\chi}_1^0$ mass.

B Higgs Bosons from Higgsino Decay

The Higgs boson decay mode of a Higgsino-like neutralino NLSP, $\widetilde{\chi}_1^0 \to h\widetilde{G}$, presents the possibility of collecting SUSY events which contain a real Higgs boson. The most promising channels which include a Higgs boson are $h\gamma\not{E}_T$ and $hh\not{E}_T$ which yield the final state signatures $\gamma bj\not{E}_T$ discussed in sections V A 1 and V A 2 and $bbbj\not{E}_T$ discussed in section V A 3. It is then interesting to consider the reach in these channels as a general function of both the Higgsino and Higgs masses [36].

The total cross section times branching ratio contours for the $\gamma bb\not{E}_T$ and $bbbb\not{E}_T$ channels as a function of the h and $\tilde{\chi}_1^0$ masses are shown in Fig. 31. These contours include $\mathrm{Br}(\chi_1^0 \to (\gamma, h)\tilde{G})$ for $\tan\beta = 3$ and $\mu/M_1 = -3/4$ and SM values for $\mathrm{Br}(h \to bb)$. The Run IIa 3σ discovery reach with 2 fb^{-1} discussed in section V A 2 for the $\gamma bj\not{E}_T$ channel corresponds to a signal times branching ratio cross section of 6 fb. For the parameters of Fig. 31 this corresponds to a Higgs mass of up to at least 120 GeV for $\tilde{\chi}_1^0$ masses in the range 140-195 GeV, with a maximum reach in Higgs mass of just over 130 GeV. The Run IIa reach is indicated by the light shaded region in Fig. 31. This is to be contrasted with the search for the SM Higgs from direct Wh and Zh production. These SM channels are background limited, and no sensitivity to a Higgs mass beyond current limits is expected in Run IIa. So the $\gamma bj\not{E}_T$ channel presents the interesting possibility for Run IIa of a SUSY signal which contains real Higgs bosons. The Run IIb 3σ discovery reaches implied by the results of section V A 2 and V A 3 with 30 fb^{-1} of integrated for the $\gamma bj\not{E}_T$ and $bbbj\not{E}_T$ channels respectively correspond to signal times branching ratio cross sections of 1.5 fb and 4 fb respectively. For the parameters of Fig. 31 the maximum reach in Higgs mass then corresponds to almost 145 GeV and 115 GeV respectively. The Run IIa reach is indicated by the dark shaded region in Fig. 31.

In order to identify the Higgs boson directly in a sample of events arising from Higgsino decays it is necessary to observe a peak in the bb invariant mass. The identifiable di-boson final states and large $\not{E}_T$ carried by the

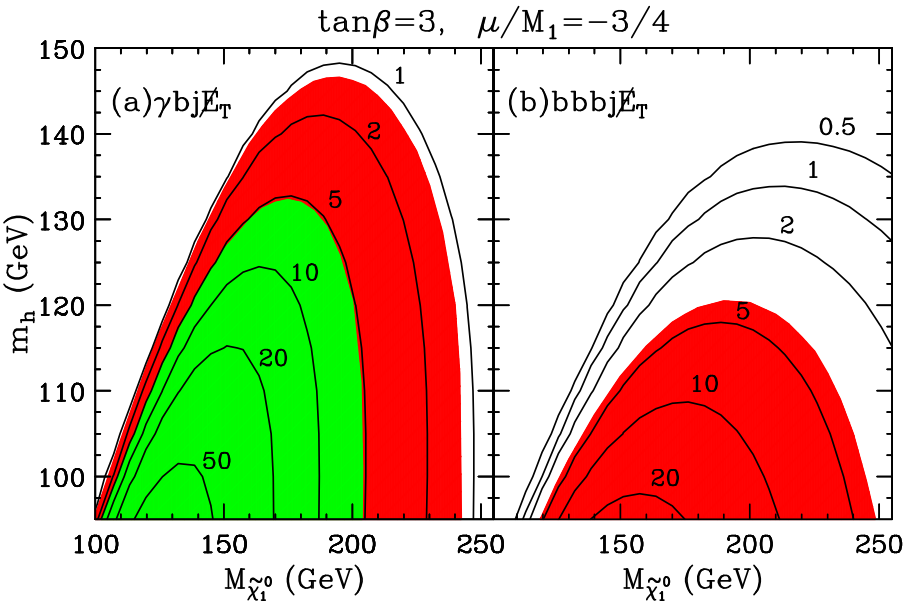

FIGURE 31. Signal cross-section times branching ratio contours in fb for the (a) $\gamma bb\not{E}_T$ and (b) $bbbb\not{E}_T$ channels, as a function of the neutralino mass $M_{\tilde{\chi}_1^0}$, and the Higgs mass m_h, for $\tan\beta = 3$ and $\mu/M_1 = -3/4$. The Run IIa(b) reach with 2(30) fb^{-1} of integrated luminosity is indicated in light(dark) region.

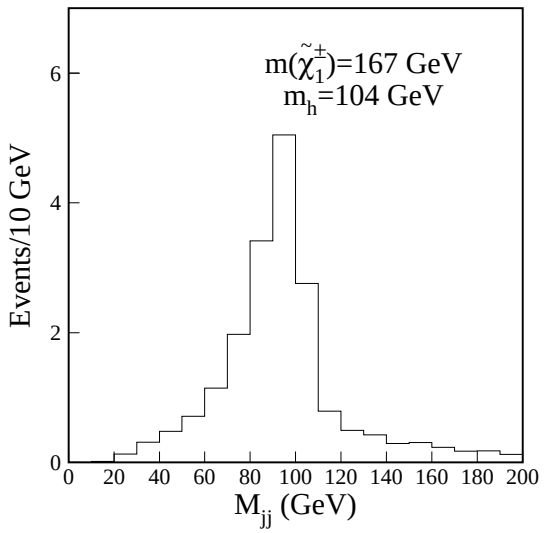

FIGURE 32. The invariant mass distribution of the two leading jets in the DØ $\gamma bj\not{E}_T$ analysis for the Model Point on the Higgsino-like Neutralino NLSP Model Line I with $m_{\tilde{\chi}_1^\pm} = 167$ GeV ($\Lambda = 80$ TeV) and with L = 2 fb^{-1}. Note that 19 signal and less than 1 background events are expected.

Goldstinos render the supersymmetric Higgs boson final states discussed here relatively clean. Reconstructing the Higgs mass peak should be relatively straightforward compared to SM Wh and Zh production modes which suffer from much larger continuum bb backgrounds. Fig. 32 shows the invariant mass distribution of the two leading jets in the DØ $\gamma bj\not{E}_T$ analysis described in section V A 2 for the Model Point on the Higgsino-like

Neutralino NLSP Model Line I with $m_{\tilde{\chi}_1^\pm} = 167$ GeV ($\Lambda = 80$ TeV) and with L = 2 fb^{-1}.

C Non-Prompt Decays to Higgs and Z Bosons

The decay length for $\widetilde{\chi}_1^0 \to (h, Z, \gamma)\widetilde{G}$ may be macroscopic, as illustrated in Fig. 2. Decay over a macroscopic distance, but within the detector volume gives displaced hard partons with finite impact parameter. Detection of displaced hard photons is discussed in section IV B.

Decays of a metastable Higgsino-like neutralino with macroscopic decay length by $\widetilde{\chi}_1^0 \to h\widetilde{G}$ with $h \to bb$ or $\widetilde{\chi}_1^0 \to Z\widetilde{G}$ with the Z decaying hadronically give rise to large E_T displaced jets with finite impact parameter and large $\not{E}_T$. Since the metastable $\widetilde{\chi}_1^0$ is non-relativistic the jets from h or Z decay have a roughly uniform angular distribution in the lab frame. This is in contrast to potential high E_T displaced jet background from heavy quark decay, which is highly boosted in the direction of motion of the relativistic heavy quark. So the angular distribution of displaced high E_T jets can greatly aid in reducing background. A useful selection criterion in this regard is the large negative impact parameter (LNIP) described in section VIII B in the context of NLSP squark decay. LNIPs select displaced jets which are emitted towards rather than away from the beam axis. Also note that since each h or Z decays to a pair of jets, the displaced jets should reconstruct displaced vertices in pairs from the point of each h or Z decay. Such pairs of displaced jets have an invariant mass appropriate to the h or Z, which could also be used as a further cut.

Decays of a neutralino with macroscopic decay length contained within the tracking region by $\widetilde{\chi}_1^0 \to Z\widetilde{G}$ with $Z \to \ell\ell$ where $\ell = e, \mu$ presents the possibility of very cleanly reconstructing the displaced Z. First, the $\ell\ell$ vertex can be accurately determined using tracking. Second the $\ell\ell$ invariant momentum can also be required to reconstruct the Z very accurately. Based in part on the possibility of observing a metastable neutralino which decays to a Z boson, CDF has carried out a search for displaced $Z \to ee$ decays in Run I [49]. Although the production cross section is too small to have been observed in Run I, as discussed in section V A 4 some channels with a leptonic Z could be observed in Run II. The search for displaced Z bosons should therefore be extended to Run II.

It is important to note that the backgrounds for any of the final state signatures for a Higgsino-like neutralino NLSP described in the previous section are greatly reduced if the $\widetilde{\chi}_1^0$ decay is displaced but contained within the tracking region. A search for Non-prompt Higgsino-like neutralino decays can therefore be implemented simply by applying an LNIP or displaced leptonic Z search to an event sample derived from any of the searches described in the previous sections on prompt decays. This interesting combination of analysis for these spectacular signatures should not be overlooked in Run II. In the case of metastable $\widetilde{\chi}_1^0 \to h$ decays with $h \to bb$, this would yield a very interesting sample of Higgs bosons.

VI STAU NLSP

A stau NLSP arises if the sleptons are lighter than the other MSSM superpartners and if the stau is more than 1.8 GeV lighter than the selectron and smuon, so that these states eventually cascade decay to $\widetilde{\tau}_1$, as discussed below. A stau NLSP decays to the Goldstino by

$$\widetilde{\tau}_1 \to \tau\widetilde{G} \tag{6.1}$$

If the supersymmetry breaking scale $\sqrt{F}$ is sufficiently low, then the decay 6.1 occurs promptly, and all supersymmetric events contain at least two high-p_T τ's. Since the decays into the $\widetilde{\tau}_1$ NLSP also typically contain τ's, the predicted events can quite often have three or even four τ leptons [4,15,16]. They can be manifested either in purely leptonic or hadronic channels. Since the heavy $\widetilde{\tau}_1$ decays to two essentially massless particles, these events will have high $\not{E}_T$ and the leptons or jets from the τ's will typically have high p_T. Furthermore, the other leptons and jets produced in the supersymmetric decay chains can have quite distinctive profiles.

If the supersymmetry breaking scale is larger, the $\widetilde{\tau}_1$ is very long-lived. It is then appears as a weakly interacting, massive, slowly-moving charged particle so it has unique characteristics. It will appear as a high-E_T track that penetrates the calorimeters and the muon system. If it is moving slowly enough, it will leave significantly more dE/dx energy than a minimum–ionizing particle. In the GMSB models, we expect two of these objects in each SUSY event, leading to a variety of spectacular signals [4,50,51]. We can consider

triggering in several ways. The first is the $\widetilde{\tau}_1$ as a muon, since it will likely be a high-E_T track that is weakly interacting so it can traverse the muon chambers. In this case there are two possible failure modes: the particle is moving too slow to reach the muon system within the timing gate, or the event is rejected because a MIP calorimeter energy cut is placed on the muon trigger track. The second trigger is a simple requirement on high-E_T isolated tracks as mentioned in the discussion of two prompt τ's. Finally, these triggers are necessary for the direct production of the sleptons, but the trigger could require the objects from cascade decays of heavier sparticles. Off-line the events can also be detected several ways. First, since they can appear as muons, they can be detected simply as an excess of muons. Since most of the $\widetilde{\tau}_1$'s will have excessive dE/dx, they can potentially be detected in any detector that records dE/dx. Finally they can be detected as slow particles by detectors with timing information.

For intermediate values of $\sqrt{F}$, the stau decays can occur inside the detector but at a macroscopic distance. In that case, the impact parameter of the stau from the interaction region or the kink in the charged particle track when the decay occurs can yield a unique signal and provide information about the decay length. Note that the decay width formula essentially depends only on the stau mass (which kinematic information can reveal) and the supersymmetry breaking order parameter $\sqrt{F}$. So measuring the physical decay length of the charged staus in this scenario may yield direct information or constraints on the supersymmetry breaking mechanism.

In the stau NLSP scenario, the heavier sleptons $\widetilde{e}_R$ and $\widetilde{\mu}_R$ must have allowed three-body decays

$$\widetilde{e}_R \to e\,\tau^{\pm}\widetilde{\tau}_1^{\mp} \qquad \text{and} \qquad \widetilde{\mu}_R \to \mu\tau^{\pm}\widetilde{\tau}_1^{\mp}. \tag{6.2}$$

These decays have been studied in some detail in Ref. [6]. The charges of the final-state τ and $\widetilde{\tau}_1$ NLSP are largely uncorrelated with the charge of the decaying slepton. This means that production of the heavier sleptons, either directly or in other sparticle decays, tends to produce a pair of final-state stau NLSPs with the same charge almost half of the time. This is also true for any supersymmetric events which involve a neutralino, either as one of the initially produced particles, or as part of the decay chain. This is because of the Majorana nature of neutralinos, which requires that they decay democratically into final states with $\tau^+\widetilde{\tau}_1^-$ and $\tau^-\widetilde{\tau}_1^+$. This observation, that many or most supersymmetric events feature like-charge staus in the final stage of the decay chain before $\widetilde{\tau}_1 \to \tau\widetilde{G}$, may be useful for defining reduced-background signals. Furthermore, the ratio of same-charge vs. opposite-charge stau events (particularly the deviation of this ratio from 1) can be an important observable in disentangling the model parameters from the data.

It is also worth noting that the three-body decays eq. (6.2) may also have a macroscopic length in the lab frame, if the total mass difference between initial and final states is less than about 1 GeV. This can occur for $\tan\beta$ in the range from 5 to 10, depending of course on the other model parameters. In this case, the τ and e or μ will be extremely soft and could be missed. This results in an interesting signal of a charge-changing HIT (CC-HIT), with the decaying slepton or smuon track turning into a stau track with the opposite charge about half the time.

For quantitative studies, we follow the general strategy outlined in Section II and define a Stau NLSP Model Line. The fixed parameters that define this Model Line are:

$$\text{Stau NLSP Model Line}: \qquad N = 2,\ \frac{M_m}{\Lambda} = 3,\ \tan\beta = 15,\ \mu > 0, \tag{6.3}$$

with Λ allowed to vary. In Fig. 33, we show the masses of the lightest few superpartners and the lightest CP-even Higgs boson h^0, as a function of 34 TeV $< \Lambda <$ 85 TeV. The relevant sparticle masses scale almost linearly with Λ. Note that $m_{\widetilde{e}_R} - m_{\widetilde{\tau}_1}$ and $m_{\widetilde{\mu}_R} - m_{\widetilde{\tau}_1}$ are greater than a few GeV for all points along this Model Line, so that all sparticles do indeed have kinematically-allowed decays to the stau NLSP. Therefore, the possible general types of experimental signatures are:

- Small C_G with prompt NLSP decays:
  Events with 2 or 3 or more high-p_T τ's, often with additional leptons and jets.

- Intermediate C_G with delayed NLSP decays:
  Events with $\widetilde{\tau}_1 \to \tau$ decay kinks.

- Large C_G with a quasi-stable NLSP:
  Events with heavy charged particle tracks featuring anomalous ionization rate or time-of-flight from slow staus, and/or fake "muons" from fast staus.

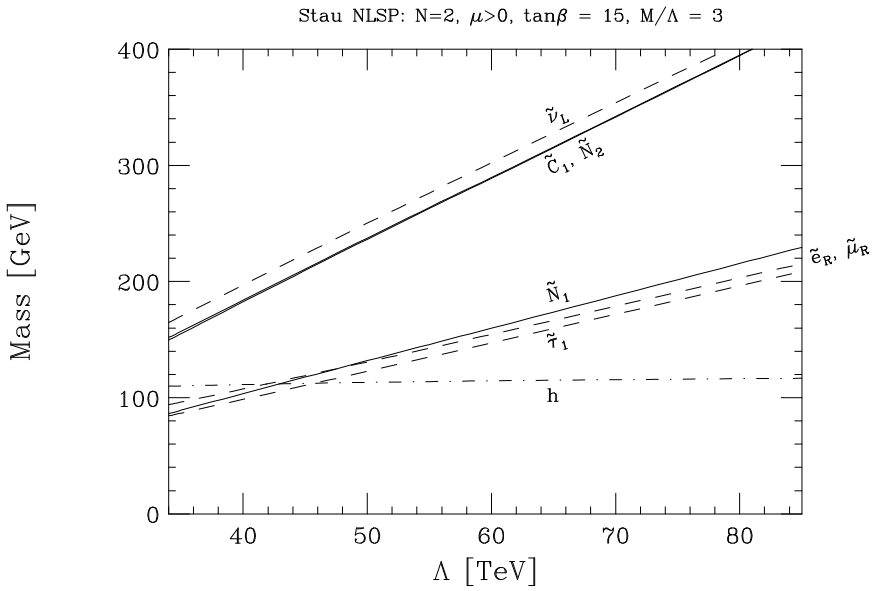

FIGURE 33. The masses of the lightest neutralinos, charginos, sleptons and CP-even Higgs boson in the Stau NLSP Model Line, as a function of Λ.

In Figure 34, we show the most important Run II production cross-sections for superpartners in this model, including $\tilde{\chi}_1^+\tilde{\chi}_1^-$, $\tilde{\chi}_1^\pm\tilde{\chi}_1^0$, $\tilde{e}_R^+\tilde{e}_R^-$, $\tilde{\mu}_R^+\tilde{\mu}_R^-$, and $\tilde{\tau}_1^+\tilde{\tau}_1^-$, as well as the total inclusive cross-section for all supersymmetric particles, as a function of $m_{\tilde{\chi}_1^\pm}$ and $m_{\tilde{\tau}_1}$.

Again, $\tilde{\chi}_1^+\tilde{\chi}_1^-$ and $\tilde{\chi}_1^\pm\tilde{\chi}_2^0$ dominate the production cross section for $\Lambda \lesssim 75$ TeV, corresponding to $m_{\tilde{\tau}_1} \lesssim 185$ GeV and $m_{\tilde{\chi}_1^\pm} \lesssim 370$ GeV. For larger Λ values, $\tilde{\tau}_1^+\tilde{\tau}_1^-$, $\tilde{e}_R^+\tilde{e}_R^-$, and $\tilde{\mu}_R^+\tilde{\mu}_R^-$ productions become relatively more important. Figures 35, 36, 37 and 38 show the most significant branching fractions for $\tilde{\chi}_1^\pm$, $\tilde{\chi}_2^0$, $\tilde{\chi}_1^0$ and $\tilde{e}_R$. As an example, branching ratios of $\tilde{\chi}_1^\pm$ and $\tilde{\chi}_2^0$ for $\Lambda = 40$ TeV are graphically displayed in Fig. 39. In the following, signatures for short-lived and for quasi-stable $\tilde{\tau}_1$'s will be discussed. It should be noted that the two analyses discussed below also have some sensitivity to the case with an intermediate $\tilde{\tau}_1$ lifetime.

A CDF study of Stau NLSP Model Line with prompt $\tilde{\tau}_1$ decay

Prompt τ decays can be investigated though the $\ell\nu\nu$ leptonic decays (17% each for e or μ), where they often contribute to the efficiency in leptonic analyses. The other approach is to search for the one– (50%) or three– (15%) charged–hadron decays (which can contain additional neutrals) [52]. For these "hadronic" τ's, the signature is the one or three charged tracks, isolated from other tracks, but associated with a calorimeter energy cluster with a narrow width. The tracks must be within 10° of the jet centroid and no other tracks are within 30°. The probably that a randomly–selected jet pass these cuts is on the order of 1%. Note that this fake rate is, in general, too large to search for τ decays in a data sample dominated by jets. If selection criteria are imposed on other parts of the event, then a good signal to noise can be achieved. Note that a selection of a leptonically–decaying τ selected with a hadronically–decaying τ has greater rejection than either two leptons or two hadronic τ's because QCD and Drell–Yan can be more effectively suppressed.

CDF has searched for the signature of two prompt τ's and $\not\!\!E_T$ in the context of a search for top decays to the charged Higgs which in turn decays to $\tau\nu$ [53,52]. The data set was collected through the $\not\!\!E_T$ trigger. The primary analysis cuts were $\not\!\!E_T > 30$ GeV, two hadronically decaying τ's with $E_T > 30$ GeV and $|\eta| < 1$, and the τ's must not be back–to–back, to remove Z decays. In 100 pb^{-1}, no events were observed while 2.2 ± 1.3 where expected from Standard Model sources, mostly $W \to \tau\nu$ with a jet faking the second τ.

Projecting this result in a straightforward way, we expect 40 events in 2 fb^{-1} or a limit of 13 events at 95% C.L. or 32 events at 5σ. Using SHW, we find 3.6% for the efficiency for a nominal model point along the Stau NLSP Model Line which has $M_{\tilde{\chi}_1^\pm}$ =193 GeV and $m_{\tilde{\tau}_1}$ =103 GeV; see Table 13. Due to the low efficiency for the τ's we do not expect to be very sensitive to this model. We might be able to set a limit on the $\tilde{\tau}_1$ near

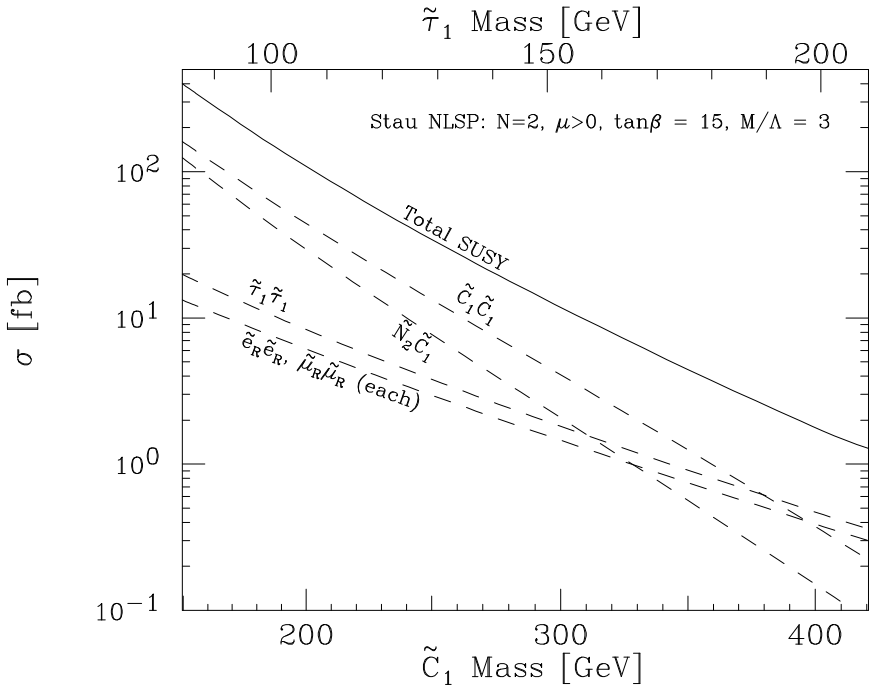

FIGURE 34. Production cross-sections in $p\overline{p}$ collisions with $\sqrt{s} = 2$ TeV, for superpartner pairs in the Stau NLSP Model Line, as a function of $m_{\tilde{\chi}_1^\pm}$ and $m_{\tilde{\tau}_1}$.

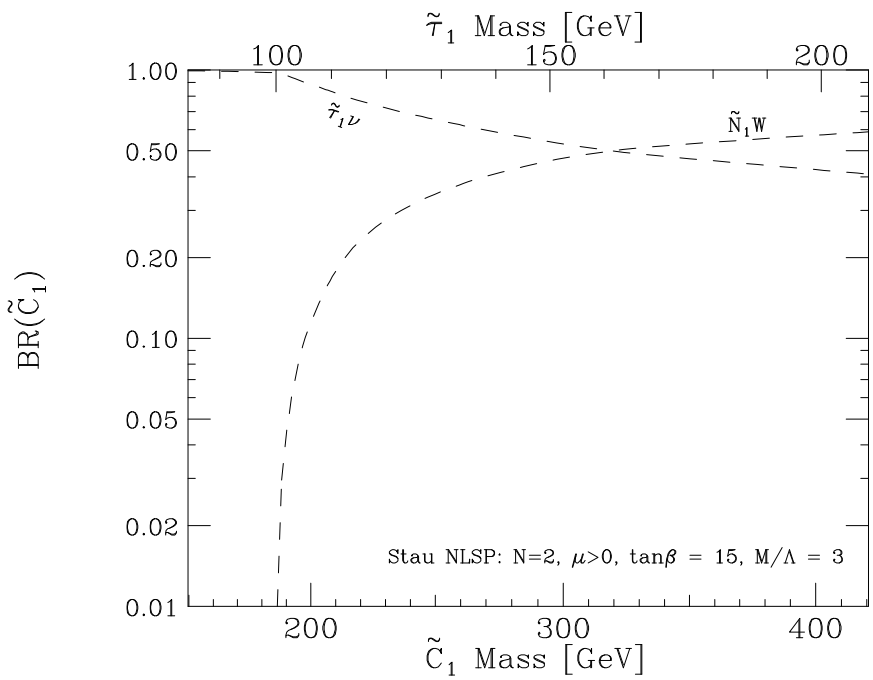

FIGURE 35. Branching fractions for the decay of $\tilde{\chi}_1^\pm$ in the Stau NLSP Model Line, as a function of $m_{\tilde{\chi}_1^\pm}$ and $m_{\tilde{\tau}_1}$.

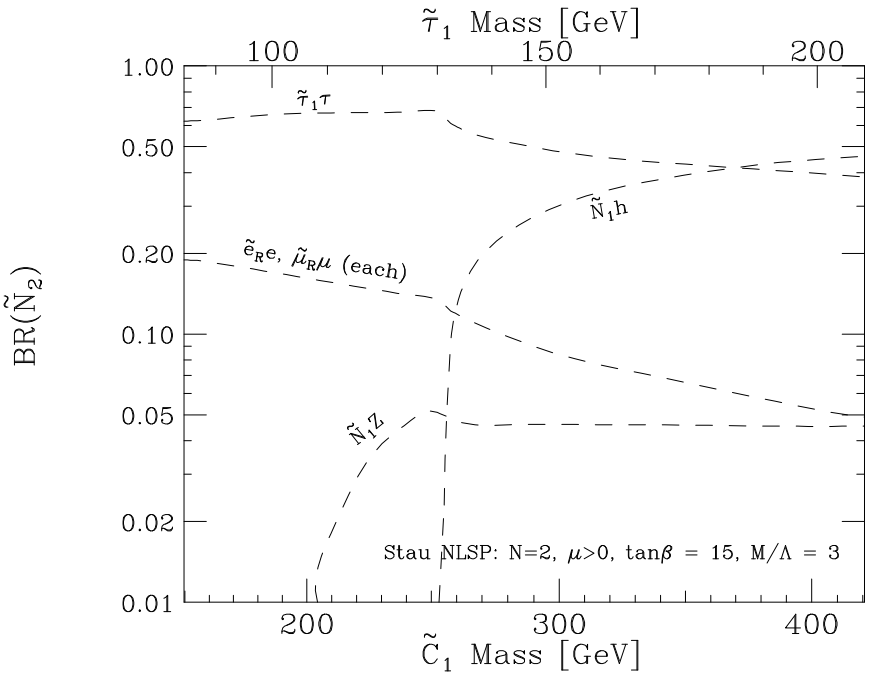

FIGURE 36. Branching fractions for the decay of $\widetilde{\chi}_2^0$ in the Stau NLSP Model Line, as a function of $m_{\tilde{\chi}_1^\pm}$ and $m_{\tilde{\tau}_1}$.

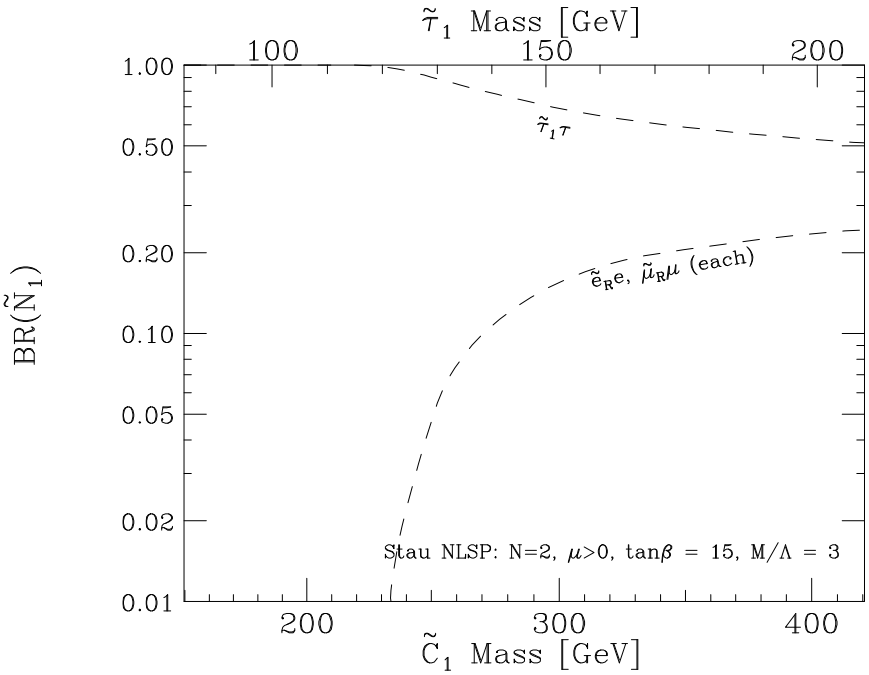

FIGURE 37. Branching fractions for the decay of $\widetilde{\chi}_1^0$ in the Stau NLSP Model Line, as a function of $m_{\tilde{\chi}_1^\pm}$ and $m_{\tilde{\tau}_1}$.

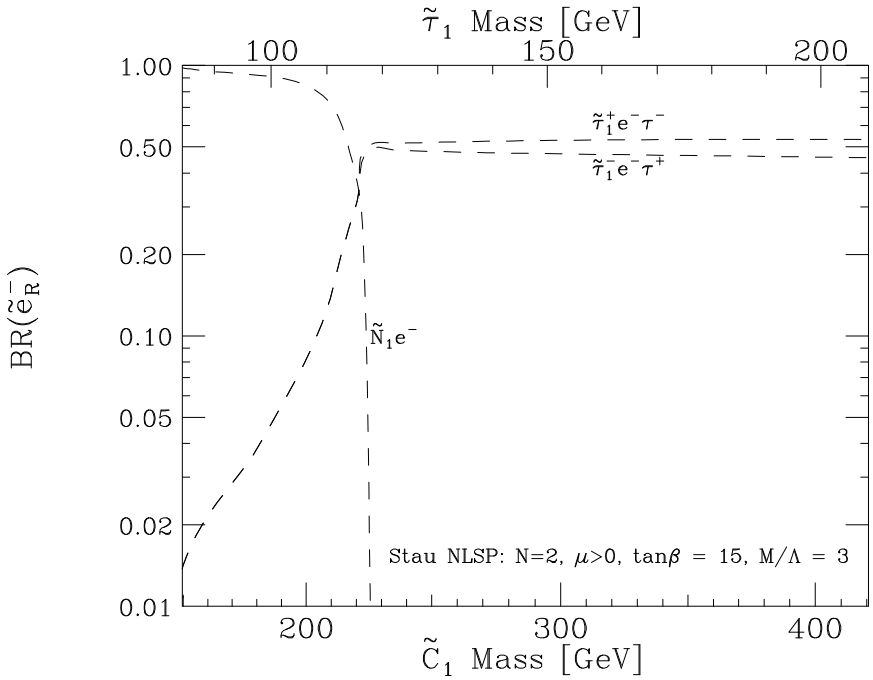

FIGURE 38. Branching fractions for the decay of $\tilde{e}_R^-$ or $\tilde{\mu}_R^-$ in the Stau NLSP Model Line, as a function of $m_{\tilde{\chi}_1^\pm}$ and $m_{\tilde{\tau}_1}$.

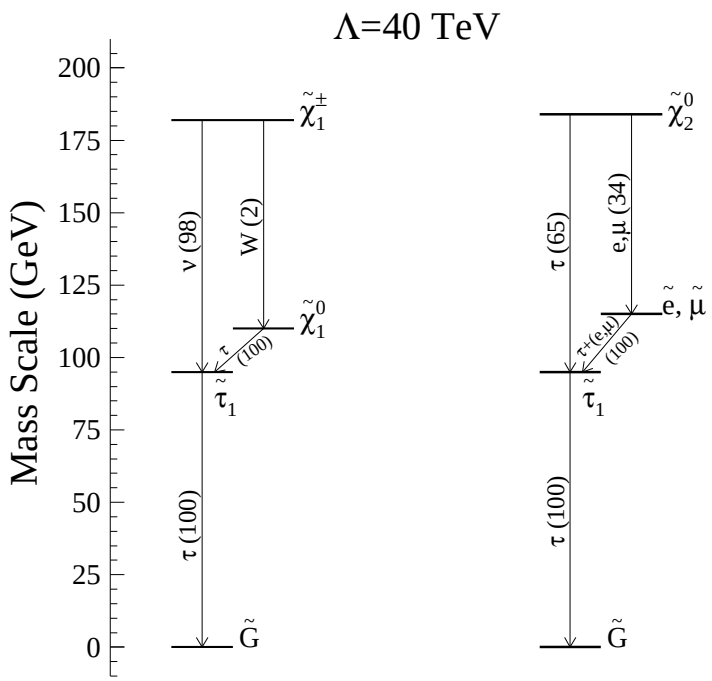

FIGURE 39. Decay schematics of $\tilde{\chi}_1^\pm$ and $\tilde{\chi}_2^0$ for $\Lambda = 40$ TeV for the Model Line with a $\tilde{\tau}_1$ as the NLSP. Percentage branching ratios for main decay modes are shown in parentheses. (The $\tilde{\tau}_1$, $\tilde{e}_R$, $\tilde{\mu}_R$ and $\tilde{\chi}_1^0$ mass levels have been displaced slightly for labelling purposes.)

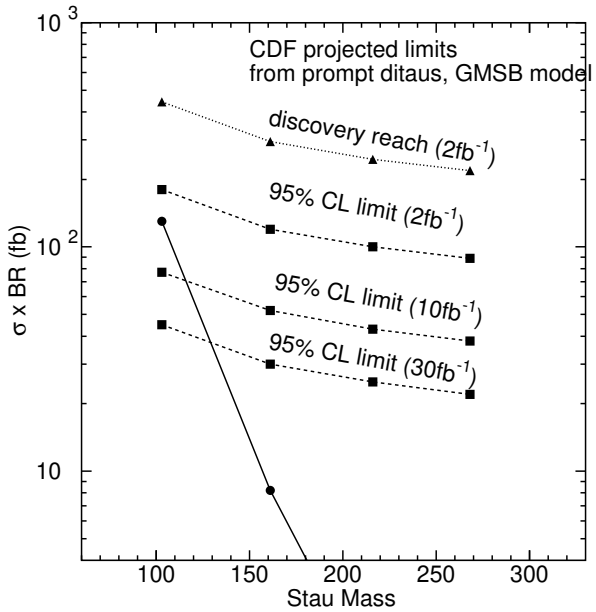

FIGURE 40. The limit on cross section times branching ratio from the CDF analysis of two τ's and $\not\!\!E_T$ applied to the Stau NLSP Model Line in Run II. The solid line is the theoretical cross-section.

100 GeV for 2 fb^{-1}, similar to the sensitivity of the final LEP configuration. For 30 fb^{-1}, we estimate we have a limit sensitivity near 130 GeV and possibly a discovery sensitivity in the region of 100 GeV. These results are shown in Figure 40.

TABLE 13. The summary of the Monte Carlo points used to investigate projected limits on the Stau NLSP Model Line for Run II (2 fb^{-1}) in the CDF study. Every event has two $\widetilde{\tau}_1$'s which decay promptly to $\tau\widetilde{G}$.

Λ (TeV)	42	66	88	109
$m_{\widetilde{\chi}_1^\pm}$ (GeV)	193	321	436	544
$m_{\widetilde{\chi}_1^0}$ (GeV)	109	176	237	296
$m_{\widetilde{\tau}_1}$ (GeV)	103	161	216	268
$\sigma\times$BR (fb)	130	8.2	1.1	.22
$A\cdot\epsilon$ (%)	3.6	5.4	6.5	7.3
$\sigma\times$BR 95% C.L. limit (fb)	180	120	100	89

This projection is based on data from a $\not\!\!E_T$ trigger and one of the obvious potential improvements is to trigger on the τ's directly. Although we don't expect much more sensitivity from reducing the $\not\!\!E_T$ requirements in this model, other searches, such as $H^\pm \to \tau\nu$ and $A \to \tau^+\tau^-$, might take advantage of this capability. In addition we are attempting to be sensitive to as many signatures as possible, with or without models.

A preliminary look at this trigger is shown in Figure 41. This Figure displays the rejection for min-bias events and efficiency for the nominal point for this gauge-mediated model ($m_{\widetilde{\tau}1}$ =103 GeV). The requirements are placed on the L1 calorimeter trigger. For each trigger tower (twice as large in η as a physical tower), this trigger compares tracks, found in the $r-\phi$ plane, to either the EM or total tower energies. We have plotted the rejection and efficiency versus the tower energy requirement for different cases of minimum track p_T. We

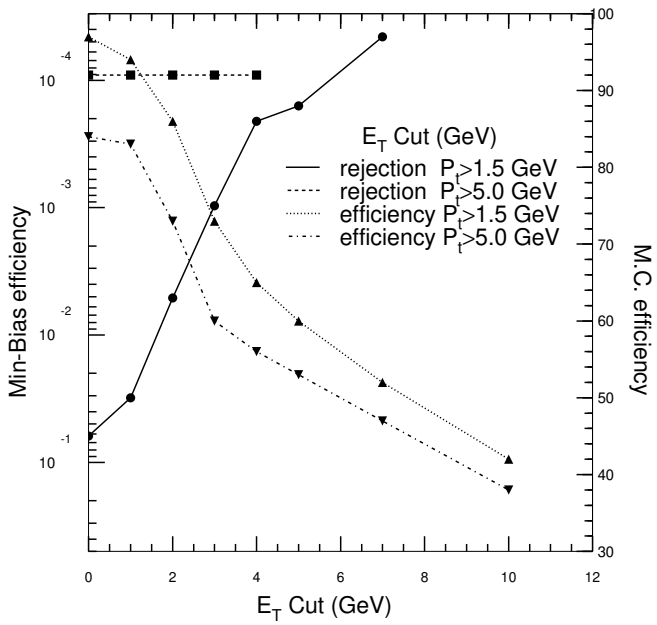

FIGURE 41. The rejection for CDF min–bias events and the efficiency for the nominal stau model point ($m_{\tilde{\tau}_1} = 103$ GeV). The requirements are two trigger ϕ sectors with the indicated requirements on minimum track p_T and trigger tower E_T. For a successful level 1 trigger, the rejection should be on the order of 2×10^{-4}.

require two ϕ sectors pass the cuts (indicating two τ's are present). The L1 trigger must be a few percent of the level 1 trigger rate to be acceptable, so the rejection should be near 2×10^{-4}. We find we can achieve this rejection with the requirement of two towers with $E_T > 6$ GeV, each associated with tracks with $p_T > 1.5$ GeV. Raising the p_T requirement does not improve the rejection rapidly. These cuts are approximately 50% efficient for the gauge-mediated model.

Work is underway to understand how to achieve the needed rejection at trigger level 2. At this level we have the additional ability to require that the jet is "thin", which is characteristic of τ's. We can require the tracks are isolated from other tracks in the event, and that the τ candidates are not back–to–back, reducing the QCD background. We anticipate being able to keep the track and tower thresholds near the L1 thresholds.

Further studies show that a single τ trigger will be significantly more difficult. Here we find we approach the required rejection with tower E_T cuts of approximately 12 GeV, and the track requirement doesn't improve the rejection.

A more inclusive trigger is to simply require two tracks above a p_T threshold. This trigger could not only find more di-τ's, it could find the long-lived $\tilde{\tau}_1$'s (or, for example, $\tilde{t}_1$'s) which do not trigger the muon system. We find we can achieve the necessary rejection when we require two tracks with $p_T > 5$ GeV. At trigger level 2, we will need to require that the tracks are well–isolated. Work to plan these triggers is continuing.

B DØ study of Stau NLSP Model Line with prompt $\tilde{\tau}_1$ decays

If the $\tilde{\tau}_1$ is short-lived and decays in the vicinity of the production vertex (*i.e.* with a decay distance $\gamma c\tau \lesssim 10$ cm), anomalous τ production will provide a visible signal in the DØ detector. Combining the $\tilde{\tau}_1 \to \tau\tilde{G}$ decays with the W^*/Z^* productions from the cascade decays of primary supersymmetric particles, these events will give rise to $\ell\ell\ell j\not{E}_T$ and $\ell^\pm\ell^\pm jj\not{E}_T$ final states from leptonic τ decays.

DØ searched for gaugino pair production using the tri-lepton signature [54] in Run I. The lepton p_T cut was typically 15 GeV for the leading lepton and 5 GeV for the non-leading leptons. The analysis also had a small $\not{E}_T$ requirement. The observable background cross section was estimated to be around 13 fb. Most of these backgrounds are due to Drell-Yan processes. We select the $\ell\ell\ell j\not{E}_T$ events using the following criteria:

1) $p_T^{\ell_1} > 15$ GeV, $p_T^{\ell_2} > 5$ GeV, $p_T^{\ell_3} > 5$ GeV;

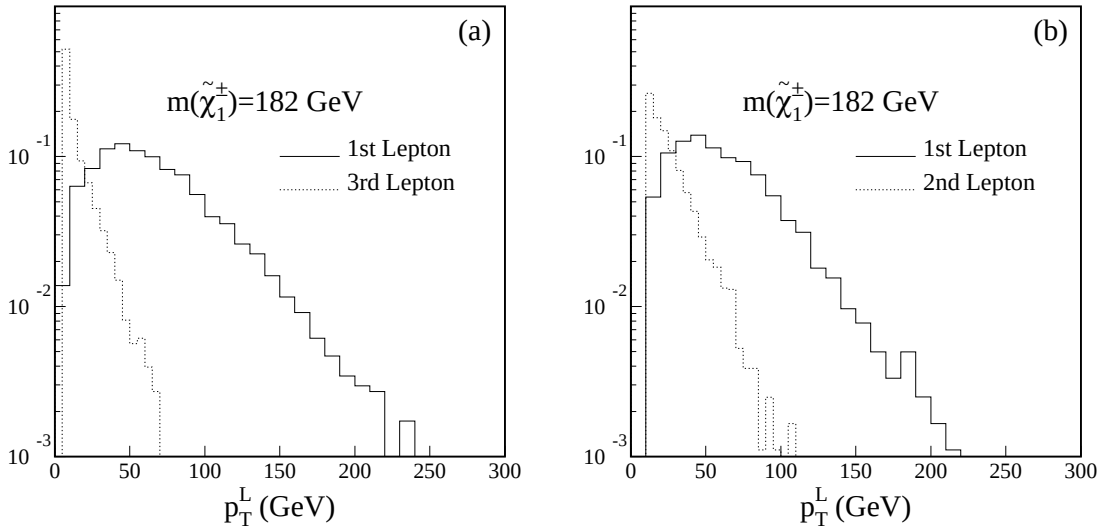

FIGURE 42. Lepton p_T distributions for (a) the $\ell\ell\ell j\not{E}_T$ events and (b) the $\ell^{\pm}\ell^{\pm}jj\not{E}_T$ events of the models with a short-lived $\tilde{\tau}_1$ for $m_{\tilde{\chi}_1^{\pm}} = 182$ GeV ($\Lambda = 40$ TeV) in the DØ study of the Stau NLSP Model Line. All distributions are normalized to unit area.

2) $\not{E}_T > 20$ GeV;

3) At least one jet with $E_T^j > 20$ GeV.

The Drell-Yan production, a major background source for the Run I analysis, is significantly reduced by the new jet requirement. The total observable background cross section is estimated to be 0.3 fb assuming background reduction factors of 10 from the jet requirement, 2 from the improved particle identification, 2 from the higher $\not{E}_T$ cut.

Same-charge di-lepton events are expected from a variety of processes which produce slepton pairs either directly or in decays, or in any processes which produce Majorana fermions such as neutralino pair or gluino pair production. They are also expected from processes with three or more leptons in the final states, but only two are identified. This final state is expected to have small backgrounds. Again without a magnetic tracker, DØ had no analysis of this nature in Run I. Based on Monte Carlo studies for several supersymmetric models, we select $\ell^{\pm}\ell^{\pm}jj\not{E}_T$ events using the following criteria:

1) Two same-charge leptons with $p_T^{\ell} > 15$ GeV;

2) At least two jets with $E_T^j > 20$ GeV;

3) $\not{E}_T > 25$ GeV.

Events with three or more identified leptons are removed to make the sample orthogonal to the $\ell\ell\ell j\not{E}_T$ sample. Since leptons are relatively soft in p_T for the new physics model we investigated using this selection, the effect of charge confusion due to a limited tracking resolution is neglected in this study. The major backgrounds are: $W +$ jets events with one of the jets misidentified as a lepton, $t\bar{t}$ events with energetic leptons from b-quark decays, and Drell-Yan (WZ, ZZ) events. The $W +$ jets background is estimated using the number of $W + 3j$ events observed in Run I, folded with $\mathcal{P}(j \to \ell)$, to be 0.2 fb. The $t\bar{t}$ and Drell-Yan backgrounds are estimated using Monte Carlo to be 0.1 and 0.1 fb respectively. Adding the three background sources together yields a total observable background cross section of 0.4 fb.

The lepton p_T distributions of the $\ell\ell\ell j\not{E}_T$ and $\ell^{\pm}\ell^{\pm}jj\not{E}_T$ events are shown in Fig. 42. Since most leptons are produced in τ decays, their p_T's are relatively soft. Table 14 shows the efficiencies of the $\ell\ell\ell j\not{E}_T$ and $\ell^{\pm}\ell^{\pm}jj\not{E}_T$ selection criteria for these events along with the theoretical cross sections, $\tilde{\chi}_1^{\pm}$ and $\tilde{\tau}_1$ masses. Note that the $\ell\ell\ell j\not{E}_T$ and $\ell^{\pm}\ell^{\pm}jj\not{E}_T$ criteria are orthogonal. The efficiencies are relatively small largely due to the small branching ratio of the events to tri-leptons. We note that the total efficiencies shown in the table are somewhat

conservative. They do not take into account the migration of the $\ell\ell\ell j\not{E}_T$ events to the $\ell^\pm\ell^\pm jj\not{E}_T$ events due to inefficiency in the lepton identification. The 5σ discovery curves are shown in Fig. 43. The lighter chargino with mass up to 160 and 230 GeV can be discovered for $\mathcal{L}$=2, 30 fb^{-1}.

TABLE 14. The $\tilde{\chi}_1^\pm$ and $\tilde{\tau}_1$ masses, theoretical cross sections, detection efficiencies of $\ell^\pm\ell^\pm jj\not{E}_T$ and $\ell\ell\ell j\not{E}_T$ selections, and significances for different values of Λ for the models with a short-lived $\tilde{\tau}_1$ as the NLSP in the DØ analysis. The relative statistical error on the efficiency is typically 25%. The combined $\ell^\pm\ell^\pm jj\not{E}_T$ and $\ell\ell\ell j\not{E}_T$ background cross section is assumed to be 0.7 fb with a 20% systematic uncertainty.

Λ (TeV)	20	40	60	80
$m_{\tilde{\chi}_1^\pm}$ (GeV)	72	182	289	394
$m_{\tilde{\tau}_1}$ (GeV)	54	99	147	196
σ_{th} (fb)	5800	149	14.4	2.1
$\ell^\pm\ell^\pm jj\not{E}_T$ ϵ (%)	–	0.6	1.0	1.3
$\ell\ell\ell j\not{E}_T$ ϵ (%)	0.5	1.0	1.6	2.0
Total ϵ (%)	0.5	1.6	2.6	3.3
$N_s/\delta N_b$ (2 fb^{-1})	48	4.0	0.6	0.1
$N_s/\delta N_b$ (30 fb^{-1})	140	12	1.8	0.3

It is often assumed that this analysis should benefit from a τ identification. However, it is not clear that it will have a dramatic impact on the reach in the supersymmetry parameter space. Though a τ identification could improve the efficiency for the signal, it will undoubtedly come with large backgrounds. Nevertheless, a τ identification is essential to narrow down theoretical models if an excess is observed in the tri-lepton final state.

C ISAJET study of Stau NLSP Model Line with prompt $\tilde{\tau}_1$ decays

Tevatron signals for the Stau NLSP Model Line parameters (6.3) have also been simulated using ISAJET [17]. In this study, we only consider $\Lambda \geq 35$ TeV. [For $\Lambda \lesssim 34$ TeV, $\tilde{\chi}_1^0 \to \tau\tilde{\tau}_1$ is kinematically forbidden, and $\tilde{\chi}_1^0$ would decay via the four body decay $\tilde{\chi}_1^0 \to \nu_\tau\tilde{\tau}_1 W^*$ (which is not yet included in ISAJET) or via its photon mode considered above.] Gluinos and squarks are then too heavy to be produced at the Tevatron, and sparticle production is dominated by chargino, neutralino and slepton pair production. We expect that SUSY events will contain tau leptons from sparticle cascade decays which are expected to result in a tau slepton which then decays via $\tilde{\tau}_1 \to \tau\tilde{G}$. The observability of SUSY realized as in this scenario thus will benefit from the capability of experiments to identify hadronically decaying tau leptons, and further, to distinguish these from QCD jets. We classify SUSY events by the number of identified taus, and further separate them into jetty and clean event topologies labeled by the number of isolated leptons (e and μ). It should be remembered that the efficiency for identifying taus is expected to be smaller than for identifying photons. First, the tau has to decay hadronically, and then the hadronic decay products have to form a jet.

We simulate this scenario using the toy ISAJET calorimeter described above. To model the experimental conditions at the Tevatron the toy calorimeter package ISAPLT is interfaced with ISAJET. The particle identifications used in ISAPLT for photons, jets, electrons, and muons, are described in section IV A 3. In addition, τ's are identified as narrow jets with just one or three charged prongs with $p_T > 2$ GeV within 10° of the jet axis and no other charged tracks in a 30° cone about this axis. The invariant mass of these tracks is required to be $\leq m_\tau$ and the net charge of the three prongs required to be ± 1. QCD jets with $E_T = 15(\geq 50)$ GeV are misidentified as taus with a probability of 0.5% (0.1%) with a linear interpolation in

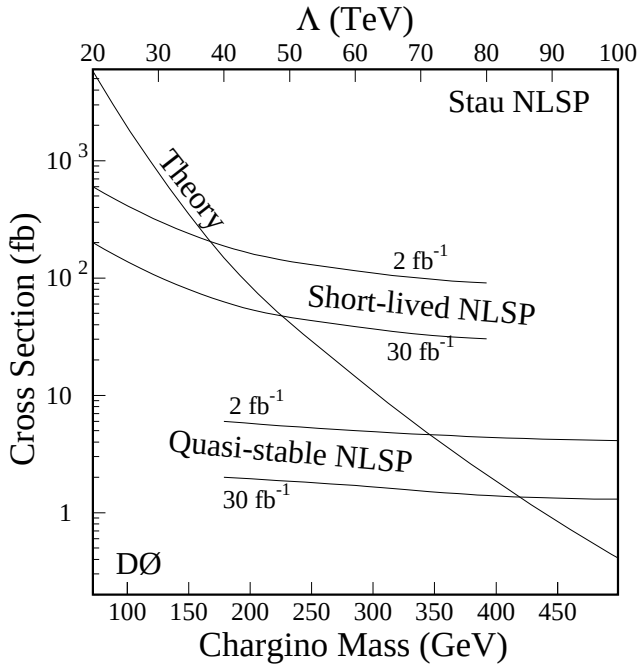

FIGURE 43. The DØ 5σ discovery cross section curves as functions of mass of the lighter chargino and the supersymmetry breaking scale Λ for the Stau NLSP Model Line, along with the theoretical cross sections. The 5σ curves are shown for both short-lived NLSPs (combining $\ell^\pm\ell^\pm jj\not{E}_T$ and $\ell\ell\ell j\not{E}_T$ selections) and quasi-stable NLSP's ($\ell\ell + dE/dx$ selection) and for integrated luminosities of 2, 30 fb^{-1}.

between. In our analysis, we require $\not{E}_T \geq 30$ GeV together with at least one of the following which serve as a trigger for the events:

- one lepton with $p_T(\ell) \geq 20$ GeV,
- two leptons each with $p_T(\ell) \geq 10$ GeV,
- $\not{E}_T \geq 35$ GeV.

The dominant physics sources of SM backgrounds to n-jet + m-leptons + $\not{E}_T$ events, possibly containing additional taus, are W,γ^* or Z + jet production, $t\bar{t}$ production and vector boson pair production. Instrumental backgrounds that we have attempted to estimate are $\not{E}_T$ from mismeasurement of jet energy and mis-identification of QCD jets as taus.

In addition to our basic requirements above, we also impose:

- a veto on opposite-charge, same-flavor dilepton events with $M_Z - 10$ GeV $\leq m(\ell\bar{\ell}) \leq M_Z + 10$ GeV to remove backgrounds from WZ and ZZ and high p_T Z production, and
- for dilepton events, we require $\Delta\phi(\ell\bar{\ell}') \leq 150°$ $(\ell, \ell' = e, \mu, \tau)$ to remove backgrounds from $Z \to \tau\bar{\tau}$ events.

We have checked that even after these cuts and triggers, SM backgrounds from W production swamp channels with no leptons or just one identified lepton (e, μ or τ). The former is the canonical $\not{E}_T$ signal, which after optimizing cuts, may be observable at Run 2 if gluinos are lighter than $\sim$ 400 GeV. We do not expect that this signal from gluino and squark production will be detectable since $m_{\tilde{g}} = 578$ GeV (with squarks somewhat heavier) even for $\Lambda = 35$ TeV. For this reason, and because there are large single lepton backgrounds from W production, we focus on signals with two or more leptons in our study. Also, because the presence of τ's is the hallmark of this scenario, we mostly concentrate on leptonic events with at least one identified τ.

We begin by considering the signal and background cross section for clean events. These are shown in Table 15. Events are classified first by the number of identified taus, and then by the lepton multiplicity; the C in the topology column denotes "clean" events. For each topology, the first row of numbers denotes the cross sections

after the basic acceptance cuts and trigger requirements along with the Z veto and the $\Delta\phi$ cut discussed above. We see that there is still a substantial background in several of the multilepton channels. This background can

TABLE 15. SM background cross sections in fb for various clean multilepton topologies from W, $Z \to \tau\tau$, VV ($V = W, Z$) and $t\bar{t}$ production at a 2 TeV $p\bar{p}$ collider, together with ISAJET signal cross sections for the $\Lambda = 40$ TeV and $\Lambda = 50$ TeV points on the Stau NLSP Model Line described in the text. For each event topology, the first number denotes the cross section after the basic acceptance cuts and trigger requirements along with the Z veto and the $\Delta\phi$ cut discussed in the text. The second number is after the additional cut, $p_{Tvis}(\tau_1) \geq 40$ GeV, for events at least one identified τ. The entries labeled $Total^*$ are the sum of all the cross sections except those in the $1\tau 1\ell$ channel. The last two rows provide a measure of the statistical significance of the signal.

Topology	W	$Z \to \tau\tau$	VV	$t\bar{t}$	$\Lambda = 40$ TeV $m_{\tilde{\chi}_1^\pm} = 183$ GeV	$\Lambda = 50$ TeV $m_{\tilde{\chi}_1^\pm} = 236$ GeV
$C3\ell$	0	0	0.39	0	0.68	0.24
	0	0	0.39	0	0.68	0.24
$C1\tau 1\ell$	1045	4.2	36	0.044	8.6	1.96
	43	2.0	10.8	0	5.3	1.27
$C1\tau 2\ell$	0	0.57	1.4	0	3.3	0.93
	0	0.045	0.43	0	1.9	0.59
$C1\tau 3\ell$	0	0	0	0	0.31	0.16
	0	0	0	0	0.21	0.10
$C2\tau 1\ell$	0	1.5	1.2	0	4.1	1.2
	0	0.57	0.79	0	3.3	1.02
$C2\tau 2\ell$	0	0	0	0	0.36	0.23
	0	0	0	0	0.33	0.22
$Total^*$	0	2.1	2.99	0	8.75	2.76
	0	0.62	1.61	0	6.42	2.17
$\sigma(sig)/\sqrt{\sigma(back)}$ (fb$^{1/2}$)					3.87	1.22
					4.30	1.45

be strongly suppressed, with modest loss of signal by imposing an additional requirement,

- $p_{Tvis}(\tau_1) \geq 40$ GeV,

on the visible energy of the hardest tau in events with at least one identified tau. In the background, the τ's typically come from vector boson decays, while in the signal a substantial fraction of these come from the direct decays of charginos and neutralinos that are substantially heavier than M_Z [even for $\Lambda = 40$ (50) TeV), $m_{\tilde{\chi}_1^0} = 103$ (132) GeV]. Thus signal taus pass this cut more easily. A few points about this Table are worth mentioning.

1. The signal cross sections in each channel are at most a few fb, and with an integrated luminosity of 2 fb^{-1}, the individual signals are below the 5σ level even for $m_{\tilde{\chi}_1^\pm} = 183$ GeV ($\Lambda = 40$ TeV). It is clear that with the luminosity expected at the MI we will be forced to add the signal in various channels and see if this inclusive signal is observable.

2. The sum of the signal in all the channels in Table 15, except the $1\tau 1\ell$ channel which has a very large background, is shown in the next two rows with and without the p_T cut on the τ, while in the last two rows we list $\sigma(sig)/\sqrt{\sigma(back)}$. We see that a somewhat better significance is obtained after the $p_{Tvis}(\tau_1) \geq 40$ GeV cut.

3. We see that the inclusive SUSY signal in the clean channels for the $m_{\tilde{\chi}_1^\pm} = 183$ GeV ($\Lambda = 40$ TeV) case should be detectable with the Run II integrated luminosity, whereas for the $m_{\tilde{\chi}_1^\pm} = 236$ GeV ($\Lambda = 50$ TeV) case an integrated luminosity of 12 fb^{-1} is needed for a 5σ signal.

4. We caution the reader that about 25-30% of the τ background comes from mis-tagging QCD jets as taus (except, of course, for the W backgrounds and the backgrounds in the $C2\tau\ell$ channels which are almost exclusively from these fake taus). Thus our estimate of the background level is somewhat dependent on the τ faking algorithm we have used. The signal, on the other hand, almost always contains only real τ's, so that improving the discrimination between τ and QCD jets will lead to an increase in the projected reach of these experiments.

5. In particular channels the background is completely dominated by fake taus. For instance, after the $p_{Tvis}(\tau)$ cut, the $C1\tau1\ell$ background from W sources of just *real taus* is only 1.9 fb, while the signal and other backgrounds remain essentially unaltered from the cross sections in Table 15. Thus if fake τ backgrounds can be greatly reduced, it may be possible to see signals in additional channels.

Next, we turn to jetty signals for the Stau NLSP Model Line. Cross sections for selected signal topologies together with SM backgrounds *after* the $p_T(\tau_1) \geq 40$ GeV cut are shown in Table 16. The other topologies appear to suffer from large SM backgrounds and we have not included them here.

TABLE 16. SM background cross sections in fb for various jetty multilepton topologies from W, $Z \to \tau\tau$, VV ($V = W, Z$) and $t\bar{t}$ production at a 2 TeV $p\bar{p}$ collider, together with ISAJET signal cross sections for $m_{\tilde{\chi}_1^\pm} = 183$ GeV ($\Lambda = 40$ TeV) and $m_{\tilde{\chi}_1^\pm} = 236$ GeV ($\Lambda = 50$ TeV) for the Stau NLSP Model Line. The cross sections are with all the cuts including the p_{Tvis} cut on the hardest τ.

Topology	W	$Z \to \tau\tau$	VV	$t\bar{t}$	$\Lambda = 40$ TeV $m_{\tilde{\chi}_1^\pm} = 183$ GeV	$\Lambda = 50$ TeV $m_{\tilde{\chi}_1^\pm} = 236$ GeV
$J3\ell$	0	0.019	0.28	0.3	1.06	0.35
$J1\tau2\ell$	0	0.19	0.29	1.2	1.92	0.79
$J2\tau1\ell$	0.11	0.79	0.41	0.8	2.25	1.18
$J2\tau2\ell$	0	0	0	0	0.31	0.22
Total	0.11	1.0	0.98	2.3	5.53	2.54
$\sigma(sig)/\sqrt{\sigma(back)}$ (fb$^{1/2}$)					2.64	1.21

The following features are worth noting:

1. We see that Stau NLSP Model Line results in smaller cross sections in jetty channels. This should not be surprising since electroweak production of charginos, neutralinos and sleptons are the dominant SUSY processes, and because staus are light, branching fractions for hadronic decays of $\tilde{\chi}^\pm$ and $\tilde{\chi}^0$ tend to be suppressed.

2. We see from Table 16 that with the present set of cuts, not only is the signal below the level of observability in any one of the channels, the inclusive signal is not expected to be observable at the MI even for the $m_{\tilde{\chi}_1^\pm} = 183$ GeV ($\Lambda = 40$ TeV) case. With an integrated luminosity of 25 fb^{-1} the signal for the $m_{\tilde{\chi}_1^\pm} = 236$ GeV ($\Lambda = 50$ TeV case is observable at the 6σ level.

3. As for the clean lepton case, a significant portion of the background comes from QCD jets faking a tau. The fraction of events with a fake tau varies from channel to channel, but for the $2\tau1\ell$ channel in Table 16 almost 60% of the background involves at least one fake τ in contrast to essentially none of the signal.

4. A major background to the jetty signal comes from $t\bar{t}$ production. To see if we could enhance the signal relative to this background we tried to impose additional cuts to selectively reduce the top background.

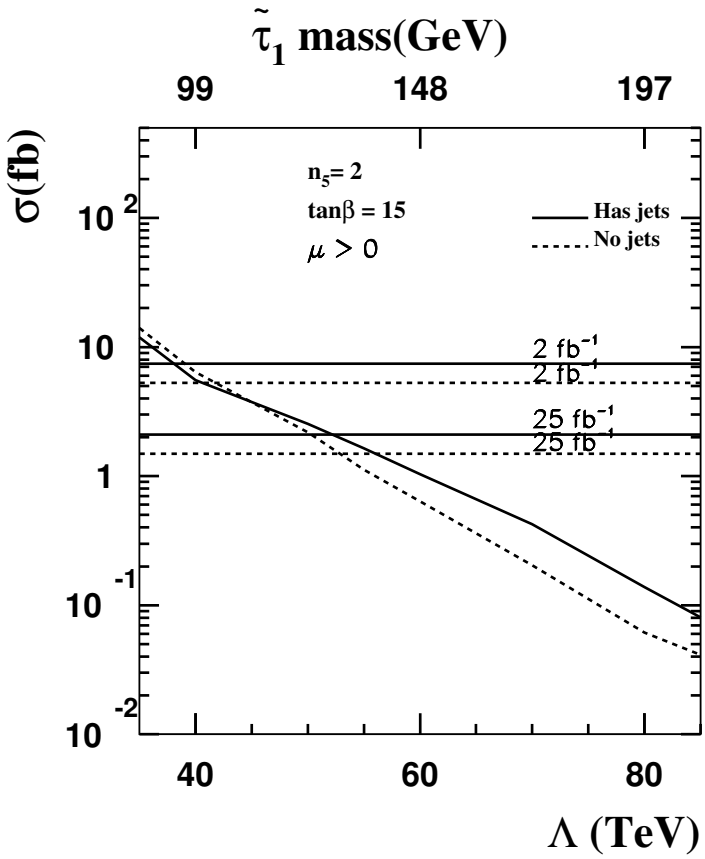

FIGURE 44. Signal cross sections after all cuts versus Λ and $m_{\tilde{\tau}_1}$ for the total signal in the clean (dashed line) and jetty (solid line) channels in the ISAJET study of the Stau NLSP Model Line. The corresponding horizontal lines denote the minimum cross section for a 5σ signal for 2 fb^{-1} and 25 fb^{-1}.

Since top events are expected to contain hard jets, we first tried to require $E_T(j) \leq 50$ GeV. We also, independently, tried vetoing events where the invariant mass of all jets exceeded 70 GeV. While both attempts lead to an improvement of the signal to background ratio, the statistical significance of the signal is not improved (and is even degraded). We do not present numbers for this for the sake of brevity. It may be possible to reduce the top background by vetoing events with identified b-jets, but we have not attempted to do so here.

For the Stau NLSP Model Line, it appears that experiments at the MI should be able to probe Λ values up to just beyond 40 TeV, corresponding to $m_{\tilde{\chi}_1^\pm} = 183$ GeV, in the inclusive clean multilepton channels. It appears, however, that it will be essential to sum up several channels to obtain a signal at the 5σ level. Confirmatory signals in inclusive jetty channels may be observable at the 3.7σ level. Of course, for an integrated luminosity of 25 fb^{-1} it may be possible to probe $\Lambda = 50$ TeV ($m_{\tilde{\chi}_1^\pm} = 236$ GeV) even in the unfavored jetty channels, and somewhat beyond in the clean channels. The situation is summarized in Fig. 44 where we show the signal cross sections summed over the selected channels for events without jets (dashed) and for events with jets (solid). The horizontal lines denote the minimum cross section needed for the signal to be observable at the 5σ level. We note that, in some channels, a substantial fraction of background events come from QCD jets faking a tau — our assessment of the Run II reach is therefore sensitive to our modeling of this jet mis-tag rate. By the same token, if this rate can be reduced, the reach may be somewhat increased.

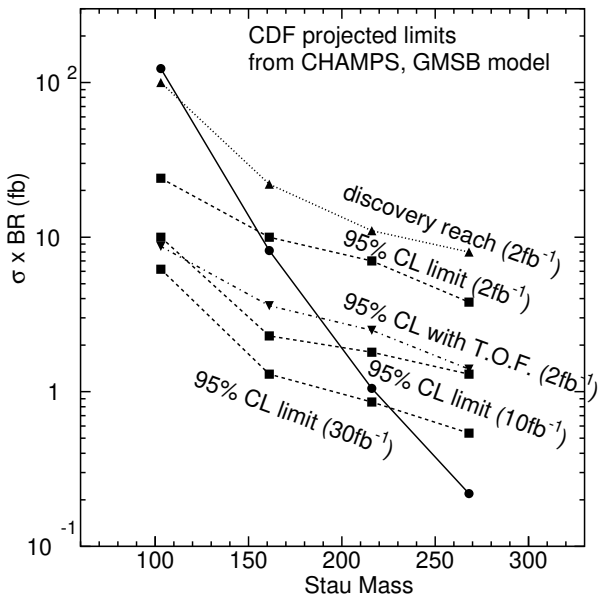

FIGURE 45. The projected CDF limits on the cross-section times branching ratio for a long-lived stau in the Stau NLSP Model Line. The SUSY production is gauginos and sleptons. All sparticles decay to final states involving the $\widetilde{\tau}_1$ NLSP. The limit is the 95% C.L. point assuming no signal and the discovery reach is a signal 5σ over background. The time-of-flight projection assumes a 100 ps timing resolution. The other projections assume only the dE/dx in the COT and SVX and an isolation cut. Adding timing information from other detectors or increasing the momentum cut could increase sensitivity.

D CDF study of quasi-stable staus in the Stau NLSP Model Line

CDF has searched for long-lived massive charged particles in Run I [55,40]. The inclusive muon trigger data sample (90 pb^{-1}) is searched for tracks with $p > 35$ GeV, $|\eta| < 1.0$, dE/dx implying $\beta\gamma < 0.85$, and a mass, calculated from the dE/dx and p_T, greater than 60 GeV. Since the $\widetilde{\tau}_1$ should be isolated, cuts requiring less than 4 GeV in a cone of 0.4 in the calorimeter and track isolation in the CTC are imposed. Two events pass all cuts while 0.85 ± 0.25 are expected. Using a model quite similar to the Stau NLSP Model Line, and allowing all SUSY production, we find the limit is approximately a factor of 6 away from excluding a 100 GeV $\widetilde{\tau}_1$.

For the Run II projection, we assume we are still using the muon triggers so one of the $\widetilde{\tau}_1$'s must pass the trigger. The limit could potentially be improved by including electron and $\not\!\!E_T$ triggers. For the offline efficiency, we require $|\eta| < 1.0$, $p > p_{\rm cut}$, $\beta\gamma < 0.85$ and isolation. We take $p_{\rm cut} = 35$ GeV to start with, and the effects of changing this cut will be discussed shortly. Once the event passes the trigger, either $\tilde{\tau}$ may pass the offline cuts. As defined by the Stau NLSP Model Line, we vary Λ to find the mass dependence.

We estimate the cross section for the background will go up by 20% due to the higher energy. From the Run I data, we estimate the background momentum distribution and for the 2 TeV projection, scale it up in momentum by 5%. The predicted background is 25 events for $m_{\tilde{\tau}_1} = 100$ GeV. The 95% C.L. point is at 2σ or 10 events and the 5σ discovery point is 25 events. We have assumed that the larger $m_{\tilde{\tau}_1}$ is, the larger we can set the minimum mass cut, which greatly reduces the background for larger masses.

Table 17 and Figure 45 summarize our conclusions on the reach in Run II. If we see no signal and set a limit it should be on the order of 150 GeV in the $\widetilde{\tau}_1$ mass. We should be sensitive to a 5σ signal out to $m_{\tilde{\tau}_1} = 110$ GeV. For higher luminosities, we scale the signal and backgrounds. As shown in Figure 45, the limits are extended to $m_{\tilde{\tau}_1} = 200$ GeV for 10 fb^{-1} and $m_{\tilde{\tau}_1} = 225$ GeV for 30 fb^{-1}.

This projection is conservative since there are several methods to improve the sensitivity. We can easily check if increasing the momentum cut can increase our sensitivity and the results are in Table 18. We conclude that the sensitivity could be significantly increased by increasing p_{cut}. We do not include this result in the prediction of the limits since it depends strongly on the model of the background momentum distribution which

TABLE 17. Results of the CDF Monte Carlo study for four points in the Stau NLSP Model Line with prompt $\widetilde{\tau}_1$ decays. The cross section is the total SUSY cross section for gauginos and sleptons. The integrated luminosity is assumed to be 2 fb^{-1}.

Λ (TeV)	42	66	88	109
$m_{\tilde{\chi}_1^\pm}$ (GeV)	193	321	436	544
$m_{\tilde{\chi}_1^0}$ (GeV)	109	176	237	296
$m_{\tilde{\tau}_1}$ (GeV)	103	161	216	268
σ (fb)	123	8.2	1.05	0.22
$A \cdot \epsilon$ (%)	21	25	31	40
signal events	52	4	.65	.18
N_{bg}	25	1.7	0.6	0.3
95% C.L. limit (fb)	24.0	10.0	7.0	4.0
5σ discovery (fb)	100.0	22.0	11.0	8.0

could have tails that degrade this result.

TABLE 18. The effect of increasing the momentum cut on the $\widetilde{\tau}_1$ candidates in the CDF study of quasi-stable stau NLSPs, for $\Lambda = 42$ TeV and $m_{\tilde{\chi}_1^\pm} = 193$ GeV, with 2 fb^{-1}.

p_{cut} (GeV)	$N_{\rm signal}$	$N_{\rm bg}$	$N_{\rm signal}/\sqrt{N_{\rm bg}}$
35	52	25	10
45	45	9	15
55	35	3	20
65	25	1	25
75	12	0.4	8

Another way to improve the sensitivity might be to require two heavy charged particles in the event. While this might reduce the signal by a factor of approximately three, the background would be zero (the fake dE/dx rate is 3×10^{-4} per track). Requiring the COT, hadron calorimeter, or muon scintillator to show a late hit consistent with the dE/dx measurement could make dramatic improvements.

Since this model has light $\tilde{\ell}$'s and W's in the cascade decays of $\widetilde{\chi}_1^\pm$ and $\widetilde{\chi}_2^0$, there should be a significant number of leptons in these events. Another way to improve the sensitivity would be to require an e or second μ in the event. The background would be greatly reduced. As a simpler alternative, the additional lepton (or ν through $\not{E}_T$) could supply the trigger to increase the efficiency.

The CDF Run II detector includes a new time of flight (TOF) system. The system consists of scintillators installed around the outside of the COT and read out with precise timing. The primary purpose is for K/π separation in B physics but it will be very useful for this analysis too.

With 100 ps timing resolution (including the uncertainty on the interaction time), we expect we could require 4σ separation at $\approx$400 ps, which is $\beta\gamma < 2.26$, or $p <$235 GeV for our baseline 103 GeV $\widetilde{\tau}_1$. This greatly increases the acceptance compared to the $\beta\gamma < 0.85$ we had to require in the baseline analysis.

The $\beta\gamma < 2.26$ requirement has a total efficiency of 58% compared to the 21% for the baseline analysis for

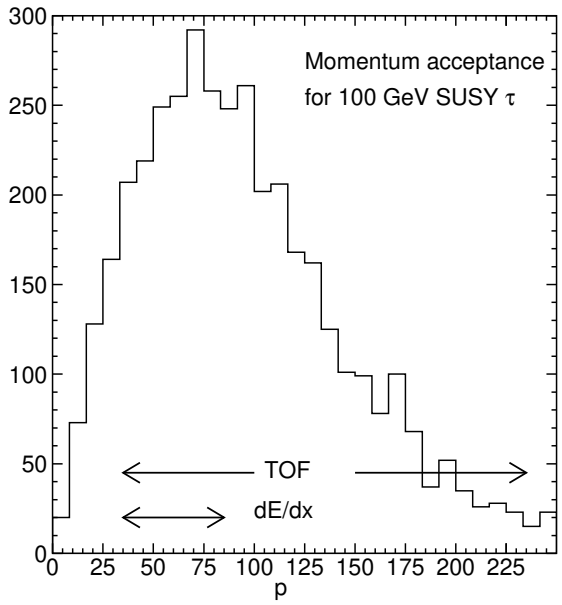

FIGURE 46. The large increase in momentum acceptance with the proposed CDF time-of-flight system installed.

the case $m_{\tilde{\chi}_1^\pm} = 193$ GeV. We would expect 144 signal events instead of 52. Figure 46 shows this significant increase in the sensitive momentum range we could expect with a time-of-flight (T.O.F.) system.

We can combine this result with the SUSY cross section to arrive at the cross section limits show in Figure 45. The T.O.F. system could extend our limit sensitivity by 40 GeV out to $m_{\tilde{\tau}_1} = 190$ GeV and our 5σ discovery sensitivity out to $m_{\tilde{\tau}_1} = 150$ GeV. In this scenario our sensitivity is significantly greater than LEP. However the limit for direct production of the $\tilde{\tau}_1$ would still be below the LEP reach. The search for massive stable strongly interacting charge particles, such as NLSP squarks discussed in section VIII, will also be significantly improved with the TOF detector.

E DØ study of quasi-stable stau signals in the Stau NLSP Model Line

If the $\tilde{\tau}_1$ has a long lifetime (quasi-stable) and decays outside the detector ($\gamma c\tau$ greater than ~ 3 m), it can appear in the detector as a slowly moving charged particle with large ionization energy losses. The signature is, therefore, two high p_T "muons" with large dE/dx values.

Though DØ had several di-lepton analyses in Run I, none of these can be extrapolated to Run II, thanks to the replacement of the central tracker. Based on the expected signatures of several supersymmetric models with heavy stable charged particles discussed below, we select high p_T di-lepton events ($\ell\ell + dE/dx$) with large dE/dx loss using the following requirements:

1) At least two "leptons" with $p_T^\ell > 50$ GeV;

2) $M_{\ell\ell} > 150$ GeV;

3) At least one "lepton" passing the dE/dx requirement.

The di-lepton mass requirement is intended to reduce Drell-Yan backgrounds. The principal backgrounds are: QCD dijet events with jets misidentified as leptons, $t\bar{t}$, and Drell-Yan events. Using $\mathcal{P}(j \to \ell) = 10^{-4}$ and the assumed rejection factor of the dE/dx cut for the MIP particles, the observable background cross sections are estimated to be 0.1 fb from QCD dijet, 0.2 fb from $t\bar{t}$ events, and 0.2 fb from Drell-Yan processes. The QCD dijet cross section for $p_T > 50$ GeV is assumed to be 1 μb in the estimation. The total observable cross section is therefore 0.5 fb for the above selection.

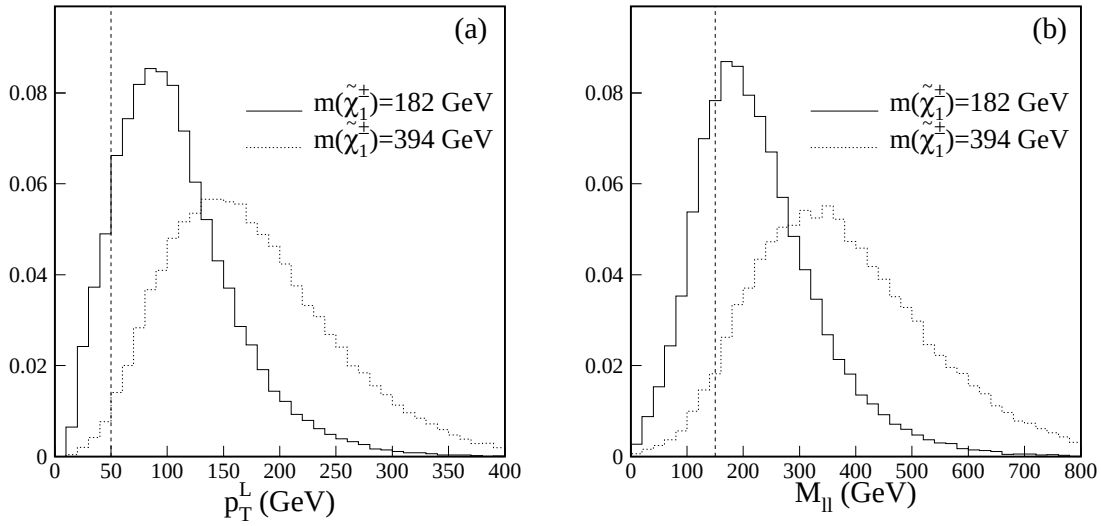

FIGURE 47. The "lepton" p_T (a) and di-"lepton" mass $M_{\ell\ell}$ (b) distributions for the models with a quasi-stable $\tilde{\tau}_1$ as the NLSP for $\Lambda = 40,\ 80$ TeV ($m_{\tilde{\chi}_1^\pm} = 182,\ 394$ GeV) in the DØ study. The "leptons" are actually quasi-stable staus. The vertical dashed lines indicate the cutoffs. All distributions are normalized to unit area.

The expected p_T distributions of the $\tilde{\tau}_1$ for two different values of Λ are shown in Fig. 47(a). The cut of $p_T > 50$ GeV of the $\ell\ell + dE/dx$ selection is efficient for the signal while it is expected to reduce backgrounds significantly. The typical invariant mass of the two 'muons' (assuming massless) is very large as shown in Fig. 47(b). A $M_{\ell\ell} > 150$ GeV requirement does little harm to the signals. Due to its large mass, the $\tilde{\tau}_1$ is expected to move slowly. However since most of the $\tilde{\tau}_1$'s are produced in the decays of massive $\tilde{\chi}_1^\pm$s and $\tilde{\chi}_2^0$s, the average speed $\beta(\equiv v/c)$ is relatively large. It is around 0.7 for the Λ values studied.

The not-so-slow moving $\tilde{\tau}_1$'s are expected to deposit large ionization energies in the detector, differentiating them from other high p_T MIP particles. Since the backgrounds for the requirements $p_T > 50$ GeV and $M_{\ell\ell} > 150$ GeV are already small, it pays to have a dE/dx requirement with a relatively high efficiency for the signal and a reasonable rejection for the MIP particles. The $\not{E}_T$ distribution of these events as shown in Fig. 48 shows two distinct regions: small and large $\not{E}_T$. The decays $\tilde{\chi}_1^\pm \to \tilde{\chi}_1^0 W \to \tilde{\tau}_1 \tau W$ and $\tilde{\chi}_2^0 \to e\tilde{e},\ \mu\tilde{\mu}$ contribute to events with small $\not{E}_T$. The decays $\tilde{\chi}_1^\pm \to \tilde{\tau}_1 \nu$ and $\tilde{\chi}_2^0 \to \tau\tilde{\tau}_1$ are responsible for events with large $\not{E}_T$. The detection efficiencies and the expected significances of the $\ell\ell + dE/dx$ selection for different values of Λ are tabulated in Table 19. The high efficiency is largely due to the high momentum expected for the quasi-stable $\tilde{\tau}_1$. The 5σ discovery curves are shown in Fig. 43 for two values of $\mathcal{L}$. The lighter chargino with mass up to 340, 410 GeV and the $\tilde{\tau}_1$ with mass up to 160, 200 GeV can be discovered for the two integrated luminosities respectively.

VII SLEPTON CO-NLSP

Slepton co-NLSPs result if the sleptons are lighter than the other MSSM superpartners and the slepton mass eigenstates $\tilde{e}_R$, $\tilde{\mu}_R$, and $\tilde{\tau}_1$ are degenerate to within less than about 1.8 GeV, so that the three body decays $\tilde{e}_R \to e\tau\tilde{\tau}_1$ and $\tilde{\mu}_R \to \mu\tau\tilde{\tau}_1$ are forbidden. Supersymmetric decay chains can therefore pass through any of $\tilde{e}_R$, $\tilde{\mu}_R$ or $\tilde{\tau}_1$. As a result, the sleptons ($\tilde{\ell} \equiv \tilde{\tau}_1, \tilde{e}_R, \tilde{\mu}_R$) effectively share the role of the NLSP. The slepton co-NLSPs decay to the Goldstino by

$$\tilde{\ell} \to \ell\tilde{G} \tag{7.1}$$

If the supersymmetry breaking scale $\sqrt{F}$ is in the lower part of the allowed range, then the slepton decays can be prompt, so that supersymmetric events will be rich in high p_T leptons and τ's, with large $\not{E}_T$ from the Goldstinos escaping the detector. The lepton flavors occurring in these decays will often be nearly democratic

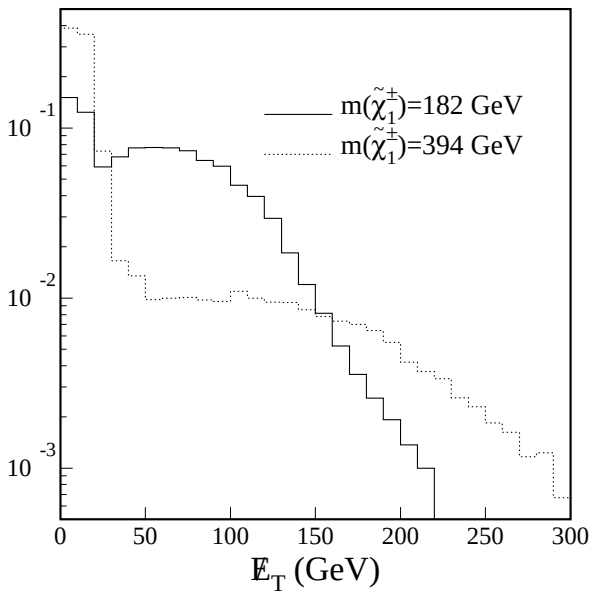

FIGURE 48. The $\not{E}_T$ distributions for the models with a quasi-stable $\tilde{\tau}_1$ as the NLSP for $\Lambda = 40$, 80 TeV ($m_{\tilde{\chi}_1^{\pm}} = 182$, 394 GeV) in the DØ study. The decays $\tilde{\chi}_1^{\pm} \to \tilde{\chi}_1^0 W^{\pm} \to \tilde{\tau}_1 \tau W^{\pm}$ and $\tilde{\chi}_2^0 \to e\tilde{e}$, $\mu\tilde{\mu}$ contribute to events with small $\not{E}_T$ while the decays $\tilde{\chi}_1^{\pm} \to \tilde{\tau}_1 \nu$ and $\tilde{\chi}_2^0 \to \tau\tilde{\tau}_1$ are the source for events with large $\not{E}_T$.

TABLE 19. The $\tilde{\chi}_1^{\pm}$ and $\tilde{\tau}_1$ masses, theoretical cross section, detection efficiencies of the $\ell\ell + dE/dx$ selection, and significances in the DØ study for different values of Λ for the models with a quasi-stable $\tilde{\tau}_1$ NLSP. The relative statistical error on the efficiency is typically 1%. The background cross section is assumed to be 0.5 fb with an uncertainty of 20%.

Λ (TeV)	40	60	80	100
$m_{\tilde{\chi}_1^{\pm}}$ (GeV)	182	289	394	499
$m_{\tilde{\tau}_1}$ (GeV)	99	147	196	246
σ_{th} (fb)	149	14.4	2.1	0.4
ϵ (%)	37.4	44.6	51.6	54.9
$N_s/\delta N_b$ (2 fb^{-1})	112	12	2.1	0.5
$N_s/\delta N_b$ (30 fb^{-1})	341	40	6.7	1.4

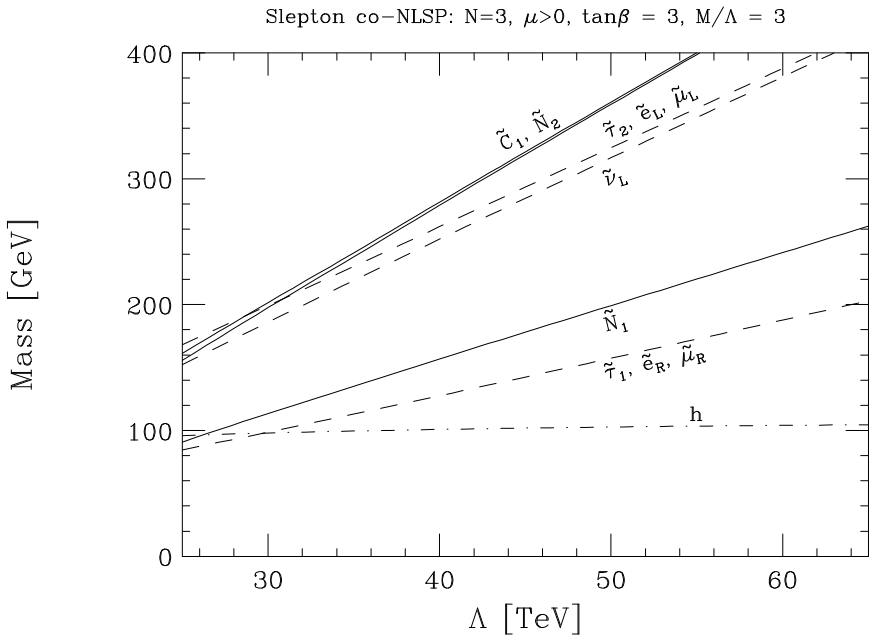

FIGURE 49. The masses of the lightest neutralinos, charginos, sleptons and CP-even Higgs boson in the Slepton co-NLSP Model Line, as a function of Λ.

because of the near-degeneracy of staus, smuons, and selectrons in the slepton co-NLSP scenario, but there is some preference for τ's, due to the effects of $\widetilde{\tau}_R$-$\widetilde{\tau}_L$ mixing which provides a stronger coupling of $\widetilde{\tau}_1$ to Winos.

For very large values of the supersymmetry breaking scale $\sqrt{F}$, the slepton NLSPs will move through the detector before decaying. Since the sleptons are required to be heavy from bounds at LEP, they may well often be produced with velocities in the lab frame that are not ultra-relativistic. This can cause them to be detected by virtue of their high ionization rate (dE/dx) or by time-of-flight measurement, just as discussed for the $\widetilde{\tau}_1$ in the Stau NLSP scenario of the previous section. Very energetic quasi-stable sleptons will penetrate all the way through the detector with a near-minimal ionization rate, and may yield signals that are identical or nearly identical to those of muons.

For intermediate values of $\sqrt{F}$, the slepton decays can occur inside the detector but at a macroscopic distance. Just as discussed above for the stau NLSP case, the impact parameter of the slepton from the interaction region or the kink in the charged particle track when the decay occurs can yield a unique signal and provide information about the decay length. Measuring the physical decay length of the charged sleptons in this scenario may yield direct information or constraints on the supersymmetry breaking mechanism, which would be one of the most theoretically interesting determinations one can make in this scenario.

In general, the signatures in the slepton co-NLSP scenario are rather similar to those in the stau NLSP case. However, the profiles of the leptons and jets coming from the sparticle decays can be quite different, with the hallmark being a tendency for lepton democracy rather than the preponderance of τ's found in the stau NLSP scenario.

For quantitative studies, we define a Slepton co-NLSP Model Line according to the general strategy outlined in Section II. The fixed parameters that define our Model Line are:

$$\text{Slepton Co} - \text{NLSP Model Line}: \qquad N = 3, \ \frac{M_m}{\Lambda} = 3, \ \tan\beta = 3, \ \mu > 0, \tag{7.2}$$

and Λ is allowed to vary. In Figure 49, we show the masses of the lightest few superpartners and the lightest CP-even Higgs boson h^0, as a function of 34 TeV $< \Lambda <$ 85 TeV. In Figure 50, we show the most important Run II production cross-sections for superpartners in this Model Line, including $\widetilde{\chi}_1^+\widetilde{\chi}_1^-$, $\widetilde{\chi}_1^\pm\widetilde{\chi}_1^0$, $\widetilde{e}_R^+\widetilde{e}_R^-$, $\widetilde{\mu}_R^+\widetilde{\mu}_R^-$, and $\widetilde{\tau}_1^+\widetilde{\tau}_1^-$, as well as the total inclusive cross-section for all supersymmetric particles, as a function of $m_{\widetilde{\chi}_1^\pm}$ and $m_{\widetilde{\tau}_1}$. Figures 51 and 52 show the most significant branching fractions for $\widetilde{\chi}_1^\pm$ and $\widetilde{\chi}_2^0$. The decay of $\widetilde{\chi}_1^0$ for these models is almost democratic into the three final states $e\widetilde{e}_R$, $\mu\widetilde{\mu}_R$, and $\tau\widetilde{\tau}_1$, with a slight preference for the last.

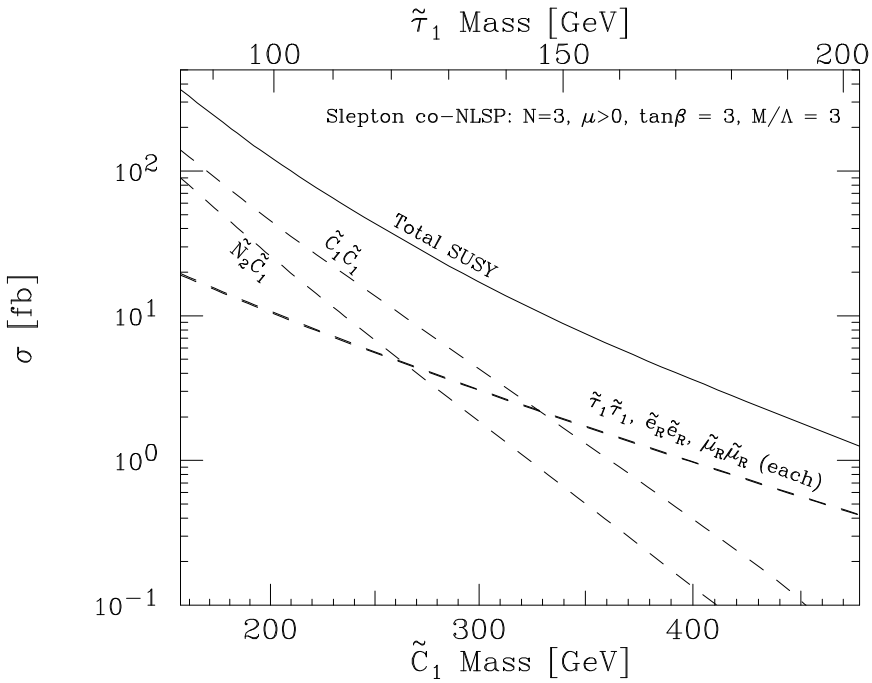

FIGURE 50. Total production cross-sections in $p\overline{p}$ collisions with $\sqrt{s} = 2$ TeV, for superpartner pairs in the Slepton co-NLSP Model Line, as a function of $m_{\tilde{\chi}_1^\pm}$ and $m_{\tilde{\tau}_1}$.

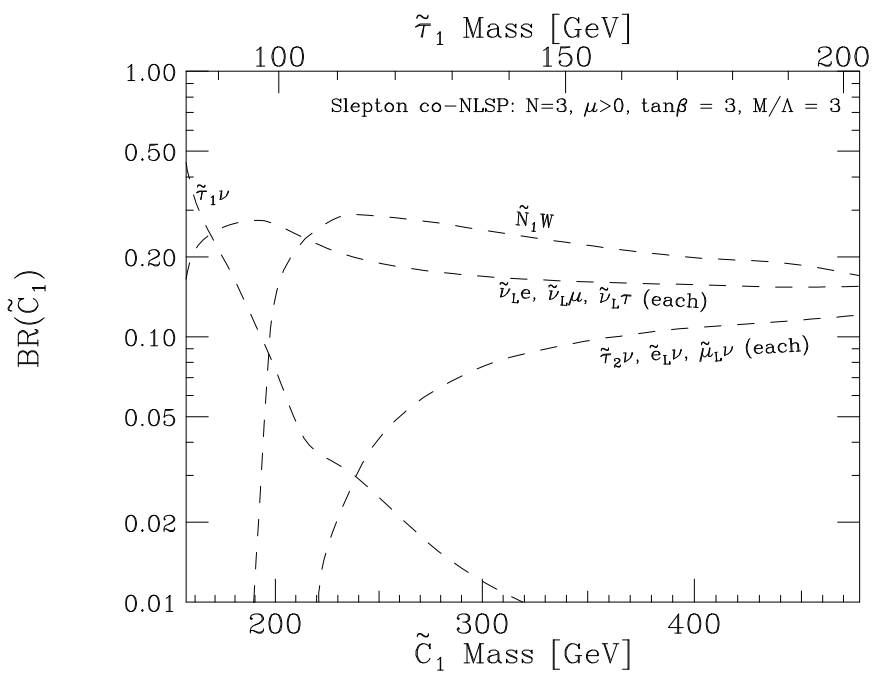

FIGURE 51. Branching fractions for the decay of $\tilde{\chi}_1^\pm$ in the Slepton co-NLSP Model Line, as a function of $m_{\tilde{\chi}_1^\pm}$ and $m_{\tilde{\tau}_1}$.

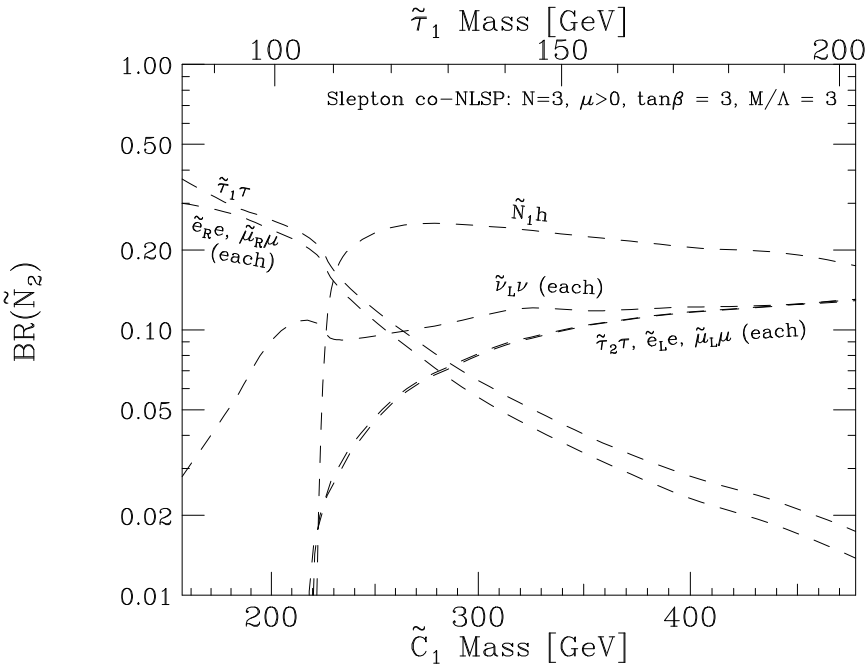

FIGURE 52. Branching fractions for the decay of $\widetilde{\chi}_2^0$ in the Slepton co-NLSP Model Line, as a function of $m_{\tilde{\chi}_1^\pm}$ and $m_{\tilde{\tau}_1}$.

In this Model Line, the three lightest mass eigenstates $\widetilde{e}_R$, $\widetilde{\mu}_R$, and $\widetilde{\tau}_1$ are separated by less than 1 GeV. Therefore, they effectively share the role of the NLSP. For small values of Λ, $\widetilde{\chi}_1^+\widetilde{\chi}_1^-$ and $\tilde{\chi}_1^\pm\tilde{\chi}_2^0$ dominate the production cross section. As illustrated in Fig. 53, $\widetilde{\chi}_1^+\widetilde{\chi}_1^-$ and $\tilde{\chi}_1^\pm\tilde{\chi}_2^0$ production will yield events with multileptons in the final state. The slepton pair production in this Model Line surpasses chargino-neutralino production if $m_{\tilde{\ell}} \gtrsim 140$ GeV.

The lifetime of $\tilde{\ell}$ determines the event topology. The general types of signals to be expected in this Model Line are:

- Small C_G with prompt NLSP decays:
  Events with 2 or 3 or more high-p_T leptons (e, μ, or τ), often accompanied by two or more jets.

- Intermediate C_G with delayed NLSP decays:
  Events with $\widetilde{\ell} \to \ell$ decay kinks.

- Large C_G with a quasi-stable NLSP:
  Events with heavy charged particle tracks featuring anomalous ionization rate or time-of-flight from slow slepton NLSPs, and/or fake "muons" from fast slepton NLSPs.

In the following, we discuss the cases with short-lived and quasi-stable $\tilde{\ell}$'s. Again, the analyses should also be sensitive to the slepton co-NLSPs with a intermediate lifetime.

A CDF study of prompt slepton decay signals in the Slepton co-NLSP Model Line

In the slepton co-NLSP scenario, supersymmetry events always produce two high–E_T leptons and may produce other leptons or jets in the cascade decays. One option for approaching this model is through a trilepton and $\not\!\!E_T$ search which overlaps with the SUGRA standard search. Another option is dileptons with jets and $\not\!\!E_T$, which also overlaps a standard SUGRA search. Finally a new search requiring only two leptons and $\not\!\!E_T$ is also potentially sensitive. The only significant background would be $WW/WZ/ZZ$ and $t\bar{t}$ production.

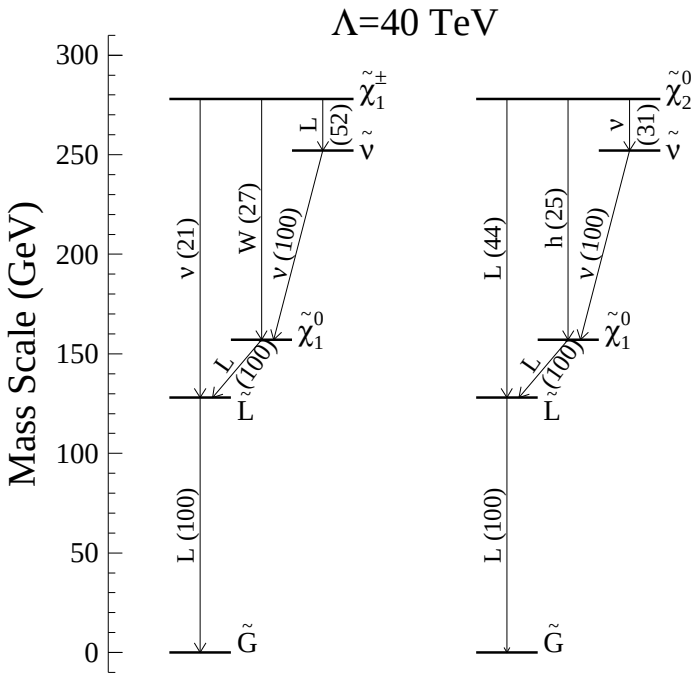

FIGURE 53. Decay schematics of $\tilde{\chi}_1^{\pm}$ and $\tilde{\chi}_2^0$ for $\Lambda = 40$ TeV for the Slepton co-NLSP Model Line. Percentage branching ratios for main decay modes are shown in parentheses.

This could be mitigated by harder cuts on the E_T and $\not\!\!E_T$, which should be more efficient for SUSY events than the Standard Model backgrounds. CDF has examined the trilepton approach by applying the results of the SUGRA trilepton analysis to the GMSB model for both the Run I data result [56] and the Run II projection.

In 107 pb^{-1} of Run I data, one lepton is required to be central, have $E_T > 11$ GeV and pass tight identification cuts. Two other leptons must have $E_T > 5$ GeV and pass looser cuts. A $\not\!\!E_T$ of more than 15 GeV is then required. No events pass all cuts and anything more than 3.2 events of anomalous production is excluded. Table 20 and Figure 54 shows the resulting limits. The branching ratio falls off when the $\tilde{\chi}_1^{\pm}$ mass is less than about 150 GeV because the $\tilde{\nu}$ becomes heavier than the $\tilde{\chi}_1^{\pm}$ and the leptonic feed–down decays are suppressed.

TABLE 20. The summary of the Monte Carlo points used to investigate the limits on the slepton co-NLSP model from the CDF Run I trilepton analysis. Cross sections include the branching ratios. The $A \cdot \epsilon$ is for events that satisfy the branching ratio criteria which is any three leptons at the generator level.

Λ (TeV)	23	26	31	35
$m_{\tilde{\chi}_1^{\pm}}$ (GeV)	139	164	206	238
$m_{\tilde{\ell}}$ (GeV)	78	87	101	114
BR(%)	16	33	37	35
$\sigma\times$BR (fb)	87	77	33	13
$A \cdot \epsilon$ (%)	15.9	27.7	38.7	40.7
$\sigma\times$BR 95% C.L. limit (fb)	188	108	77.3	73.4

The SUGRA trilepton analysis has been projected to Run II and it has been estimated that approximately

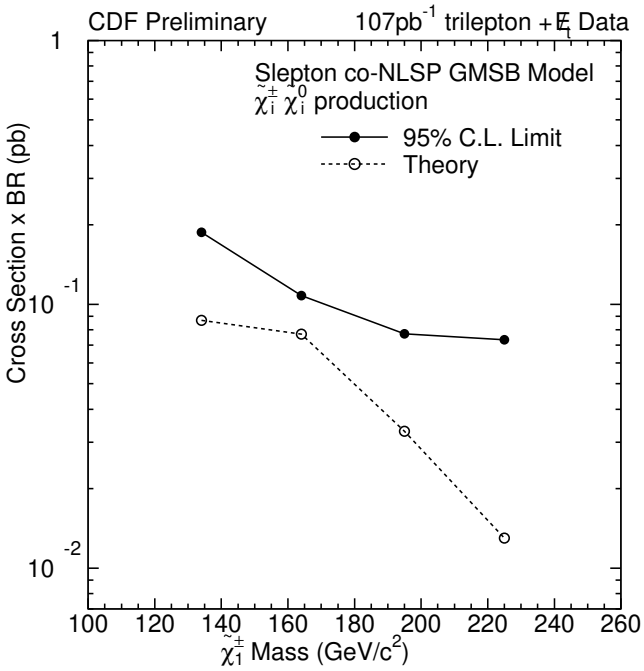

FIGURE 54. The CDF Run I limit on cross section times branching ratio from the trilepton analysis applied to the Slepton co-NLSP Model Line.

one background event will remain in 2 fb^{-1} if the $\not\!\!E_T$ cut is raised to 25 GeV. With 20% systematics on the background and efficiency, we expect limits of 4 events at 95% C.L. and 17 events at 5σ. Table 21 and Figure 55 show the projected limits.

For 2 fb^{-1} we expect to have a 5σ discovery reach of 280 GeV in chargino mass and a limit reach of 330 GeV. For larger luminosities, we have not attempted to re–optimize the cuts; we simply scale the signals and backgrounds. Figure 55 again shows the result, which indicate the chargino mass reach is extended by 50 GeV for 10 fb^{-1} and 70 GeV for 30 fb^{-1}.

B DØ study of prompt slepton decay signals for the Slepton co-NLSP Model Line

If the decay $\tilde{\ell} \to \ell\tilde{G}$ is prompt ($\gamma c\tau \lesssim$ 10 cm), $\ell\ell\not\!\!E_T$ events are expected from supersymmetry. Unfortunately, this final state has large backgrounds from the Standard Model processes such as $t\bar{t}$, WW, WZ and ZZ productions as well as from $W+$jets production with one of the jets misidentified as a lepton. However we note that these events typically have multiple leptons in the final state and most of them are in the central pseudorapidity region with good lepton identification. Apart from those from $\tilde{\ell}$ decays, leptons are also expected from W^*'s and Z^*'s produced in the cascade decays of $\tilde{\chi}_1^{\pm}$ and $\tilde{\chi}_2^0$ of supersymmetry originated events. Therefore, they can be selected using the $\ell\ell\ell j\not\!\!E_T$ criteria. The p_T distributions of the leading lepton and the third lepton of these events are shown in Fig. 56(a). Since most of the leading leptons are produced in the direct decays of heavy $\tilde{\ell}$'s, its p_T spectrum is relatively hard as shown in the figure. The detection efficiencies and the expected significances are summarized in Table 22. The reduction in the relative cross section of the tri-lepton producing $\tilde{\chi}_1^+\tilde{\chi}_1^-$ and $\tilde{\chi}_1^{\pm}\tilde{\chi}_2^0$ processes is responsible for the decrease in efficiency as Λ increases. For $\Lambda \gtrsim$ 50 TeV corresponding to $m_{\tilde{\ell}} \gtrsim$ 160 GeV and $m_{\tilde{\chi}_1^{\pm}} \gtrsim$ 360 GeV, the $\tilde{\ell}\tilde{\ell}$ production cross section surpasses that of the $\tilde{\chi}_1^+\tilde{\chi}_1^-$ and $\tilde{\chi}_1^{\pm}\tilde{\chi}_2^0$. With the $\tilde{\ell} \to \ell\tilde{G}$ decay, $\tilde{\ell}\tilde{\ell}$ events will result in a high p_T $\ell\ell\not\!\!E_T$ final state. We note that the improvement by adding the $\ell^{\pm}\ell^{\pm}jj\not\!\!E_T$ selection is minimal in this case. The 5σ discovery curves are compared with the theoretical cross sections in Fig. 57. With integrated luminosities of 2 and 30 fb^{-1}, the lighter chargino with mass up to 310 and 360 GeV can be discovered, respectively.

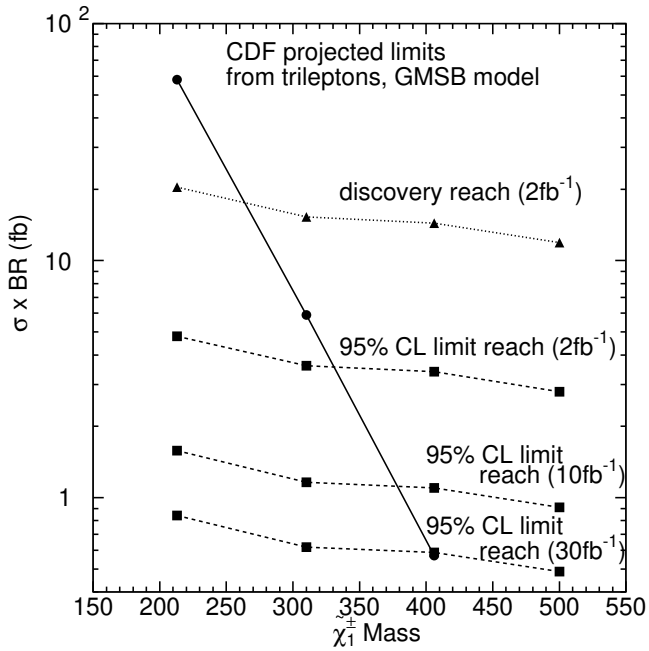

FIGURE 55. The projected Run II CDF limit on cross section times branching ratio from the trilepton analysis applied to the Slepton co-NLSP Model Line. The solid line is the theoretical prediction.

TABLE 21. The summary of the Monte Carlo points used to investigate projected limits on the slepton co-NLSP model for Run II (2 fb^{-1}) in the CDF study. Cross sections include the branching ratios. The $A \cdot \epsilon$ is for events that satisfy the branching ratio criteria which is any three leptons at the generator level.

Λ (TeV)	32	44	56	68
$M_{\tilde{\chi}_1^\pm}$ (GeV)	213	310	406	500
$M_{\tilde{\ell}}$ (GeV)	104	140	176	212
BR(%)	61	39	16	5
$\sigma \times$BR (fb)	58.0	5.9	0.57	0.056
$A \cdot \epsilon$ (%)	41	56	59	71
$\sigma \times$BR 95% C.L. limit (fb)	4.8	3.6	3.4	2.8

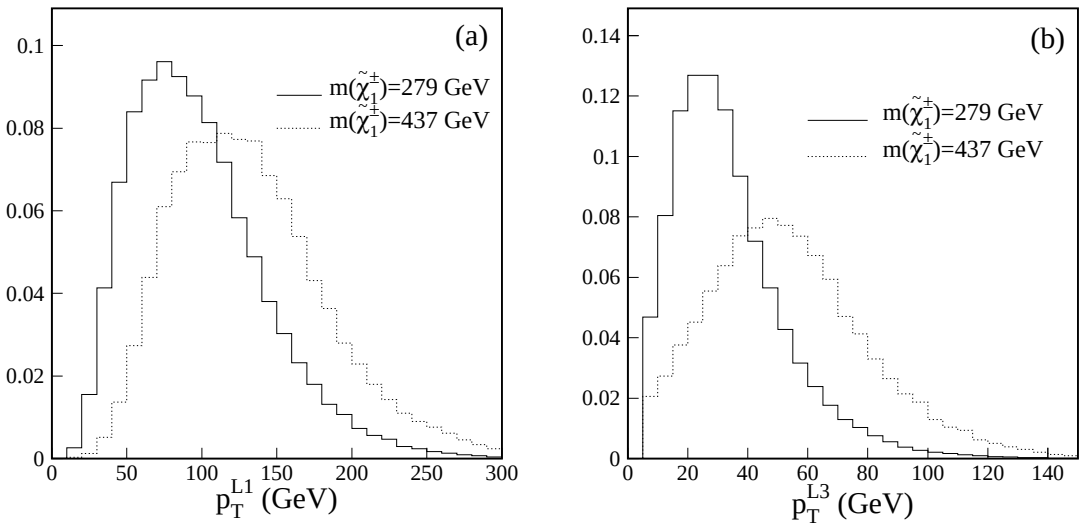

FIGURE 56. The p_T distributions of (a) the leading lepton and (b) the third lepton for the models with short-lived sleptons as co-NLSPs for $m_{\tilde{\chi}_1^\pm} = 279,\ 437$ GeV ($\Lambda = 40,\ 60$ TeV) in the DØ study. Note that the p_T requirement is 15 GeV for the leading lepton and 5 GeV for the non-leading leptons. All distributions are normalized to unit area.

TABLE 22. The theoretical cross sections, $\tilde{\chi}_1^\pm$ and $\tilde{\ell}$ masses, detection efficiencies of the $\ell\ell\ell j \not{E}_T$ selection criteria, and significances for different values of Λ for points on the Slepton co-NLSP Model Line with prompt decays, in the DØ analysis. The efficiencies typically have a relative statistical uncertainty of 4%. The observable background cross section is assumed to be 0.3 fb with a 20% systematic uncertainty.

Λ (TeV)	30	40	50	60	70
$m_{\tilde{\chi}_1^\pm}$ (GeV)	197	279	358	437	517
$m_{\tilde{\ell}}$ (GeV)	99	128	158	188	218
σ_{th} (fb)	121	24.5	6.7	2.3	0.9
ϵ (%)	14.7	15.4	9.6	4.7	1.4
$N_s/\delta N_b$ (2 fb^{-1})	44	9.4	1.6	0.3	–
$N_s/\delta N_b$ (30 fb^{-1})	152	32	5.5	0.9	0.1

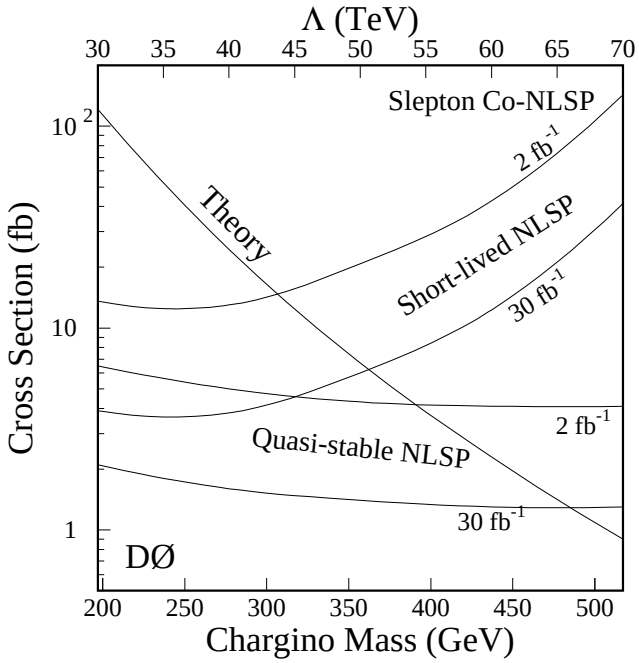

FIGURE 57. The DØ 5σ discovery cross section curves as functions of mass of the lighter chargino and Λ for the Slepton co-NLSP Model Line, along with the theoretical cross sections. The 5σ curves are shown for both short-lived NLSPs ($\ell\ell\ell j\not{E}_T$selection criteria) and quasi-stable slepton co-NLSPs ($\ell\ell+dE/dx$selection) and for integrated luminosities of 2, 30 fb^{-1}.

C DØ study of quasi-stable slepton signals for the Slepton co-NLSP Model Line

If the slepton co-NLSPs have a long lifetime, it can decay outside the detector ($\gamma c\tau \gtrsim 3$ m). In this case, the $\tilde{\ell}$ will appear in the detector like a 'muon' except that the ionization energy loss will be large. This signature is identical to that of a quasi-stable $\tilde{\tau}_1$ discussed above. Therefore, the signal events can be identified using the same $\ell\ell + dE/dx$ selection. The expected p_T and β distributions of the $\tilde{\ell}$ for $\Lambda = 40,\ 60$ TeV are shown in Fig. 58. Note that the β distribution is very similar to that shown in Fig. 58(b) for the models with $\tilde{\tau}_1$ as the sole NLSP. The $\tilde{\ell}$s typically have very large p_T and are mostly central. For example, about 90% of the $\tilde{\ell}$s are in central pseudorapidity region with the tracking coverage for the case of $\Lambda = 70$ TeV ($m_{\tilde{\ell}} = 218$ GeV). Table 23 shows the detection efficiencies and the expected significances for different Λ values. The 5σ discovery curves are shown in Fig. 57. The lighter chargino mass discovery reach is about 390 GeV for $\mathcal{L}$=2 fb^{-1} and 480 GeV for $\mathcal{L}$=30 fb^{-1}.

VIII SQUARK NLSP

A squark may arise as the NLSP in theories of gauge-mediated supersymmetry breaking in which the strongly interacting messenger fields have suppressed couplings to spontaneous supersymmetry breaking. In addition, any non-gauge couplings between the standard model superpartners and the messenger or supersymmetry breaking sectors have an *a priori* unknown effect on the superpartner spectrum. If kinematically open, a squark NLSP can decay to the Goldstino through emission of its partner quark,

$$\widetilde{Q} \to q\widetilde{G} \tag{8.1}$$

The lightest squark is likely to be mostly stop-like because of left-right stop level repulsion, and negative renormalization group evolution contribution to the squared masses, both proportional to the square of the top Yukawa coupling. For a stop-like squark lighter than the top quark, the only kinematically allowed two-body

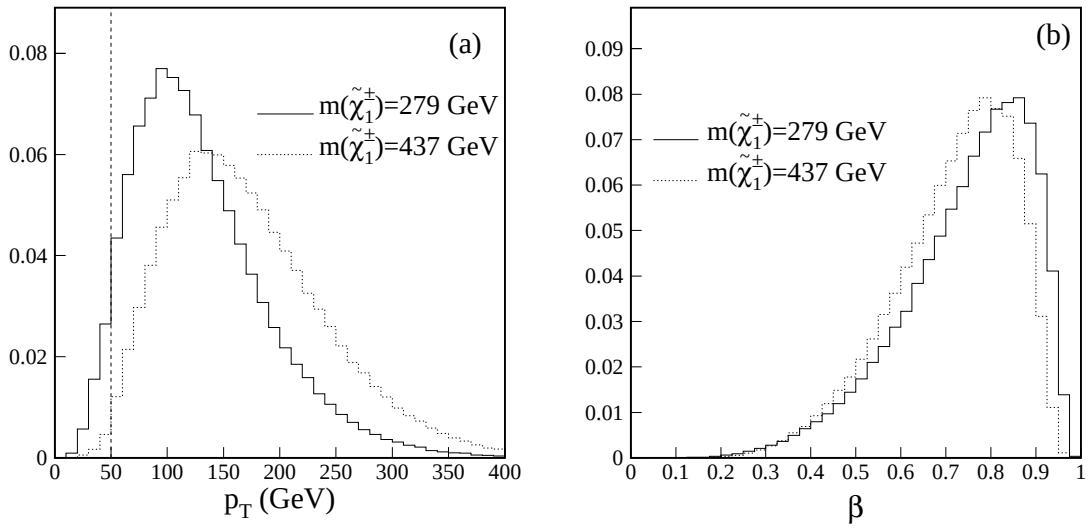

FIGURE 58. The lepton p_T (a) and the NLSP speed β (b) distributions expected for models with quasi-stable sleptons as co-NLSPs, for $m_{\tilde{\chi}_1^{\pm}} = 279,\ 437$ GeV ($\Lambda = 40, 60$ TeV) Here β is measured in units of the speed of light c. All distributions are normalized to unit area.

TABLE 23. The theoretical cross section, $\tilde{\chi}_1^{\pm}$ and $\tilde{\ell}$ masses, detection efficiency of the $\ell\ell + dE/dx$ selection, and significances for different values of Λ for the models with quasi-stable $\tilde{\ell}$'s as co-NLSPs, in the DØ analysis. The relative statistical error on the efficiency is typically 1%. The background cross section is assumed to be 0.5 fb with a systematic uncertainty of 20%.

Λ (TeV)	30	40	50	60	70
$m_{\tilde{\chi}_1^{\pm}}$ (GeV)	197	279	358	437	517
$m_{\tilde{\ell}}$ (GeV)	99	128	158	188	218
σ_{th} (fb)	121	24.5	6.7	2.3	0.9
ϵ (%)	34.8	45.2	52.6	54.9	55.1
$N_s/\delta N_b$ (2 fb^{-1})	83	22	7.0	2.6	1.0
$N_s/\delta N_b$ (30 fb^{-1})	257	68	21	7.8	3.1

decays are through flavor violating suppressed modes to light quarks. Since mixing between the second and third generations is expected to be larger than between the first and third generations,

$$\tilde{t} \to c\widetilde{G} \tag{8.2}$$

should be the dominant two-body decay mode. Three body decay through a charged current interaction,

$$\tilde{t} \to bW\widetilde{G} \tag{8.3}$$

is not suppressed by flavor violation, but is phase-space suppressed. Depending of the precise parameters, the three-body mode $\tilde{t} \to bW\widetilde{G}$ dominates over the two body mode $\tilde{t} \to c\widetilde{G}$ for values of the scharm-stop mixing angle $\sin\theta_{\tilde{c}\tilde{t}} \lesssim$ few $\times 10^{-3}$ [57]. For a stop-like squark heavier than the top quark, the two-body decay $\tilde{t} \to t\widetilde{G}$ generally dominates. With the top decay $t \to bW$ this give the same decay pattern as (8.3), but with different kinematics. Expressions for the two- and three-body squark decays to the Goldstino are given in Appendix XI 2.

For any reasonable supersymmetry breaking scale above the electroweak scale, coupling to the Goldstino is weak enough so that the squark decay length easily exceeds the hadronization length scale. A NLSP squark therefore always hadronizes before decaying. Hadronization with a light antiquark leads to a neutral or charged mesino bound state, $\mathcal{M}_{\widetilde{Q}\bar{q}} \equiv (\widetilde{Q}\bar{q})$, while hadronization with two light quarks leads to a neutral or charged sbaryon bound state $\mathcal{B}_{\widetilde{Q}qq} \equiv (\widetilde{Q}qq)$, and likewise for the antiparticle states. The existence of these strongly interacting bound states can lead to a number of novel signatures discussed below.

If the supersymmetry breaking scale is below a few 100 TeV, the decay length for the decay (8.1) or (8.2) and (8.3) is short enough so that the decay products appear to originate from the interaction region. The experimental signatures for general prompt squark decay are

$$\bullet \text{ Prompt decays } \quad \widetilde{Q} \to g\widetilde{G} \quad : \quad jj\not{E}_T \tag{8.4}$$

For a stop-like NLSP squark, the experimental signatures depend on the relative importance of the two- or three-body decay modes

$$\begin{aligned} &\bullet \text{ Prompt decays } \quad \tilde{t} \to bW\widetilde{G} \text{ or } \tilde{t} \to t\widetilde{G} \quad : \quad bbWW\not{E}_T \text{ or } tt\not{E}_T \\ &\bullet \text{ Prompt decays } \quad \tilde{t} \to c\widetilde{G} \quad : \quad cc\not{E}_T \end{aligned} \tag{8.5}$$

Observation of any of these signatures interpreted as arising from decay to Goldstino pairs, would of course imply a squark NLSP with a low supersymmetry breaking scale. Observation of either $bbWW\not{E}_T$ or $tt\not{E}_T$ would imply the NLSP squark is stop-like. In conjunction with a bound on the $cc\not{E}_T$ signature, this would also provide a very stringent upper limit on the scharm-stop mixing angle [57].

If the supersymmetry breaking scale is larger than a few 100 TeV the squark decays (8.1) or (8.2) and (8.3) within a hadronized mesino or sbaryon can take place over a macroscopic distance. In this case displaced jets arise from the squark decay. If the displaced decays are short enough, Standard Model backgrounds from heavy quark production with displaced secondary vertices are possible, but may be controlled by the use of angular distributions. Longer decay lengths can be distinguished by the magnitude of the jet impact parameter with the production vertex. Slowly moving charged mesinos and sbaryons which live long enough to traverse the tracking region of a detector will yield highly ionizing tracks (HITs), much like a quasi-stable stau slepton discussed in sections VI D and VI E. Hadronic interactions of an antimesino or sbaryon give rise to additional hadronic activity along the track and also allow charge exchange with the detector material. Slowly moving antimesinos or sbaryons therefore give rise to intermittent charge exchange associated with highly ionizing tracks (CE-HITs). Mesinos and antisbaryons do not undergo as rapid charge exchange as the antiparticle counterparts. But for a charged state there can still be additional hadronic activity along a highly ionizing track (H-HIT). This is due to inelastic hadronic interactions of the bound state in the calorimeter materials [61]. Neutral mesino and sbaryon states, as well as the intermittent nature of antimesino or sbaryon CE-HITs, contribute to missing energy. The experimental signatures of a squark NLSP with macroscopic decay length to the Goldstino are therefore:

$$\begin{aligned} &\bullet \text{ Macroscopic decays } \quad \widetilde{Q} \to g\widetilde{G} \quad : \quad \text{Displaced jets} \\ &\qquad\qquad\qquad\qquad\qquad\qquad\qquad\quad \text{CE} - \text{HITs} \\ &\qquad\qquad\qquad\qquad\qquad\qquad\qquad\quad \text{H} - \text{HITs} \\ &\qquad\qquad\qquad\qquad\qquad\qquad\qquad\quad \not{E}_T \end{aligned} \tag{8.6}$$

A number of techniques to identify displaced jets, and the difficulty in identifying hadronic highly ionizing tracks are detailed below in sections VIII B and VIII C. Observation of any signature associated with macroscopic decay of an NLSP squark would imply a low SUSY breaking scale. Measurement of the decay length distribution would give a measure of the SUSY breaking scale. Flavor tagging of the final states would yield information about the NLSP squark flavor.

An NLSP squark also presents the interesting possibility of neutral mesino-antimesino oscillations analogous to meson-antimeson oscillations [57]. Rather than representing a very specialized process which could only be observed once the existence of an NLSP squark is established, mesino oscillation can in fact provide a discovery channel, as detailed in section VIII D. Observation of mesino oscillation would provide a very sensitive probe of sflavor violation in the squark sector.

For the quantitative studies below, the signals are assumed to arise entirely from direct squark pair production mainly through s-channel gluon exchange. The squark NLSP Model Line is therefore simply defined to be a single squark with a mass which is allowed to vary. Squark pair production is very likely to be the largest SUSY production cross section in the squark NLSP scenario. It is, however, possible that gluino pair production could also contribute to the signals if the gluino is not too much heavier than the NLSP squark. In this case additional prompt partons would arise from gluino cascade decays, which are likely to be dominated by $\widetilde{g} \to q\widetilde{Q}$.

A Prompt Squark Decay

The lightest squark is likely to be mostly stop-like because of left-right stop level repulsion, and negative renormalization group evolution contribution to the squared mass, both proportional to the square of the top Yukawa coupling. Without any sflavor violation, the dominant decay mode for an NLSP stop squark heavier than about 90 GeV but lighter than the top quark is the three body decay $\widetilde{t} \to bW\widetilde{G}$. Top squark pair production then yields the signature $bbWW\not{E}_T$. Unfortunately this is the identical signature which arises from top quark pair production. One possibility would be to search for an excess in the top sample at large missing energy. This can be significantly improved by using additional kinematic information to distinguish top and stop decays.

One observable which is available at the Tevatron which can distinguish top and stop decays is the invariant mass of the observed b-jet plus lepton system which results from a leptonic W decay [58]. Because the Goldstino is derivatively coupled, the stop decay amplitude is peaked at large values of the Goldstino momentum, which implies small values of the invariant mass for the remaining (visible) decay products. In contrast, top quark decays favor large values of the invariant mass of the visible decay products. Fig. 59 shows the lepton-b invariant mass distribution for the top quark and two values of the stop mass with typical parameters [58]. The b-W invariant mass for stop decay is also shown. As is apparent, the stop excess in a top quark sample could be enhanced by a cut on the lepton-b-jet invariant mass. In order to avoid combinatoric problems this would be applied in the channel in which one W decays hadronically while the other decays leptonically.

It should be noted that at present, the available Pythia and ISAJET Monte Carlo simulations of the three body decay $\tilde{t} \to bW\widetilde{G}$ do not incorporate a derivatively coupled Goldstino in the decay amplitude, and so would not reproduce the correct invariant mass distributions. This should be rectified in future studies of this process.

Another observable which can distinguish top and stop decays is the W longitudinal polarization [58]. A W boson arising from top decay is highly longitudinally polarized because of the large longitudinal Goldstone component coupling proportional to the top mass. The W longitudinal polarization arising from stop decay depends on the relative importance of various amplitudes. If the decay is dominated by diagrams in which the Goldstino is emitted from the stop squark or intermediate off-shell bottom squark the polarization is similar to that for top quark decay. However, diagrams in which the Goldstino is radiated from an intermediate chargino which is mostly Wino contribute transverse polarization [58]. The latter diagrams are important if the chargino is not much heavier than the stop squark or top quark. Fig. 60 shows the longitudinal W polarization for top quark decays and stop squark decays as a function of the Wino mass for various stop mixing angles and typical parameters [58]. This observable is model dependent and therefore sensitive to the underlying superpartner spectrum. Because of the missing energy carried by the Goldstinos, a measurement of the W longitudinal polarization in stop decay can not make use of techniques which require the neutrino four-vector. However, the polarization can be determined from the W decay angle determined from four-vectors of the two jets assigned to the hadronic W [58].

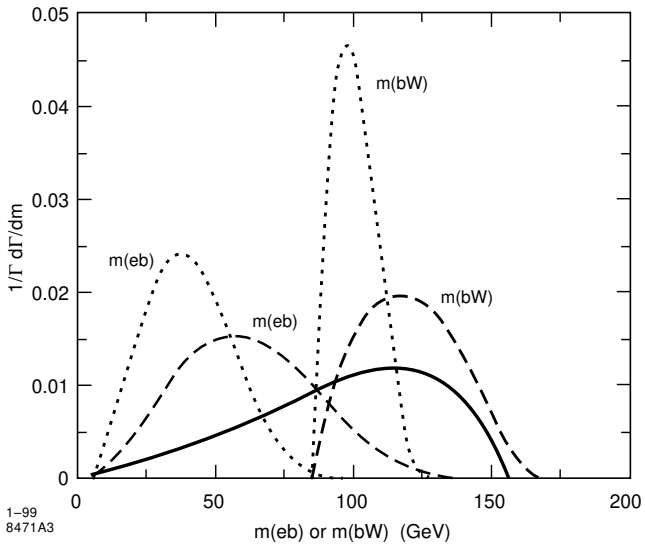

FIGURE 59. m_{eb} and m_{bW} invariant mass spectra for stop squark decay $\tilde{t} \to bW\widetilde{G}$ for $m_{\tilde{t}} = 130$ GeV (dot) and $m_{\tilde{t}} = 170$ GeV (dash) with $m_2 = 200$ GeV, $\mu = 1000$ GeV, $\tan\beta = 1$, $m_{\tilde{b}_L} = 300$ GeV, and the left-right stop mixing angle $\sin\theta_t = -0.8$. The m_{eb} invariant mass spectrum for top quark decay $t \to bW$ is shown for comparison (solid).

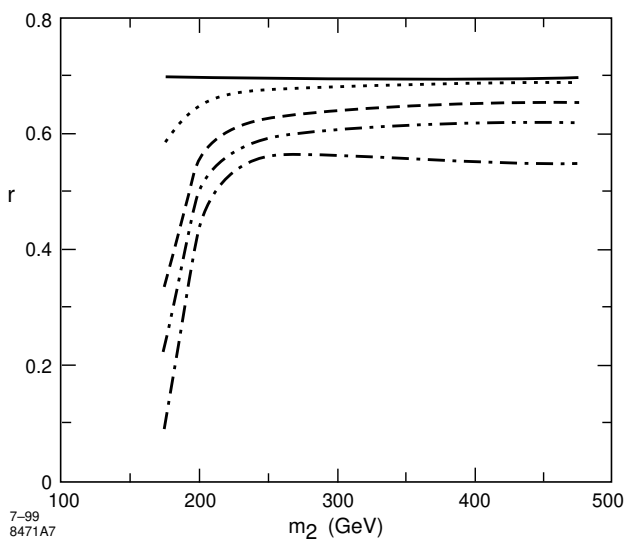

FIGURE 60. Longitudinal W boson polarization $r \equiv \Gamma(W_0)/\Gamma(\text{all})$ for stop squark decay $\tilde{t} \to bW\widetilde{G}$ as a function of the $SU(2)_L$ Wino mass m_2 for the left-right stop mixing angle $\sin\theta_t = -0.98$ (dot), -0.8 (dash), -0.6 (dot-dot-dash), and 0 (dot-dash), with $m_{\tilde{t}} = 170$ GeV, $\tan\beta = 1$, $\mu = 1000$ GeV, and $m_{\tilde{b}_L} = 300$ GeV. The longitudinal polarization for top quark decay $t \to bW$ is shown for comparison (solid).

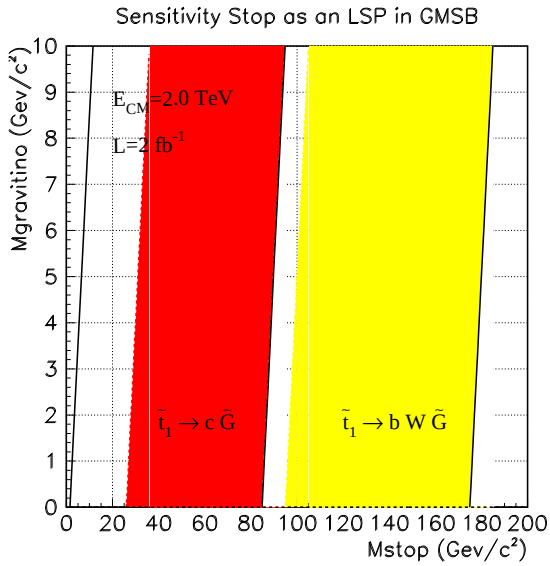

FIGURE 61. Projected CDF Run II limits on a stop NLSP.

With non-trivial scharm-stop mixing the decay $\tilde{t} \to c\widetilde{G}$ can dominate for stop squarks less massive than the top quark. Even without sflavor violation, standard quark mixing results in this decay mode dominating for a stop mass less than about 90 GeV. Stop pair production $\tilde{t}\tilde{t}$ then leads to events with two charm jets and $\not{E}_T$. A search for this mode can be handled as a special case of a SUGRA search for $\widetilde{t}_1 \to c\widetilde{\chi}_1^0$ with the $\widetilde{\chi}_1^0$ mass approaching zero.

1 CDF study of Prompt Squark Decay

CDF has performed a search for $\widetilde{t}_1\widetilde{t}_1$ pair production with $\widetilde{t}_1 \to c\widetilde{\chi}_1^0$ in 88 pb^{-1} of Run I data [59]. The primary analysis cuts include two jets with $E_T > 15$ GeV, 40 GeV of $\not{E}_T$, and one of the jets must have displaced tracks in the SVX. The results include the region where the $\widetilde{\chi}_1^0$ mass approaches zero where the limit applies to the low scale SUSY breaking decay $\widetilde{t}_1 \to c\widetilde{G}$. The results rule out this scenario for a $\widetilde{t}_1$ mass between 40 and 85 GeV.

To project to Run II, the cross sections are simply scaled to 2 fb^{-1} and the efficiency for tagging displaced tracks is assumed to increase by a factor of two. The lowest $\widetilde{t}_1$ mass exclusion region boundary, where the luminosity could overcome the decreasing efficiency of the $\not{E}_T$ cut, is expected to go down to approximately 25 GeV as shown in Fig. 61. The upper limit will remain at 85 GeV because that is where the $\widetilde{t}_1 \to Wb\widetilde{G}$ becomes kinematically available and dominates in the absence some non-trivial stop-scharm mixing.

CDF has also performed the search for $\widetilde{t}_1\widetilde{t}_1$ pair production in the lepton-plus-jets top data mode [60] which applies for heavier $\widetilde{t}_1$'s which decay by $\widetilde{t}_1 \to Wb\widetilde{G}$. The signal is discriminated from the top quark background based on the shape of the transverse mass distribution of the lepton and $\not{E}_T$. This analysis is sensitive only for $\widetilde{t}_1$ masses greater than 90 GeV due to the lepton E_T and $\not{E}_T$ cuts. This analysis is expected to be sensitive up to the threshold where the decay $\widetilde{t}_1 \to t\widetilde{G}$ dominates.

B Mesino and Sbaryon Displaced Decay Signals

The NLSP squark decay length to the Goldstino depends very sensitively on the supersymmetry breaking scale, and may take place over a macroscopic distance. For example, using the expressions for squark decay

rate to the Goldstino given in Appendix XI 2, for $m_{\tilde{t}} = 150$ GeV $\Gamma^{-1}(\tilde{t}_R \to bW\widetilde{G}) \simeq 75$ cm $(\sqrt{F}/100\ \text{TeV})^4$, while for $m_{\tilde{t}} = 190$ GeV $\Gamma^{-1}(\tilde{t} \to t\widetilde{G}) \simeq 0.75$ cm $(\sqrt{F}/100\ \text{TeV})^4$. The visible decay products of the squark decay can therefore be displaced from the production vertex. Since the decay products always involve strongly interacting partons, an NLSP squark hadronized in a mesino or sbaryon bound state can give rise to displaced jets with both large transverse energy (E_T) and large missing transverse energy ($\not{E}_T$).

Any search for squark decay involving displaced jets well within the tracking volume must contend with backgrounds from analogous heavy (c- and b-) quark decays which can also give large E_T displaced jets. This is particularly true for a metastable stop squark which decays to heavy quark flavors so that the background can not be reduced by simply anti-tagging on heavy flavor displaced jets. For sufficiently large squark decay length, the signal can be distinguished from the heavy quark background by the large beam axis impact parameter. An $\not{E}_T$ cut can also significantly reduces background involving heavy quark hadronic decay modes. In addition, since the massive mesinos and sbaryons are non-relativistic, the decay products are not significantly boosted in the lab frame, and are distributed roughly uniformly. This is in contrast to high E_T displaced jets from heavy quark decay, which are highly boosted in the direction of the relativistic heavy quark motion, namely away from the interaction vertex. So the angular distribution of displaced high momentum jets can greatly aid in the separation of a squark signal from heavy quark background. A useful observable in this regard is [57]

$$\cos\varphi \equiv \frac{\vec{p}_{\text{jet}} \cdot \vec{n}}{|\vec{p}_{\text{jet}}|} \tag{8.7}$$

where $\vec{p}_{\text{jet}}$ is the three-momentum vector of the displaced jet and $\vec{n}$ is the unit normal from the beam axis to the origin of the displaced jet. The distribution of high E_T displaced jets from direct heavy quark production and decay is concentrated in $0 \lesssim \cos\varphi \lesssim 1$, with $\cos\varphi \sim 0$ corresponding to high pseudorapidity. In contrast, the distribution from mesino or sbaryon decay is roughly uniformly distributed in $-1 \lesssim \cos\varphi \lesssim 1$. Mesino and sbaryon decay may therefore be distinguished by high E_T jets with large $\not{E}_T$ and with large negative impact parameters (LNIPs), where the sign of the impact parameter is taken to be $\text{sgn}(\cos\varphi)$. Negative impact parameters defined in this way result if the visible decay products recoil against the invisible Goldstino in a direction towards, rather than away from the production vertex. Equivalently, the jet appears to originate on the "wrong side" of the production vertex.

Stop squarks which decay with a macroscopic decay length either by $\tilde{t} \to c\widetilde{G}$ or $\tilde{t} \to bW\widetilde{G}$ or $\tilde{t} \to t\widetilde{G}$ could be uncovered with an LNIP search. In the case of the charm final state an LNIP search could be applied to the SUGRA search for stop pair production in events with two charm jets and $\not{E}_T$. In the case of the top-like final states, the top quark background could be significantly reduced by requiring large impact parameters for the W decay products in a top quark sample. This could easily be implemented by requiring that none of the leptons be associated with the interaction vertex in a di-lepton or lepton-hadron top quark sample.

LNIPs provide an efficient means to search for any exotic massive metastable particles which decay to hadronic final states. In particular, a search for LNIPs would also be sensitive to a Higgsino-like neutralino NLSP, discussed in section V and V C, which decays with a macroscopic decay length by $\widetilde{\chi}_1^0 \to h\widetilde{G}$ with $h \to bb$ or $\widetilde{\chi}_1^0 \to Z\widetilde{G}$ with the Z decaying hadronically.

Displaced jets arising from neutral mesinos or sbaryons which decay within the tracking region would appear as incomplete tracks leading to jets with very large impact parameter. A charged mesino or sbaryon which decays within the tracking region might be identified as a HIT stub intersecting a displaced jet. A search for decay lengths in this regime would require rather specialized analysis of events with large hadronic E_T and $\not{E}_T$.

C Quasi-stable Mesino and Sbaryon Signals

Quasi-stable NLSP squarks hadronized in mesino and sbaryons with long enough life times to partially or completely traverse a detector lead to a number of interesting phenomena. It should first be noted that even though squarks carry significant momentum from the production vertex, there can only be very soft hadronic activity associated with squark hadronization. This is because massive squarks are non-relativistic, and in the heavy particle limit it is the relative velocity which determines the magnitude of any jet activity associated with hadronization. Likewise, when a non-relativistic hadronized mesino or sbaryon decays by decay of the constituent squark, the bound state light quark(s) do not lead to significant jet activity since by decoupling the high momentum squark decay products can not transfer significant energy to the low momentum light quark(s).

The energy of the bound state quark(s) are only of order the QCD scale binding energy. These observations about jet activity are of course also true for any of the non-prompt squark decay signatures discussed in sections VIII B or VIII D, and also for the prompt squark decay signatures discussed in section VIII A since in that case the decay length still greatly exceeds the hadronization scale.

Long-lived squarks may hadronize as either neutral or charged mesinos or sbaryons. A neutral non-relativistic strongly interacting bound state will experience only a few rather soft hadronic interactions as it moves through a detector. The calorimeters will therefore only detect a small fraction of its energy compared with a usual relativistic jet of showering particles. This will result in an apparent $\not{E}_T$ signature [61,62]. Since there are two NLSPs produced in each event, and since there is minimal jet activity associated with squark hadronization, the total missing transverse momentum vector can point in a direction different from any jet in the event.

A charged non-relativistic quasi-stable mesino or sbaryon is very similar to a quasi-stable stau slepton. Because of the increased ionization of a slowly moving massive charged particle, highly ionizing tracks (HITs) result in the tracking region of a detector. However, a non-relativistic strongly interacting bound state which contains light quarks can exchange isospin and charge with background material in a detector through hadronic interactions [61,62]. Such particles make transitions between neutral and charged states as they pass through matter. It is important to note that in the non-relativistic limit, only bound states which contain light quarks (rather than anti-quarks), namely anti-mesinos and sbaryons, can significantly charge exchange with matter [61]. Non-relativistic anti-mesinos and sbaryons moving through a detector therefore yield the phenomenon of intermittent charge exchange associated with highly ionizing tracks (CE-HITs). Depositions in the calorimeter alternate between highly ionizing charged and neutral segments.

The oscillation length between charged and neutral anti-mesino states can be estimated in the heavy squark and chiral limits from the forward scattering isospin exchange amplitude in matter. In the chiral limit the neutral and charged states are degenerate (ignoring electromagnetic mass splittings), and isospin exchange operators are of the form $(4\pi/\Lambda_\chi)^2\ \overline{\mathcal{M}}\vec{\tau}\Gamma\mathcal{M}\cdot\overline{N}\vec{\tau}\Gamma N$ where $\mathcal{M}$ and N are the mesino and nucleon operators respectively, τ is the Pauli isospin matrix, Γ is a Dirac matrix representing the general Lorentz structure, $\Lambda_\chi \simeq 1.1$ GeV is the chiral symmetry breaking or cut off scale, and the estimate of the coefficient follows from consistency of the cutoff chiral Lagrangian. This yields an oscillation length in matter of

$$\lambda(\overline{\mathcal{M}}^{\pm} \leftrightarrow \overline{\mathcal{M}}^{0}) \sim \frac{1.2\ \mathrm{m}}{\rho/(\mathrm{gm\ cm}^{-3})} \tag{8.8}$$

where ρ is the material density. It should be noted that the actual oscillation length may differ from this estimate by up to a factor of a few.

The exchange length per unit density for a CE-HIT is small enough so that an antimesino or sbaryon is unlikely to charge exchange in the inner tracking region of a detector. However charge exchange in the calorimeter region is possible. This can have the effect of converting a charged antimesino or sbaryon which leaves a HIT in the inner tracking region to a neutral state which does not register in the outer muon system. Conversely intermittent tracks in the muon system can arise from an initial neutral antimesino or sbaryon which does not register in the inner tracking region. The intermittent nature of CE-HITs can also reduce charge track trigger efficiency and contribute to $\not{E}_T$. Mis-identification of CE-HITs can also contribute to $\not{E}_T$.

A non-relativistic charged mesino or anti-sbaryon contain light antiquarks, and are therefore less likely to charge exchange in matter than the anti-particle counterparts. These slowly moving charged states experience a few rather soft hadronic interactions as it moves through a detector, just as the neutral states. Because of the additional hadronic activity along the track, these particles yield hadronic highly ionizing tracks (H-HITs). In the inner tracking region H-HITs are likely to appear simply as HITs. However, the additional hadronic activity could be recorded by the calorimeter.

Using CE-HITs as a discovery mode for a long lived NLSP squark is problematic because of possibly significant backgrounds from, for example, cosmics and because of the uncertainty in the charge exchange rate. More useful would be a HIT search based only on the inner tracking region. Both CE-HITs and H-HITs should appear as HITs in the inner tracker. Reconstruction of CE-HITs and H-HITs in the outer tracking region might be attempted in a sample of inner tracker HITs. TOF information utilizing the outer muon system might also be used, but with reduced efficiency compared with a stau HIT due to charge exchange in the calorimeter. The $\not{E}_T$ implied by the intermittency of CE-HITs, or the $\not{E}_T$ from squarks hadronized in a neutral bound state might also be useful in identifying events.

It is interesting to note that a bound state NLSP squark could be identified as either an up- or down-type squark if the sign of the charged segments of CE-HITs could be determined. An up-type anti-squark bound in an antimesino with a quark is either negatively charged or neutral, $\overline{\mathcal{M}}^{-}$ or $\overline{\mathcal{M}}^{0}$. Conversely, a down-type

anti-squark bound in an antimesino with a quark is either positively charged or negative, $\overline{\mathcal{M}}^+$ or $\overline{\mathcal{M}}^0$. Since hadronization in (anti)sbaryon states is less likely than in (anti)mesino states, and since CE-HITs arise mainly for antimesinos rather than mesinos, an excess of negative over positive CE-HITs would imply an up-type NLSP anti-squark, while an excess of positive over negative CE-HITs would imply a down-type NLSP anti-squark.

Finally, a bound state squark which decays within the detector might be observed by a H-HIT which ends with a jet, an H-HIT to jet kink. Events of this type might be identified by HITs in the inner tracking region which end in a jet or deposited energy in the calorimeter.

D Mesino Oscillations

A mesino bound state of a squark and antiquark, $\mathcal{M}_{\widetilde{Q}\bar{q}} \equiv (\widetilde{Q}\bar{q})$, is a spin $\frac{1}{2}$ Dirac fermion. A neutral mesino and its antiparticle differ by two units of (s)flavor, fermion number, F, and R-charge. All of these quantum numbers are, however, manifestly violated in any supersymmetric theory. (S)quark flavor is violated by Yukawa couplings and squark flavor may also be violated by scalar tri-linear couplings and possibly the scalar mass-squared matrices. Fermion number and R-symmetry are violated by gaugino masses. Since no conserved quantum number distinguishes a mesino from antimesino, these states can mix. So hadronization of squarks into neutral mesino bound states allows for the interesting phenomenon of particle–antiparticle oscillations which is impossible for an isolated charged particle.

Mesino oscillations are analogous to meson oscillations. At the microscopic level the $\Delta\tilde{Q} = \Delta q = \Delta F = \Delta R = 2$ amplitudes which mix mesino and antimesino are typically dominated by tree level gluino exchange [57]. For a stop-like neutral mesino the gluino contribution to the $\mathcal{M}_{\tilde{t}\overline{u}} \leftrightarrow \overline{\mathcal{M}}_{\tilde{t}^*u}$ oscillation wavelength, $\beta\gamma\lambda$, is numerically [57]

$$\lambda \simeq (4 \text{ nm}) \left(\frac{m_{\tilde{g}}}{250 \text{ GeV}}\right)^2 \frac{f(m_{\tilde{t}}/m_{\tilde{g}})}{\sin^2\theta_{\tilde{u}\tilde{t}}} \tag{8.9}$$

where $\sin\theta_{\tilde{u}\tilde{t}}$ is the up squark-stop mixing angle, $f(y) = y(1-y^2)$, and by assumption $y < 1$ so $0 < f(y) < \sqrt[3]{2/3} \simeq 0.38$. Oscillations on the scale of a detector could occur for $\sin\varphi_{\tilde{u}\tilde{t}}$ as small as 5×10^{-5}. Up-type sflavor violation involving the third generation is essentially unconstrained by present data, so extremely rapid oscillations compared with the decay length and scale of a detector are conceivable.

The time-integrated probability for an NLSP squark hadronized as a mesino to oscillate to an antimesino and decay as an antisquark depends on the oscillation frequency and decay rate

$$\mathcal{P}(\mathcal{M} \to \overline{\mathcal{M}}) = \frac{x^2}{2(1+x^2)} \tag{8.10}$$

where $x = (2\pi/\Gamma)/\lambda$ is the ratio of the decay length to oscillation length. Rapid oscillations, $x \gg 1$, yield $\mathcal{P}(\mathcal{M} \to \overline{\mathcal{M}}) = \frac{1}{2}$, while for slow oscillations, $x \ll 1$, $\mathcal{P}(\mathcal{M} \to \overline{\mathcal{M}}) \to \frac{1}{2}x^2$.

Neutral mesino–antimesino oscillations present the possibility of novel experimental signatures, even for decay lengths which are too short to be resolved in real space. Oscillations may be revealed in any decay mode which tags the sign of the (anti)squark in a neutral (anti)mesino. Squark–antisquark production events in combination with mesino–antimesino oscillation can then lead to same-sign events. For example, the antisquark may hadronize as a neutral antimesino which oscillates to a mesino before decaying, while the squark hadronizes as a charged mesino or sbaryon which can not oscillate. Summing over all possibilities, the time-integrated ratio of same- to opposite-sign events is

$$R \equiv \frac{N_{++} + N_{--}}{N_{+-} + N_{-+}} = \frac{2\mathcal{P}f_0(1-\mathcal{P}f_0)}{1 - 2\mathcal{P}f_0 + 2\mathcal{P}^2 f_0^2} \simeq 2\mathcal{P}f_0 + 2\mathcal{P}^2 f_0^2 \tag{8.11}$$

where $\mathcal{P} \equiv \mathcal{P}(\mathcal{M} \to \overline{\mathcal{M}})$, and f_0 is the neutral mesino hadronization fraction. Thus, for $x \gtrsim 1$ a significant fraction of squark–antisquark events will yield same-sign events.

The feasibility of determining the sign of an (anti)squark at decay depends on the decay products. For stop-like squark decays $\tilde{t} \to bW\widetilde{G}$ or $\tilde{t} \to t\widetilde{G}$ with $t \to bW$, the W-bosons reliably tag the sign of the (anti)squark. The W-bosons signs may in turn be determined with the leptonic decay mode $W \to \ell\nu$ where $\ell = e, \mu$. This requires isolating these primary leptons from any secondary leptons arising from b-quark decay. Such

distinctive, essentially background free events have the topology of same-sign top-top events in the di-lepton channel, and provide a possible discovery mode for SUSY. The largest background is probably from top-antitop production with the very small probability of misidentification of the primary leptons or mismeasurement of the charges. At the Fermilab Tevatron Run IIa with 2 fb^{-1} of integrated luminosity, a 175 GeV stop squark with dominant decay $\tilde{t} \to bW\widetilde{G}$ and oscillation parameter $x \sim 1$ would yield ~ 10 same-sign dilepton top-top events, while $x \gg 1$ would yield ~ 20 events. A detection acceptance times efficiency $\gtrsim 30\%$ should give a detectable signal for these parameters.

Observation of stop mesino oscillations requires, and very sensitively probes, up-type squark sflavor violation. For example, for a stop decay length $\Gamma^{-1} \sim 10$ cm, maximal $\mathcal{M}_{\tilde{t}\bar{u}} \leftrightarrow \overline{\mathcal{M}}_{\tilde{t}^*u}$ mixing, $x \gtrsim 1$, occurs for all $\epsilon_{(N)13} \gtrsim 5 \times 10^{-5}$. Even for $\Gamma^{-1} \sim 2$ μm (which could not be resolved as a displaced vertex), maximal mixing occurs for any $\epsilon_{(N)13} \gtrsim 10^{-2}$. The magnitude of squark sflavor violation depends on the scale at which (s)quark flavor is broken. If the flavor scale is not too much larger than the messenger scale for transmitting supersymmetry breaking, interesting levels of sflavor mixing are expected, and observable mesino oscillations can occur.

The flavor violating two-body decay $\tilde{t} \to c\widetilde{G}$ can dominate if sflavor violation is large enough, as discussed above. This mode also dominates if the NLSP squark is scharm-like, $\tilde{c} \to c\widetilde{G}$. Semi-leptonic decay of the c-quarks hadronized in $D^{0,\pm}$-mesons could then be used to tag same-sign events in high E_T charm-jets with large $\not{E}_T$. $D^0 \leftrightarrow \overline{D}^0$ oscillation is negligible and would not contaminate a mesino oscillation signal at the discovery level in a relatively clean sample of LNIPs. However, squark decays in this mode with a decay length that is too short to resolve using LNIPs would be contaminated by standard model production of b-jets which are not easily distinguished from charm-jets. This standard model background could be significant since $B^0 \leftrightarrow \overline{B}^0$ oscillations are non-negligible. Self-tagging of the heavy flavor at production to determine its sign or measuring total jet charge after decay to isolate $D^{\pm}$ mesons which do not oscillate could reduce this background, but requires large statistics, and is probably not applicable at the discovery level.

Observing oscillations for a squark NLSP which decays to other flavors is more problematic. For a sbottom-like squark which decays by $\tilde{b} \to b\widetilde{G}$, the B^0-meson backgrounds discussed above are important. Decays to lighter quarks, $\widetilde{Q} \to (u, d, s)\widetilde{G}$, are difficult to sign using self tagging. So a stop-like NLSP squark provides the best opportunity to observe mesino oscillations, in particular in same-sign events in the di-lepton top-top channel [57].

It is worth noting that if the mesino decay length is macroscopic *and* the oscillation length is fortuitously of the same order, $x \sim 1$, mesino oscillations could be observed in real space in the signed decay length distributions. This would allow a direct measure of the oscillation length, and give an accurate determination of the up-squark-stop mixing angle.

1 CDF study of Mesino Oscillations

The CDF top quark analysis results may be used to investigate the like sign top-top mode in the di-lepton channel. In Run I with 109 pb^{-1} of integrated luminosity, 9 events with opposite–sign leptons, $\not{E}_T$ and two jets were found, with an expected background of 2.4 ± 0.5. Two events with like–sign leptons were also found, with an expected background of 0.61 ± 0.44 [63]. Using simple Poisson statistics, it is possible to exclude more than approximately 6 events of anomalous like-sign top-top production. To set the scale, note that 6 events is approximately the same as what is expected from the top cross section of 5 pb. So Run I would not be sensitive to stop pair production with mesino oscillation for a stop mass similar to the top quark mass since in this case the stop pair production cross section is an order of magnitude smaller than for top pair production.

IX OTHER NLSP SCENARIOS

In principle any of the MSSM superpartners may be an NLSP. It is therefore worth considering the signatures associated with NLSP types not studied in detail as part of the Run II workshop. While perhaps unconventional and not as well studied, because of some novel and unique signatures associated with other NLSP types, these possibilities should not be overlooked in the search for SUSY in Run II.

A Gluino NLSP

The gluino is most likely to arise as the NLSP in theories of GMSB with both suppressed supersymmetry breaking for the strongly interacting messenger fields and suppressed $U(1)_R$ breaking. Since the gluino does not mix with any other states, it can only decay to the Goldstino through emission of a gluon,

$$\widetilde{g} \to g\widetilde{G} \tag{9.1}$$

Direct gluino pair production is the largest SUSY production cross in the gluino NLSP scenario.

If the decay $\widetilde{g} \to g\widetilde{G}$ occurs promptly, then the signature will be a pair of very hard gluon jets, accompanied by large $\not{E}_T$. A detailed study of this signal has not been performed. But there may be some reach, possibly significant, in this channel at Run II, provided that the cuts on the $\not{E}_T$ and the E_T of the two hardest jets in an event are chosen suitably high to defeat backgrounds from $Z \to \nu\overline{\nu}$ production, jet energy mismeasurements, missed partons, etc.

A gluino NLSP with macroscopic decay length can lead to other interesting signatures. An NLSP gluino, which is an octet of $SU(3)_C$, hadronizes with either a gluon or light quark and antiquark to form what is generally referred to as an R-hadron bound state, $\widetilde{R}^0 \equiv (\widetilde{g}g)$ or $\widetilde{R}^{0,\pm} \equiv (\widetilde{g}q\bar{q})$. If the decay length is macroscopic, but contained within the tracking region, large E_T displaced jets with large $\not{E}_T$ result. These can be identified in an LNIP search described in section VIII B in the context of a squark NLSP.

For decay lengths comparable to or larger than a detector, the signatures of the charged or neutral R-hadron bound states are similar to the quasi-stable mesino and sbaryon signatures discussed in section VIII C. If the mass difference between $\widetilde{R}^{\pm}$ and $\widetilde{R}^0$ is less than the pion mass, then both are effectively stable on the scale of the detector. A neutral $\widetilde{R}^0$ contributes to $\not{E}_T$. A charge $\widetilde{R}^{\pm}$ should appear as a HIT in the inner tracking region. In addition, an R-hadron can charge exchange with detector material, yielding an intermittent charge exchange associated with a highly ionizing track (CE-HIT) as described in more detail for a squark NLSP in section VIII C. Since charge exchange is probably not significant in the inner tracking region of the detector, the best search strategy may be an attempt to identify CE-HIT signatures in the outer tracking region in a sample of inner tracking region HITs. The $\not{E}_T$ which arises neutral neutral $\widetilde{R}^0$-hadrons and the intermittent nature of CE-HIT from charged $\widetilde{R}^{\pm}$-hadrons may also be useful in identifying events. Unlike antimesino and sbaryon CE-HITs, the charged segments of R-hadron CE-HITs are equally likely to have positive or negative charge.

B Singletino NLSP

Some extensions of the MSSM contain singlet superfields without Standard Model quantum numbers. Gauge invariance implies that such scalar singlet and fermionic singletino fields can mix at the renormalizable level only with the Higgs and Higgsino fields. Singlet fields may in fact be motivated in GMSB by the necessity of additional interactions in the Higgs sector [10,64] discussed in Appendix A2i. If the NLSP is a neutralino with a large fermionic singletino component, it decays mainly through its mixing with the Higgsino to a Higgs or Z boson,

$$\widetilde{\chi}_1^0 \to (h, Z)\widetilde{G} \tag{9.2}$$

The signatures for prompt decay are then very similar to the Higgsino-like neutralino NLSP discussed in section V. If the scalar singlet, ϕ, is lighter than $\widetilde{\chi}_1^0$, the NLSP decay

$$\widetilde{\chi}_1^0 \to \phi\widetilde{G} \tag{9.3}$$

dominates. However, this still generally gives rise to visible signatures since ϕ is likely to decay mainly through its mixing with Higgs by $\phi \to bb$ [64].

C Neutralino-Stau Co-NLSP

The slepton co-NLSP scenario discussed in section VII in which the splitting between the sleptons is smaller than the lepton masses is natural if the messenger interactions do not violate lepton flavor, as is the case in

the MGM. It is also possible that some of the superpartners just happen to be close enough in mass to give a co-NLSP scenario, even though no symmetry enforces this near degeneracy. This in fact occurs in the MGM at low to moderate $\tan\beta$ with $N = 2$ generations of messengers and the messenger scale not too far above the supersymmetry breaking scale. In this case the lightest neutralino, $\widetilde{\chi}_1^0$, and the right handed sleptons, $\tilde{l}_R$, just happen to be nearly degenerate [4]. A near degeneracy between $\widetilde{\chi}_1^0$ and $\widetilde{\tau}_1$ can also occur in a somewhat smaller region of parameter space for $N = 3$ with large $\tan\beta$. For $|m_{\tilde{\chi}_1^0} - m_{\tilde{\tau}_1}| < m_\tau$, either the decays $\widetilde{\chi}_1^0 \to \tau\widetilde{\tau}_1$ or $\widetilde{\tau} \to \tau\widetilde{\chi}_1^0$ are blocked kinematically, depending on the mass ordering. In this case $\widetilde{\chi}_1^0$ and $\widetilde{\tau}_1$ share the role of NLSP, since they each have no kinematically allowed decays except into the Goldstino. In this scenario, all SUSY decay chains terminate either in

$$\widetilde{\chi}_1^0 \to \gamma\widetilde{G} \quad \text{or} \quad \widetilde{\tau}_1 \to \tau\widetilde{G} \tag{9.4}$$

Cascades passing through $\widetilde{\chi}_1^0\widetilde{\chi}_1^0$ or $\widetilde{\tau}_1\widetilde{\tau}_1$ should give similar signatures to those of the Bino-like Neutralino NLSP discussed in section IV or the stau NLSP discussed in section VI respectively. Cascades passing through $\widetilde{\chi}_1^0\widetilde{\tau}_1$ would give a mixed signature, and could be searched for in a $\gamma X \not{E}_T$ event sample. The sensitivity in each these modes of course depends on the precise branching ratios of the cascade decays.

D Sneutrino NLSP

Finally, for completeness the possibility of a sneutrino NLSP may also be considered. Both $\widetilde{\nu}$ and ν interact only weakly, and so escape the detector without depositing energy. An NLSP decay $\widetilde{\nu} \to \nu\widetilde{G}$ is therefore unobservable. In this case the only signatures available would be from cascade decays, $X\not{E}_T$, to the NLSP $\tilde{\nu}$.

X DIRECT GOLDSTINO PAIR PRODUCTION

The overall mass scale for Standard Model superpartners could be related to the electroweak scale, but may still be too heavy to allow direct superparticle production in Run II. However, with low scale supersymmetry breaking the gravitino is very light compared with collider energies, and is always kinematically accessible. In principle then, final states could arise with the Goldstino components of the gravitino as the only supersymmetric particles. With R-parity conservation supersymmetric particles are produced in pairs, so the simplest example of this type is Goldstino pair production. At a hadron collider the dominant contribution is likely to come from t- and u-channel virtual squark exchange [65]. The weakly interacting Goldstinos escape the detector, yielding an invisible event. However, initial–state radiation may be used to tag such events, giving a signature of one jet and $\not{E}_T$ or one photon and $\not{E}_T$. The supersymmetry breaking scale must be extremely low (right at the electroweak scale) in order for this process to yield an observable signal. If this interesting scenario were realized in nature, essentially all the superpartners would probably be very strongly coupled to the supersymmetry breaking sector.

1 CDF studies of direct Goldstino production

CDF has searched for the one jet and $\not{E}_T$ signature in the Run I data [66]. The trigger is based on $\not{E}_T$ which has a nominal 35 GeV threshold. A large set of clean–up cuts are necessary to remove the copious backgrounds from cosmic rays and from QCD events with severely mismeasured $\not{E}_T$. In addition, the leading jet must have $E_T > 80$ GeV and there must be no leptons with $E_T > 10$ GeV, which could indicate a $W \to \ell\nu$ decay. The final $\not{E}_T$ requirement is optimized to be 175 GeV.

With this set of cuts, 19 events remain while 22 ± 7 are expected from Standard Model sources, mostly from $Z \to \nu\nu$ plus an initial–state radiation jet. Comparing to cross section estimates for Goldstino pair production [65], the result excludes approximately $\sqrt{F} > 217$ GeV which corresponds to $m_{\tilde{G}} \geq 1.1 \times 10^{-5}$ eV. For Run II, the important backgrounds have been extrapolated using the ratio of the cross sections at 1.8 TeV and 2.0 TeV. The result is an expected 20% increase in the backgrounds. Assuming that the systematic uncertainty in the background remains at 30%, the expected limit with 2 fb^{-1} of integrated luminosity is $\sqrt{F} > 260$ GeV or $m_{\tilde{G}} \geq 1.6 \times 10^{-5}$ eV. The rather modest increase in the expected bound on the supersymmetry breaking scale

(or equivalently the Goldstino decay constant) over the Run I limit follows from the derivative coupling of the Goldstino which implies the cross section is a rapidly falling function of the supersymmetry breaking scale, proportional to $(1/\sqrt{F})^8$ or $(1/m_{\tilde{G}})^4$.

XI SUMMARY

In this report the potential of the Fermilab Tevatron Run II for discovery and study of low-scale supersymmetry breaking has been assessed. Low scale gauge mediated supersymmetry breaking provides a particularly attractive theoretical solution to the problem of flavor-violation in the supersymmetric Standard Model. The existence of a nearly massless Goldstino to which the NLSP can decay, provides an attractive and rich set of experimental possibilities for Run II, with a variety of potentially spectacular signals. The various classes of signals depend on the identity of the NLSP and its decay length.

The experimental signatures which have been identified in this report as being useful for the Tevatron Run II and future upgrades are summarized in Table 24 and below:

1. Bino-Like NLSP
   - For prompt decays of a Bino-like $\tilde{\chi}_1^0$ NLSP, there will be a very substantial reach in the $\gamma\gamma$ X $\not{E}_T$ channel, where X can be anything, but likely includes jets.
   - Cascade decays to the Bino-like $\tilde{\chi}_1^0$ NLSP can include a neutral Higgs boson, h, with fairly high probability. The SUSY signature of two hard photons and $\not{E}_T$ could then be used as a unique method of obtaining a sample of Higgs bosons.
   - For macroscopic decay lengths of a Bino-like $\tilde{\chi}_1^0$ NLSP, the resulting displaced photons can be resolved and provide a useful signal. The properties of the DØ preradiator allow for a particularly sensitive probe of decay lengths down to the few centimeter level.
2. Higgsino-Like NLSP
   - Prompt decays of a Higgsino-like $\tilde{\chi}_1^0$ NLSP can yield γ, h, and Z bosons, giving rise to signatures with photons, b-jets, jets, and reconstructed leptonic Z bosons in combinations that depend strongly on the underlying SUSY parameters. This allows for a particularly rich set of possibilities for event selections. Many of the signatures are interesting on general grounds, since they can arise in other, unrelated, new physics scenarios.
   - The presence of Higgs bosons from $\tilde{\chi}_1^0$ decays can lead to a interesting source of tagged Higgs events.
   - For decays of a Higgsino-like $\tilde{\chi}_1^0$ NLSP with macroscopic decay length, but contained within the detector, displaced photons, displaced Z bosons, or displaced Higgs bosons arise. The displaced hadronic final states, including b-jets from displaced Higgs decay, yield tracks with large negative impact parameters (LNIPs) with reconstructed displaced jets pointing towards, rather than away from, the beam axis.
3. Stau NLSP
   - Prompt decays of a $\tilde{\tau}_1$ NLSP give rise to events with same-charge taus (either manifested as hadronic one-prong or three-prong decays, or as leptonic decays). Depending on the underlying SUSY parameters a variety of different multi-lepton and multi-tau event selections are possible. In some cases, it is best to require an additional one or two hard jets, since these occur in SUSY cascade decays but not in relevant backgrounds. All these signatures depend crucially on tau identification efficiency, which will need to be evaluated once the detectors are operating.
   - Stau decays that take place within the instrumented region of a detector yield events with a decay kink. Such a non-relativistic stau leaves a highly ionizing track (HIT) with a kink to a hadronic tau jet or an e or μ from a leptonic tau decay.
   - Quasi-stable staus which traverse the entire detector before decaying will appear either as HITs or an excess of fake "muons", i.e. minimum ionizing tracks (MITs). Both CDF and DØ have found a significant reach in this search. In addition, the CDF time-of-flight (TOF) detector has been found to be quite useful in this search since the staus are non-relativistic. Stau pairs will often have the same charge, allowing another useful handle on the events.

TABLE 24. Experimental signatures for different NLSP scenarios. LNIP $\equiv$ Large Negative Impact Parameter. MIT $\equiv$ Minimum Ionizing Track (muon candidate). HIT $\equiv$ Highly Ionizing Track (anomalously large dE/dx). CC-HIT $\equiv$ Charge Changing Highly Ionizing Track. CE-HIT $\equiv$ Charge Exchange Highly Ionizing Track. H-HIT $\equiv$ Hadronic Highly Ionizing Track. TOF $\equiv$ large Time of Flight measurement. $X \equiv$ Additional partons in the final state. If the decay length is comparable to the size of the detector, then signatures from two or three columns can appear simultaneously.

NLSP	Prompt Decay	Macroscopic Decay Length	Long-lived
Bino-$\widetilde{\chi}_1^0$	$\gamma\gamma\ X\ \not{E}_T$	(Displaced γ) $X\ \not{E}_T$ TOF	$X\ \not{E}_T$
Higgsino-$\widetilde{\chi}_1^0$	$(\gamma,h,Z)(\gamma,h,Z)\ X\ \not{E}_T$ $[\gamma b\ X\ \not{E}_T,\quad \gamma bjX\not{E}_T,$ $\gamma jj\ X\ \not{E}_T,\quad \gamma X\not{E}_T,$ $b\overline{b}\ X\ \not{E}_T,\quad bbb\ X\ \not{E}_T,$ $\gamma\ell\ell\ X\ \not{E}_T,\quad \ell\ell\ell\ell\ X\ \not{E}_T]$	(Displaced γ , Displaced Z , LNIP b-jets) $X\ \not{E}_T$ TOF	$X\ \not{E}_T$
$\widetilde{\tau}_1$	$\tau^\pm\tau^\pm\ X\ \not{E}_T$ $\ell^\pm\ell^\pm\ X\ \not{E}_T$ $\tau\tau\tau\ X\ \not{E}_T$ $\tau\tau\ell\ X\ \not{E}_T$ $\tau\ell\ell\ X\ \not{E}_T$ $\ell\ell\ell\ X\ \not{E}_T$ $\tau\tau\ell\ell\ X\ \not{E}_T$ $\tau\ell\ell\ell\ X\ \not{E}_T$	HIT $\rightarrow \tau$ kinks HIT $\rightarrow e,\mu$ kinks	HITs Same-Charge HITs Same-Charge MITs $\ell\ell\ell X\not{E}_T$ $\ell\ell\ell\ell X\not{E}_T$ CC-HITs TOF
$\widetilde{\ell}$ co-NLSP	(as for Stau NLSP, but with different profiles, lepton democracy) $\ell\ell\ell\ell\ X\ \not{E}_T$	HIT $\rightarrow e,\mu,\tau$ kinks	HITs $\ell\ell\ell X\not{E}_T$ $\ell\ell\ell\ell X\not{E}_T$ TOF
$\widetilde{Q}$	$jj\ X$ $cc\ X\ \not{E}_T$ $bb\ X\ \not{E}_T$ $tt\ X\ \not{E}_T$ Same-Charge $tt\ X\ \not{E}_T$	Displaced jets H-HIT $\rightarrow$ jet kinks LNIPs Mesino Oscillations	CE-HITs H-HITs $\not{E}_T$ TOF
$\widetilde{g}$	$jj\ X\ \not{E}_T$	Displaced jets LNIPs	CE-HITs H-HITs $\not{E}_T$ TOF

- The charge changing three-body cascade decays of selectrons and smuons, for example, $\widetilde{e}_R^+ \to e^+\tau^+\widetilde{\tau}_1^-$, can also have a macroscopic decay length if the selectron (or smuon) is nearly degenerate with the stau. The electron and tau released in the decay are typically very soft (and could easily be missed) with the final state stau traveling in the forward direction. This gives rise to charge-changing HITs (CC-HITs), since the non-relativistic selectron (or smuon) can convert to a stau of the opposite charge within the tracking region.

4. Slepton Co-NLSP

   - If the three lightest sleptons $\widetilde{\tau}_1$, $\widetilde{e}_R$, and $\widetilde{\mu}_R$ are degenerate in mass to within 1.8 GeV, then all three play the role of the NLSP. If the decays of the slepton co-NLSPs are prompt, a variety of signatures involving taus and leptons result. The event topologies are very similar to those in the Stau NLSP case, but the flavor and multiplicity profiles can be quite different. In particular, there is a greater tendency for lepton democracy in the events.
   - As in the case of a Stau NLSP, macroscopic or long decay lengths for slepton co-NLSPs can give rise to HIT$\to$ lepton kinks, HITs through the detector, an excess of fake "muons", and an anomalous TOF.

5. Squark NLSP

   - Prompt decay of a stop-like squark NLSP to a top-like final state gives a signature with a top quark event topology. Large $\not\!\!E_T$, lepton-b-jet invariant mass, and W boson polarization can be used to partially separate these from top quark backgrounds. Prompt decay to a charm final state can be searched for in a standard SUGRA analysis for stop pair production.
   - Decay of a squark NLSP over a macroscopic distance, but contained within the tracking region, gives rise to displaced jets with large E_T and $\not\!\!E_T$. The angular distribution of the displaced jets is roughly uniform, and may be searched for in events with large negative impact parameters (LNIPs) with the reconstructed displaced jets pointing towards, rather than away from, the beams axis.
   - Quasi-stable squarks (anti-squarks) will hadronize to form mesinos and sbaryons (anti-mesinos and anti-sbaryons). The slowly-moving anti-mesino and sbaryon bound states can exchange isospin and charge with background material in the course of traversing a detector. Non-relativistic bound states of these types therefore yield intermittent charge-exchange associated with highly ionizing tracks (CE-HITs) which alternate between highly ionizing charged and neutral segments in the calorimeter. Mis-identification of CE-HITs can contribute to $\not\!\!E_T$. Quasi-stable mesinos or anti-sbaryons do not as readily charge exchange. Squark and gluino bound states can also yield fairly soft hadronic activity along a highly ionizing track (H-HIT). This is due to inelastic hadronic interactions of the bound state with the calorimeter materials. Even though non-relativistic hadronized NLSP squarks can carry significant momentum, they deposit little energy in the calorimeters. Both CE-HITs and H-HITs are likely to appear as HITs in the inner tracking region.
   - NLSP squarks hadronized in mesino bound states can undergo mesino-antimesino oscillations. For stop-like squarks this yields events with a same sign top-top topology. Mesino oscillations might also be observed directly as oscillations in the signed decay length distributions.

6. Gluino NLSP

   - Prompt decay of a gluino NLSP will lead to events with two very hard gluon jets and very large $\not\!\!E_T$.
   - For decays of a gluino NLSP with macroscopic decay length, but contained within the detector, large E_T displaced gluon jets with large $\not\!\!E_T$ result. These can be searched for in a sample of LNIPs.
   - Quasi-stable gluino NLSPs hadronize as R-hadrons and can charge exchange with matter, resulting in CE-HITs. Charged non-relativistic R-hadrons should appear as HITs in the inner tracking region and have anomalous TOF.

We look forward to the implementation of these signatures in searches for low-scale supersymmetry using real Run II data.

APPENDIX A: MINIMAL GAUGE MEDIATION AND VARIATIONS

The precise definition of the minimal model of gauge-mediated supersymmetry breaking (MGM) used in many of the studies presented in this report is outlined below. This model, however, can not represent a full theory of gauge-mediated supersymmetry breaking. Some of the important variations and extensions of the minimal model which affect the phenomenology are therefore also described below. For reviews of the MGM see Ref. [4,12].

1 Minimal model of gauge mediation

Gauge-mediated supersymmetry breaking results if some of the fields in the messenger sector which feel supersymmetry breaking also transform under the Standard Model gauge group. Soft masses for visible sector superpartners then arise radiatively. The successful supersymmetric prediction of gauge coupling unification is not affected if the messenger fields form unifiable representations. In the MGM the messenger fields are taken to be N generations of chiral supermultiplets, Φ_i and $\overline{\Phi}_i$, each transforming as $\mathbf{5} \oplus \overline{\mathbf{5}} \in SU(5) \supset SU(3)_C \times SU(2)_L \times U(1)_Y$. The messenger fields couple to a Standard Model singlet chiral superfield, S, through the superpotential coupling

$$W = \lambda S \Phi_i \overline{\Phi}_i, \tag{A.1}$$

where λ is a dimensionless coupling. Both the scalar component of the singlet superfield, S, and auxiliary component, F_S, are assumed to acquire expectation values. The origin of the these expectation values are not specified in the MGM, and may simply be taken as background spurions. In a full theory the F_S auxiliary expectation value felt by the messengers may not coincide with the intrinsic supersymmetry breaking order parameter F which determines the Goldstino decay constant. For this reason it is useful to define a factor $C_G \geq 1$ which relates the Goldstino decay constant with F_S:

$$F = C_G F_S. \tag{A.2}$$

For a fixed value of F_S, the decay rate of the NLSP to its Standard Model partner and Goldstino is therefore proportional to $1/C_G^2$. In a full theory the auxiliary expectation values would presumably arise ultimately from non-perturbative gauge dynamics in the supersymmetry breaking sector.

The fermionic components of Φ_i and $\overline{\Phi}_i$ obtain Dirac masses from the S scalar expectation value

$$m_{\psi_i} = \lambda S \equiv M_m. \tag{A.3}$$

The auxiliary expectation value gives rise to a holomorphic soft supersymmetry breaking mass for the scalar messengers. The resulting scalar mass squared matrix

$$\begin{pmatrix} m_{\psi_i}^2 & \lambda F_S \\ \lambda F_S & m_{\psi_i}^2 \end{pmatrix} \tag{A.4}$$

has mass eigenvalues

$$m_{\pm i} = m_{\psi_i} \sqrt{1 \pm \Lambda / m_{\psi_i}}, \tag{A.5}$$

where

$$\Lambda \equiv \frac{F_S}{S} \tag{A.6}$$

The scalar expectation value S sets the overall mass scale for the messengers, while the auxiliary expectation value, F_S, sets the supersymmetry breaking scale through the mass splitting $m_{\psi_i} - m_{\pm i}$ between the messenger fermions and scalars.

Supersymmetry breaking in the messenger fermion and scalar spectrum is transmitted radiatively to the visible sector superpartners by gauge interactions. The gauginos couple directly to the messengers and acquire a mass radiatively from a single messenger loop,[†]

$$M_a = k_a N \Lambda \, \frac{\alpha_a}{4\pi} \tag{A.7}$$

where $a = 1, 2, 3$ for the Bino, Wino, and gluino respectively, and $k_1 = \frac{5}{3}$, $k_2 = k_3 = 1$. The scalars gain mass at two loops from a gauge loop coupling the scalars to a messenger loop

$$m_\phi^2 = 2N\Lambda^2 \left[\frac{5}{3} \left(\frac{Y}{2} \right)^2 \left(\frac{\alpha_1}{4\pi} \right)^2 + C_2 \left(\frac{\alpha_2}{4\pi} \right)^2 + C_3 \left(\frac{\alpha_3}{4\pi} \right)^2 \right], \tag{A.8}$$

where Y is the ordinary weak hypercharge normalized as $Q = T_3 + \frac{1}{2}Y$, $C_2 = \frac{3}{4}$ for weak isodoublet scalars and zero for weak isosinglets, and $C_3 = \frac{4}{3}$ for squarks and zero for other scalars. Since gaugino masses arise at one loop while scalar masses squared at two loops, the gaugino and scalar masses are the same order. In addition, since the supersymmetry breaking is transmitted by the Standard Model gauge interactions, the superpartner masses are roughly in proportion to their gauge couplings squared. The factors of N in (A.7) and (A.8) count the multiplicity of messenger generations in the messenger loops. Gaugino masses scale like N while scalar masses scale like $\sqrt{N}$. Finally, it is worth noting that the scalar masses squared (A.8) are fortuitously positive. A negative result would have rendered this class of models untenable.

The visible sector gaugino and scalar radiative masses (A.7) and (A.8) are generated at the messenger scale M_m with the appropriate gauge couplings evaluated at that scale. These masses must therefore be evolved to the electroweak scale by renormalization group running.

The dimensionful Higgs sector parameters which determine the electroweak scale must be linked in some way to supersymmetry breaking. These parameters violate $U(1)_{PQ}$ in the superpotential mass term which determines the Higgsino Dirac mass:

$$W = \mu H_u H_d, \tag{A.9}$$

and $U(1)_{R-PQ}$ in the Higgs soft mass parameter

$$V = -m_{ud}^2 H_u H_d \; + \; h.c. \tag{A.10}$$

Unlike the gaugino and scalar masses, these terms are not generated simply by gauge couplings to the messenger sector. These mass parameters must arise in a viable model, implying there must be additional interactions between the visible and messenger sectors which violate $U(1)_{PQ}$ and $U(1)_{R-PQ}$ symmetries. In the MGM the detailed form of these interactions is not specified and μ and m_{ud}^2 are taken to be free parameters. For phenomenological studies it is most useful to eliminate these parameters in favor of $\tan\beta$ and m_Z by imposing the constraints of electroweak symmetry breaking. Radiative electroweak symmetry breaking, in which the up-type Higgs mass squared is driven negative by the stop squark soft mass through the large top quark Yukawa coupling under renormalization group evolution, naturally occurs in the MGM. Most numerical codes which evolve the soft masses from the messenger scale using the renormalization group equations and solve the constraints of electroweak symmetry breaking, such as ISAJET in versions 7.34 and later, employ the full one-loop corrected Higgs potential. In the MGM the boundary condition for the soft Higgs masses at the messenger scale are identical to the left handed sleptons which have the same gauge quantum numbers.

Soft tri-linear A-terms are not generated directly at one-loop by gauge interactions with the messenger sector fields. These terms therefore vanish at the messenger scale, but are generated under renormalization group evolution below the messenger scale. For this reason A-terms are typically smaller in magnitude than the soft masses in the MGM unless the messenger scale is quite large.

An appealing feature of gauge-mediated supersymmetry breaking is the natural lack of supersymmetric flavor violation. Since the Standard Model gauge interactions are flavor independent, the radiatively induced superpartner soft masses do not violate flavor. In a full theory this would be the case if the scale for determining the flavor structure of the Standard Model Yukawa couplings is well above the messenger scale. If this scale is at or below the messenger scale, however, interesting levels of supersymmetric flavor mixing could occur.

[†] Note that here and in the following the Standard Model normalization $\alpha_1 = g'^2/4\pi$ is employed. In the literature, the GUT normalization, which absorbs the factor of $k_1 = \frac{5}{3}$ into α_1, is often used. Due care should be exercised when comparing formulas from different sources.

2 Beyond minimal gauge mediation

The minimal model of gauge mediation described above can not represent the full theory of supersymmetry breaking. Even so it does capture some of the important features expected in many classes of theories of gauge-mediated supersymmetry breaking. Important features of more complete theories can, however, differ significantly from the minimal model. Some of the more important variations and extensions of the minimal model and the effects on accelerator phenomenology are described below.

i) *Non-gauge corrections to Higgs masses*

The most serious deficiency of the MGM is the lack of specific interactions which break the $U(1)_{PQ}$ and $U(1)_{R-PQ}$ symmetries and give rise to the Higgs sector mass parameters μ and m_{ud}^2 described above. Any realistic theory must contain additional interactions between the Higgs superfields and messenger sector which give rise to these terms. In the MGM the Higgs soft masses at the messenger scale are assumed to be equal to the left handed slepton soft masses since these fields have the same gauge quantum numbers $m_{H_u}^2(M_m) = m_{H_d}^2(M_m) = m_{\tilde{\ell}_L}^2(M_m)$. However, it is possible that the additional interactions required to break $U(1)_{PQ}$ and $U(1)_{R-PQ}$ symmetries also contribute, either constructively or destructively, to the gauge mediated soft Higgs masses. If this is the case, the MGM relations between Higgs sector parameters μ and m_{ud}^2 and the electroweak parameters $\tan\beta$ and m_Z, implied by the constraints of electroweak symmetry breaking, are modified by the additional contributions to $m_{H_u}^2$ and $m_{H_d}^2$. From the phenomenological perspective this has the practical effect that the μ parameter, which determines the Higgsino Dirac mass, may be regarded as a free parameter.

The most important phenomenological effect of the Higgsino Dirac mass μ is on the Higgsino content of the lightest neutralino, $\tilde{\chi}_1^0$. In the MGM, with only gauge-mediated contributions to the Higgs soft masses, the constraints of electroweak symmetry breaking typically imply $\mu \sim \text{few} \times M_1$. In this case the lightest neutralino is Bino-like. However, taking μ as a free parameter leads to the possibility of a Higgsino like $\tilde{\chi}_1^0$. Some of the signatures associated with a Higgsino-like neutralino NLSP are discussed in section V.

ii) *$U(1)_R$-symmetry suppression of gaugino masses*

Gaugino masses require the breaking of both $U(1)_R$ symmetry and supersymmetry, while scalar masses require only supersymmetry breaking. In the MGM $U(1)_R$ and supersymmetry in the messenger sector are broken at the same scale by the auxiliary expectation value F_S. It is possible however with multiple spurions that $U(1)_R$ is an approximate symmetry at the supersymmetry breaking scale, and is only broken at a slightly lower scale [4]. In this case the gaugino masses are suppressed with respect to the scalar masses. The suppression can be parameterized with a parameter $\not{R} \leq 1$, which relates the gaugino masses M_a to the MGM predictions:

$$M_a = \not{R}\, M_a|_{\text{MGM}} \,. \tag{A.11}$$

With suppressed $U(1)_R$ breaking in the messenger sector the gauginos are somewhat lighter (in comparison with the MGM) than the scalars with similar quantum numbers. It should be noted that while gaugino masses require continuous $U(1)_R$ breaking they are invariant under discrete Z_2 R-parity. The breaking of continuous $U(1)_R$ symmetry therefore does not necessarily have anything at all to do with the conservation or possible violation of R-parity.

iii) *Messenger threshold corrections*

In the MGM all the messenger sector superfields are assumed to be approximately degenerate. The off-diagonal supersymmetry breaking contributions to the scalar mass squared matrix (A.4) are assumed to be small compared with the diagonal supersymmetric masses, amounting to $\Lambda \ll M_m$. This could be modified in several ways. First, it may be that there are significant hierarchies between the masses of different messenger fields. If there are two distinct messenger scales M and M', then there will be additional contributions to scalar squared masses proportional to $(\alpha_a M_a^2/4\pi)\ln(M/M')$ for each gauge group ($a = 1, 2, 3$). Second, it could be that the off-diagonal supersymmetry breaking contributions to scalar messenger masses are comparable to the diagonal supersymmetric masses. This effect can be computed in terms of a parameter $x = \Lambda/M_m$. The multiplicative threshold correction for the contributions to Standard Model gaugino masses is then $g(x) = 1 + \frac{1}{6}x^2 + \cdots$ while the multiplicative correction for scalar masses squared is $f(x) = 1 + \frac{1}{36}x^2 + \cdots$. Full expressions for these threshold corrections can be found in Refs. [67] and [11]. It should be noted that these corrections tend to be quite small in cases with moderate hierarchies, and do not violate the degeneracy of scalar partner masses with the same Standard Model gauge quantum numbers.

iv) *Non-$SU(5)$ multiplet messengers*

In the MGM the messenger fields are assumed to form complete multiplets of $SU(5) \supset SU(3)_C \times SU(2)_L \times U(1)_Y$. This has the advantage of naturally maintaining the successful supersymmetric prediction of gauge-coupling unification. However, it is also possible to view this apparent unification of gauge couplings as accidental, in whole or in part. The possibility of messenger fields which do not transform as complete $SU(5)$ multiplets may therefore be considered. In this case the expressions for the Standard Model gaugino and scalar partner masses at the messenger mass scale can be generalized to

$$M_a = k_a N_a \Lambda \frac{\alpha_a}{4\pi} \tag{A.12}$$

where $a = 1, 2, 3$, and

$$m_\phi^2 = 2\Lambda^2 \left[N_1 \frac{5}{3} \left(\frac{Y}{2}\right)^2 \left(\frac{\alpha_1}{4\pi}\right)^2 + N_2 C_2 \left(\frac{\alpha_2}{4\pi}\right)^2 + N_3 C_3 \left(\frac{\alpha_3}{4\pi}\right)^2 \right]. \tag{A.13}$$

Here N_a is the Dynkin index for the messenger fields for the appropriate gauge group, in a normalization in which $N_a = 1$ for $a = 1, 2, 3$ for a complete $\mathbf{5} \oplus \overline{\mathbf{5}} \in SU(5)$. In general, for vector messenger representations which can form Dirac states, N_2 and N_3 are required to be integers by non-Abelian gauge invariance. However, for the Abelian case of weak hypercharge,

$$N_1 = \frac{6}{5} \sum_i \left(\frac{Y_i}{2}\right)^2 \tag{A.14}$$

where the sum $\sum_i$ is over all messenger pairs. In general, N_1 must be an integer multiple of $1/5$. To see this, note that $(Y_i/2)^2 = (Q_i - T_{3i})^2$ where Q_i is the electric charge and T_{3i} is the weak isospin. Now, if fractional electric charges are confined by QCD (which is always the case for unifiable representations), then $3Q_i$ must be equal to the $SU(3)_C$ triality of the representation mod 3. This follows because it is always possible to combine the messenger field with some combination of ordinary Standard Model quark and anti-quark states to get a confined color singlet state with vanishing triality mod 3. Now, $SU(3)_C$ representations with non-zero triality have dimensions that are integer multiples of 3. Furthermore, T_{3i} is an integer(half-integer) for odd(even) dimensional representations of $SU(2)_L$. So if fractional charges are confined by QCD, then for any representation the quantity $(Y_i/2)^2 = (Q_i - T_{3i})^2$ multiplied by the dimension of the representation must be an integer multiple of $1/6$. This implies that N_1 is always an integer multiple of $1/5$ as long as QCD confines all fractional charges.

Clearly, choosing N_1, N_2 and N_3 independently (instead of $N = N_1 = N_2 = N_3$ as in the MGM) can give rise to a much more general set of possibilities for the gauge-mediated superpartner spectrum. Some of the possibilities for non-$SU(5)$ multiplet messengers have been studied in Ref. [11]. Another possibility is that the messenger fields do form complete $SU(5)$ multiplets, but that the supersymmetry breaking auxiliary expectation value(s) does not couple in an $SU(5)$-invariant manner [4].

v) *Gauge-multiplet messengers*

The massive messenger sector fields of the MGM are scalars and fermions that comprise chiral supermultiplets. However, it is also possible that some of the messengers are gauge bosons and gaugino fields which gain mass at the messenger scale. These fields comprise gauge multiplets corresponding to spontaneously broken gauge groups in the messenger or supersymmetry breaking sectors beyond the Standard Model gauge group. Such gauge-multiplet messengers always arise by virtue of the super-Higgs mechanism if chiral multiplets in the messenger sector which gain an expectation value transform under both the Standard Model gauge group and these additional gauge group(s). In this case $SU(3)_C \times SU(2)_L \times U(1)_Y \subset G$, where G also contains (some of) the messenger or supersymmetry breaking sector gauge groups which are spontaneously broken at the messenger scale.

The spectrum of the heavy gauge supermultiplets may break supersymmetry. Radiative masses for the visible sector gauginos and scalars are then generated analogously to the case of chiral messenger multiplets [68]. The most important feature of gauge multiplet messengers is that *negative* contributions to the visible sector scalar masses squared are induced. This effect poses a serious problem for such models since squark and/or slepton expectation values would result leading to color and/or charge breaking. Models which contain gauge-multiplet messengers must also in general contain chiral multiplet messengers to offset the negative contributions to scalar

masses squared. In this case the scalars are likely to be somewhat lighter (in comparison with the MGM) than the gauginos with similar quantum numbers.

vi) *Non-holomorphic messenger masses*

In the MGM, supersymmetry breaking in the messenger spectrum appears in the superpotential coupling (A.1), resulting in the off-diagonal holomorphic messenger soft masses in the scalar mass squared matrix (A.4). The diagonal scalar messenger masses in (A.4) are not affected by the auxiliary expectation value and are identical to the messenger fermion masses. This holomorphic form of supersymmetry breaking in the messenger sector has the special property $\mathcal{S}\mathrm{Tr}\ m^2 = 0$ where the supertrace is over all messenger particles, $\mathcal{S}\mathrm{Tr} \equiv \sum(-1)^f$ and $f = 0(1)$ for bosons(fermions), and each spin degree of freedom is counted separately. This has the important effect that the messenger soft masses to not mix with (or induce) visible sector scalar superpartner soft masses under renormalization group evolution. Only the finite, radiatively induced, two-loop soft scalar masses (A.8) result from messenger sector holomorphic supersymmetry breaking. The lack of renormalization group mixing can also be understood in terms of the messenger sector global symmetries carried by the holomorphic soft terms. The visible sector scalar superpartner soft masses do not transform under these symmetries. Since operators with different global quantum numbers can not mix, visible sector soft masses are therefore not induced under renormalization group evolution.

With a general messenger sector, supersymmetry breaking may appear in the messenger spectrum in a more general way than through the holomorphic superpotential coupling (A.1). The general form of the messenger scalar mass squared matrix may then be taken to be

$$\begin{pmatrix} m^2_{\psi_i} + \delta m^2_+ & \lambda F_S + \delta m^2 \\ \lambda F_S + \delta m^2 & m^2_{\psi_i} + \delta m^2_- \end{pmatrix} \tag{A.15}$$

where δm^2 is a holomorphic soft mass squared parameter while δm^2_+ and δm^2_- are non-holomorphic soft mass squared parameters. The inclusion of these diagonal non-holomorphic soft masses leads to $\mathcal{S}\mathrm{Tr}\ m^2 = 2(\delta m^2_+ + \delta m^2_-) \neq 0$. Because of this, non-holomorphic messenger soft masses can induce [69] visible sector soft masses squared at two loops under renormalization group evolution [70]. This occurs because no symmetry forbids non-holomorphic soft masses in the messenger sector from mixing with visible sector soft masses. Because of the renormalization group contribution, two-loop soft squared masses induced by non-holomorphic terms in the messenger sector are larger than the finite two-loop soft squared masses induced by holomorphic terms by a factor $\ln(M_m/m_m)$, where M_m is the messenger scale at which the non-holomorphic messenger masses are generated and m_m is the mass of the messengers. Likewise, since gaugino masses require $U(1)_R$ breaking which only appears in (A.15) from the off-diagonal holomorphic soft masses, the non-holomorphic renormalization group contribution to the visible sector scalar squared masses are also larger than the gaugino masses by the same $\ln(M_m/m_m)$ factor. So in theories with non-holomorphic messenger masses and $M_m \gg m_m$ the magnitude of the visible sector scalar squared masses are larger than the associated gaugino masses with similar gauge quantum numbers. It is also worth noting that for $\mathcal{S}\mathrm{Tr}\ m^2 = 2(\delta m^2_+ + \delta m^2_-) > 0$ in (A.15) the induced visible sector soft masses squared are negative, which is phenomenologically unacceptable. Non-holomorphic messenger masses are therefore only viable for $\delta m^2_+ + \delta m^2_- < 0$.

Non-holomorphic messenger soft masses can arise in theories in which the Standard Model gauge group is embedded directly in the supersymmetry breaking sector. In such theories it is possible that some of the moduli (or sigma model degrees of freedom) in the supersymmetry breaking sector transform under the Standard Model gauge group and act as messengers. Such moduli naturally receive non-holomorphic soft masses from Kahler potential couplings due to non-trivial curvature of the Kahler manifold. The messenger scale, M_m, in such theories is set by the mass of other chiral supermultiplet and gauge supermultiplet messenger fields which gain a mass via the super-Higgs mechanism due to gauge symmetry breaking expectation values. If the supersymmetry sector is non-renormalizable the moduli with non-holomorphic soft masses gain a mass m_m, at a hierarchically smaller scale than the messenger scale, $m_m \ll M_m$. The logarithmic enhancement of the visible sector soft squared masses, $\ln(M_m/m_m)$, can then be sizeable. In most non-renormalizable gauge-mediated supersymmetry breaking theories of this type the magnitude of the logarithm is large enough to require some degree of fine tuning to obtain electroweak symmetry breaking consistent with current bounds on gaugino masses. Ignoring this problem of fine tuning, and assuming $\mathcal{S}\mathrm{Tr}\ m^2 < 0$ so that visible sector soft masses squared are positive, the gauginos are generally lighter than the associated scalars with similar quantum numbers by the logarithmic factor $\ln(M_m/m_m)$.

vii) *D-term contributions to scalar masses*

In addition to the radiatively generated scalar soft masses arising from F-term auxiliary expectation values in the messenger sector, it is possible for scalar soft masses to receive contributions directly from a non-zero D-term expectation value for $U(1)_Y$ hypercharge. This leads to a shift in the soft scalar masses proportional to the weak hypercharge according to

$$\Delta m_\phi^2 = -Y_\phi g' \langle D_Y \rangle. \tag{A.16}$$

where Y_ϕ is the weak $U(1)_Y$ hypercharge of the scalar ϕ and D_Y is the $U(1)_Y$ auxiliary field. More generally, if the unbroken gauge symmetry at the supersymmetry-breaking scale contains an additional Abelian factor(s) $U(1)_X$, then similar contributions can arise

$$\Delta m_\phi^2 = -X_\phi g_X \langle D_X \rangle, \tag{A.17}$$

where X_ϕ is the $U(1)_X$ charge of ϕ and D_X is the $U(1)_X$ auxiliary field. If present, these D-term contributions will not affect the MSSM gaugino mass parameters, but can leave a "fingerprint" on the MSSM scalar mass spectrum which can be quite distinct from that of the MGM. Note that since Tr $Y = 0$ and Tr $X = 0$ in order to ensure vanishing of gravitational anomalies and quadratic divergences, some scalar field(s) necessarily receive a negative mass squared contribution from D-term expectation values.

Non-vanishing D-terms may arise either at tree-level or radiatively. Tree-level D-term expectation values for unbroken $U(1)$ gauge symmetries generally arise if there is chiral matter in the supersymmetry breaking sector which gains a scalar expectation value and transforms under the $U(1)$. In non-renormalizable models with large scalar moduli expectation values these D-terms are generally hierarchically smaller than the supersymmetry breaking scale and unimportant. In renormalizable models however the non-vanishing D-terms are generally only suppressed compared with the supersymmetry breaking scale by some power of a Yukawa coupling in this sector. D-term expectation values can also be generated radiatively at one loop from messenger fields which transform under the $U(1)$. This occurs if $\delta m_+ \neq \delta m_-$ in the scalar mass squared matrix (A.15).

Both tree-level and radiatively generated D-term expectation values automatically vanish if there is an unbroken discrete symmetry under which D transforms. In the MGM messenger parity provides such a discrete symmetry, and $D_Y = 0$ at leading order.

viii) *Strongly coupled messengers*

The calculation of gaugino and scalar superpartner masses in the MGM assumes that the messenger dynamics can be treated perturbatively. However, it is likely that the ultimate source of supersymmetry breaking involves non-perturbative dynamics which may be strongly coupled. It is then natural in certain classes of renormalizable theories in which the messenger and supersymmetry breaking scales coincide to consider the possibility that the messengers are strongly coupled [71]. Assuming the Standard Model gauginos are elementary at the messenger scale, the induced gaugino masses may be estimated using the standard rules of naive dimensional analysis for strongly coupled theories [72]

$$M_a \sim N \, \frac{\alpha_a}{4\pi} \, \frac{4\pi F}{M} \tag{A.18}$$

where the supersymmetry breaking scale $\sqrt{F}$ and cutoff or messenger scale M are related by $F \sim 4\pi M^2$. For elementary Standard Model scalar superpartners, the induced scalar masses are of the order [72]

$$m_\phi^2 \sim N \, \left(\frac{\alpha_a}{4\pi}\right)^2 \left(\frac{4\pi F}{M}\right)^2 \tag{A.19}$$

As in the perturbative case, the scalar and gaugino masses are the same order. However, relative to these masses, the Goldstino decay constant F is roughly a factor of 4π *smaller* than for the perturbative case.

Another interesting possibility is that some of the Standard Model matter supermultiplets are composite and/or directly coupled to the messenger and supersymmetry breaking sectors. In this case the scalar superpartners of these supermultiplets could naturally gain a mass at the supersymmetry breaking scale. For example if the first two generations are composite, with supersymmetry breaking and compositeness scales of the same order, it is likely that only the gauginos and third generation scalars would be accessible at accelerator energies [73].

APPENDIX B: DECAYS TO THE GOLDSTINO

The spontaneous breaking of global supersymmetry leads to the existence of a massless Goldstone fermion, the Goldstino. The lowest order derivative coupling for emission or absorption of a single on-shell Goldstino is fixed by the supersymmetric Goldberger-Treiman low energy theorem to be proportional to

$$\frac{1}{F}\partial_\mu G^\alpha j^\mu{}_\alpha \; + \; h.c. \tag{B.1}$$

where $\sqrt{F}$ is the supersymmetry breaking scale, and $j^\mu{}_\alpha$ the supercurrent. This allows the model independent decay rate of a sparticle to its partner plus the Goldstino to be calculated in terms of the supersymmetry breaking scale. Since cascade decays of heavy superpartners through tree-level interactions are generally very rapid, decay by Goldstino emission is generally only relevant for the lightest Standard Model superpartner(s).

For a slepton or squark the decay rate to its partner plus the Goldstino in the absence of any supersymmetric flavor mixing is [38,4]

$$\Gamma(\tilde{f} \to f\widetilde{G}) = \frac{m_{\tilde{f}}^5}{16\pi F^2}\left(1 - \frac{m_f^2}{m_{\tilde{f}}^2}\right)^4 . \tag{B.2}$$

Because the Goldstino is derivatively coupled, the two body decay rate to any massive final state suffers a β^4 suppression near threshold, where β is the massive final state velocity in the decay rest frame.

Non-vanishing supersymmetric flavor mixing in general introduces flavor violation in decay to the Goldstino. For example, the general decay rate of an up-type squark to a quark and the Goldstino is

$$\Gamma(\widetilde{Q}_a \to q_i\widetilde{G}) = \frac{m_{\tilde{Q}}^5}{16\pi F^2}\left(|U_{Lai}|^2 + |U_{Rai}|^2\right)\left(1 - \frac{m_{q_i}^2}{m_{\tilde{Q}}^2}\right)^4 \tag{B.3}$$

where here U_{Lai} and U_{Rai} are the up-squark mixing matrices between the mass eigenstates $a = 1, \ldots, 6$ and left and right flavor eigenstates $i = 1, 2, 3$. These are defined with respect to the up-quark mass eigenstates, $\widetilde{Q}_a = U_{Lai}\widetilde{Q}_{Li} + U_{Rai}\widetilde{Q}_{Ri}$, with $U^\dagger_{Lia}U_{Laj} = \delta_{ij}$, $U^\dagger_{Ria}U_{Raj} = \delta_{ij}$, and $U^\dagger_{Lia}U_{Raj} = 0$. There are no $L - R$ mixing contributions to (B.3) since the Goldstino is massless. Similar expressions hold for the down-type squarks and sleptons. For squarks lighter than the top quark, two-body decays to the Goldstino and top quark are kinematically forbidden. In this case three-body decays to the W-boson, quark, and Goldstino can become relevant depending on the magnitude of supersymmetric flavor mixing [57]. In general these decays proceed through an off-shell squark, quark, or chargino. In the limit $m_{\widetilde{\chi}_i^\pm} \gg m_{\tilde{Q}_a}$ and $m_{\tilde{Q}_b} \gg m_{\tilde{Q}_a}$, the three-body decay of the a-th up-type squark takes place predominantly through an off-shell quark plus diagrams related by gauge invariance. The general expression for the three-body decay simplifies in this limit to [57]

$$\Gamma(\widetilde{Q}_a \to q_j W\widetilde{G}) = \frac{\alpha_2 m_{\tilde{Q}}^5}{128\pi^2 F^2}\left[\left|U_{Lai}V^\dagger_{ij}\right|^2 \; I\left(m_W^2/m_{\tilde{Q}}^2, m_{q_i}^2/m_{\tilde{Q}}^2\right)\right.$$
$$\left. + \left|U_{Rai}V^\dagger_{ij}\right|^2 \; J\left(m_W^2/m_{\tilde{Q}}^2, m_{q_i}^2/m_{\tilde{Q}}^2\right)\right], \tag{B.4}$$

where here V_{ij} is the CKM quark mixing matrix, and the phase space integrals are

$$I(a,b) = \int_a^1 dx \frac{(1-x)^4(x-a)^2}{12x^3a}\left(\frac{6x^3(3a+x)}{(x-b)^2} + \frac{4x^2(4a-x)}{(x-b)} + x^2 + 2xa + 3a^2\right) \tag{B.5}$$

$$J(a,b) = \int_a^1 dx \frac{b(1-x)^4(x-a)^2(2a+x)}{2x^2a(x-b)^2}. \tag{B.6}$$

These three-body decays are particularly relevant for a stop-like squark lighter than the top quark, which can decay by $\tilde{t} \to bW\widetilde{G}$.

Neutralinos are in general mixtures of gaugino and Higgsino eigenstates, and so can decay to neutral gauge bosons and Higgs bosons if kinematically accessible through Goldstino emission. The decay rates to the photon final state through the gaugino components, and Z-boson final state through the gaugino and Higgsino components are [38,4]

$$\Gamma(\widetilde{\chi}_i^0 \to \gamma\widetilde{G}) = |\cos\theta_W N_{1\tilde{B}} + \sin\theta_W N_{1\tilde{W}}|^2 \frac{m^5_{\widetilde{\chi}_i^0}}{16\pi F^2} \tag{B.7}$$

$$\Gamma(\widetilde{\chi}_i^0 \to Z\widetilde{G}) = \left(|\sin\theta_W N_{1\tilde{B}} - \cos\theta_W N_{1\tilde{W}}|^2 + \frac{1}{2}|\cos\beta N_{1d} - \sin\beta N_{1u}|^2\right) \frac{m^5_{\widetilde{\chi}_i^0}}{16\pi F^2}\left(1 - \frac{m_Z^2}{m^2_{\widetilde{\chi}_i^0}}\right)^4 \tag{B.8}$$

where N_{ij} are the neutralino eigenvectors which diagonalize the neutralino mass matrix $M_D = N^* M N^{-1}$ [18]. The decay rates to Higgs boson final states through the Higgsino components are [38,4]

$$\Gamma(\widetilde{\chi}_i^0 \to h^0\widetilde{G}) = \frac{1}{2}|\sin\alpha N_{1d} - \cos\alpha N_{1u}|^2 \frac{m^5_{\widetilde{\chi}_i^0}}{16\pi F^2}\left(1 - \frac{m_{h^0}^2}{m^2_{\widetilde{\chi}_i^0}}\right)^4 \tag{B.9}$$

$$\Gamma(\widetilde{\chi}_i^0 \to H^0\widetilde{G}) = \frac{1}{2}|\cos\alpha N_{1d} + \sin\alpha N_{1u}|^2 \frac{m^5_{\widetilde{\chi}_i^0}}{16\pi F^2}\left(1 - \frac{m_{H^0}^2}{m^2_{\widetilde{\chi}_i^0}}\right)^4 \tag{B.10}$$

$$\Gamma(\widetilde{\chi}_i^0 \to A^0\widetilde{G}) = \frac{1}{2}|\sin\beta N_{1d} + \cos\beta N_{1u}|^2 \frac{m^5_{\widetilde{\chi}_i^0}}{16\pi F^2}\left(1 - \frac{m_{A^0}^2}{m^2_{\widetilde{\chi}_i^0}}\right)^4 \tag{B.11}$$

where α is the $h^0 - H^0$ Higgs mixing angle. In the Higgs decoupling limit in which only h^0 remains light, this angle is related to $\tan\beta$ by $\sin\alpha \simeq -\cos\beta$ and $\cos\alpha \simeq \sin\beta$ [74].

Decay of neutralinos through Goldstino emission to three-body final states can take place through an off-shell intermediate gauge boson [38]. The most important of these are Dalitz decays of neutralinos through an off-shell photon to fermion final states, $\widetilde{\chi}_i^0 \to \gamma^*\widetilde{G}$ with $\gamma^* \to f\bar{f}$. The neutralino Dalitz decay rate to a Goldstino is

$$\frac{\Gamma(\widetilde{\chi}_i^0 \to f\bar{f}\widetilde{G})}{\Gamma(\widetilde{\chi}_i^0 \to \gamma\widetilde{G})} = \frac{\alpha Q_f^2 N_c^f}{3\pi}\left(\ln(m^2_{\widetilde{\chi}_i^0}/m_f^2) - \frac{15}{4}\right) \tag{B.12}$$

where Q_f and m_f are the fermion electric charge and mass respectively, and $N_c^f = 1$ for leptons and 3 for quarks. For light quarks m_f should be replaced with an infrared cutoff of order Λ_{QCD}.

Charginos are in general mixtures of Wino and charged Higgsino eigenstates, and so can decay to $W^\pm$-boson and $H^\pm$ charged Higgs final states through Goldstino emission. The chargino decay rates are [38]

$$\Gamma(\widetilde{\chi}_i^\pm \to W^\pm\widetilde{G}) = \frac{1}{2}\left(|V_{i\tilde{W}}|^2 + |U_{i\tilde{W}}|^2 + \sin^2\beta|V_{i\tilde{H}}|^2 + \cos^2\beta|U_{i\tilde{H}}|^2\right)\frac{m^5_{\widetilde{\chi}_i^\pm}}{16\pi F^2}\left(1 - \frac{m_{W^\pm}^2}{m^2_{\widetilde{\chi}_i^\pm}}\right)^4 \tag{B.13}$$

$$\Gamma(\widetilde{\chi}_i^\pm \to H^\pm\widetilde{G}) = \frac{1}{2}\left(\cos^2\beta|V_{i\tilde{H}}|^2 + \sin^2\beta|U_{i\tilde{H}}|^2\right)\frac{m^5_{\widetilde{\chi}_i^\pm}}{16\pi F^2}\left(1 - \frac{m_{H^\pm}^2}{m^2_{\widetilde{\chi}_i^\pm}}\right)^4, \tag{B.14}$$

where here U_{ij} and V_{ij} are the chargino eigenvectors which diagonalize the chargino mass matrix by the bi-unitary transformation $M_D = U^* M V^{-1}$ [18].

Gluinos do not mix with other states, and so decay through Goldstino emission only to gluon final states, with decay rate [38]

$$\Gamma(\widetilde{g} \to g\widetilde{G}) = \frac{m^5_{\widetilde{g}}}{16\pi F^2}. \tag{B.15}$$

APPENDIX C: LIST OF MODEL LINES STUDIED

The Model Lines selected for this study are listed below. In each case, Λ is varied with the other parameters or ratios held fixed as shown. Different workers may obtain slightly different masses and branching fractions due to using different Standard Model gauge couplings, top mass, etc.

- Bino-like Neutralino NLSP Model Line: $N = 1$; $M_m/\Lambda = 2$; $\tan\beta = 2.5$; $\mu > 0$ fixed by EWSB.
- Higgsino-like Neutralino NLSP Model Line I: $N = 2$; $M_m/\Lambda = 3$; $\tan\beta = 3$; $\mu = -\frac{3}{4}M_1$.
- Higgsino-like Neutralino NLSP Model Line II: $N = 2$; $M_m/\Lambda = 3$; $\tan\beta = 3$; $\mu = \frac{1}{3}M_1$.
- Stau NLSP Model Line: $N = 2$; $M_m/\Lambda = 3$; $\tan\beta = 15$; $\mu > 0$ fixed by EWSB.
- Slepton co-NLSP Model Line: $N = 3$; $M_m/\Lambda = 3$; $\tan\beta = 3$; $\mu > 0$ fixed by EWSB.
- Squark NLSP Model Line: Single squark with varying mass.

APPENDIX D: GLOSSARY OF ACRONYMS

Acronyms used in this report which are peculiar to signals of low-scale supersymmetry breaking:

- **CC-HIT** Charge-changing highly ionizing track. These can arise when a charged slepton decays to a nearly degenerate stau of the opposite charge, by emitting a very soft lepton and tau, with the stau traveling in the forward direction. This decay can have a macroscopic length for non-relativistic sleptons, and so leads to a highly ionizing track which appears to change sign.
- **CE-HIT** Charge-exchange highly ionizing track. Strongly interacting squark or gluino bound states can exchange isospin and charge with matter in the course of traversing a detector. Non-relativistic bound states of this type therefore give rise to calorimeter deposits which alternate between highly ionizing charged and neutral segments associated with highly ionizing tracks (HITs) in the tracking and vertex detectors.
- **DCA** The distance of closest approach to the primary vertex for a displaced photon or charged track.
- **GMSB** Gauge-mediated supersymmetry breaking, the most concrete and perhaps the best-motivated example of low-scale supersymmetry breaking.
- **HIT** Highly ionizing track left by a long-lived charged particle such as a stau, selectron, smuon, squark in a mesino or sbaryon hadronic bound state, or gluino in a R-hadron bound state. These massive particles can travel slowly enough to deposit energy at a rate dE/dx which is much larger than for a MIP.
- **H-HIT** A highly ionizing track associated with additional soft hadronic activity. These can result from inelastic hadronic interactions of slowly-moving squark or gluino bound states in the calorimeters.
- **LNIP** Large negative impact parameter. The sign of the impact parameter is defined to be $\mathrm{sgn}(\cos\varphi)$, where φ is the angle between the reconstructed momentum vector of a displaced parton and the unit normal from the beam axis to the origin of the displaced jet. (See section VIII B.) Negative values arise from massive slowly moving long-lived unstable particles which decay to visible partons in a direction towards, rather than away from (as for a light relativistic unstable particle), the production vertex.
- **MGM** Minimal gauge mediation. GMSB with N generations of messengers and the μ-parameter determined (up to a sign) by EWSB.
- **MIP** A minimum ionizing particle, such as a muon or a long-lived stau with $\beta\gamma \gtrsim 0.85$.
- **NLSP** The next-to-lightest supersymmetric particle (or particles), which decay to the nearly massless Goldstino.

REFERENCES

1. P. Fayet, Phys. Lett. B **70** (1977) 461; Phys. Lett. B **84** (1979) 416; Phys. Lett. B **84** (1979) 241.
2. S. Dimopoulos, M. Dine, S. Raby, and S. Thomas, Phys. Rev. Lett. **76** (1996) 3494.
3. S. Dimopoulos, M. Dine, S. Raby, S. Thomas, and J. Wells, hep-ph/9607450, Nucl. Phys. Proc. Suppl. A **52** (1997) 38.
4. S. Dimopoulos, S. Thomas, and J. Wells, Nucl. Phys. B **488** (1997) 39.
5. S. Ambrosanio, G.D. Kribs and S.P. Martin, Phys. Rev. **D56**, 1761 (1997).
6. S. Ambrosanio, G.D. Kribs, and S.P. Martin, Nucl. Phys. B **516** (1998) 55.
7. S. Abel *et al.* [SUGRA Working Group Collaboration], "Report of the SUGRA working group for run II of the Tevatron," hep-ph/0003154 and these proceedings.
8. M. Dine, W. Fischler, and M. Srednicki, Nucl. Phys. B **189** (1981) 575; S. Dimopoulos and S. Raby, Nucl. Phys. B **192** (1981) 353; M. Dine and W. Fischler, Phys. Lett. B **110** (1982) 227; M. Dine and M. Srednicki, Nucl. Phys. B **202** (1982) 238; L. Alvarez-Gaumé, M. Claudson, and M. Wise, Nucl. Phys. B **207** (1982) 96; C. Nappi and B. Ovrut, Phys. Lett. B **113** (1982) 175.
9. M. Dine and W. Fischler, Nucl. Phys. B **204** (1982) 346; S. Dimopoulos and S. Raby, Nucl. Phys. B **219** (1983) 479.
10. M. Dine and A. Nelson, hep-ph/9303230, Phys. Rev. D **48** (1993) 1277; M. Dine, A. Nelson, and Y. Shirman, hep-ph/9408384, Phys. Rev. D **51** (1995) 1362; M. Dine, A. Nelson, Y. Nir, and Y. Shirman, hep-ph/9507378, Phys. Rev. D **53** (1996) 2658.
11. S.P. Martin, Phys. Rev. **D55**, 3177 (1997).
12. G.F. Giudice and R. Rattazzi, Phys. Rept. **322**, 419 (1999) [hep-ph/9801271].
13. S. Thomas, SU-ITP-99-47.
14. H. Baer, P.G. Mercadante, X. Tata and Y. Wang, Phys. Rev. **D60**, 055001 (1999).
15. B. Dutta and S. Nandi, hep-ph/9709511.
16. B. Dutta, D.J. Muller and S. Nandi, Nucl. Phys. **B544**, 451 (1999). D.J. Muller and S. Nandi, Phys. Rev. **D60**, 015008 (1999).
17. F. Paige and S. Protopopescu, BNL Report No. 38304, 1986 (unpublished), releases v7.37 and v7.42; H. Baer, F. E. Paige, S. D. Protopopescu and X. Tata, hep-ph/9810440, hep-ph/0001086 and references therein.
18. H. Haber and G. Kane, Phys. Rept. **117** (1985) 75.
19. S.P. Martin, "A Supersymmetry Primer", hep-ph/9709356, and in *Perspectives on supersymmetry*, ed. G.L. Kane, World Scientific, 1998..
20. W. Beenakker, M. Kramer, T. Plehn, and M. Spira, hep-ph/9810290; W. Beenakker, M. Klasen, M. Kramer, T. Plehn, M. Spira, P.M. Zerwas, Phys. Rev. Lett. 83 (1999) 3780.
21. "Report of the Higgs Working Group", these proceedings.
22. D. Cutts and G. Landsberg, private communication.
23. Yu. Gershtein, "*Level-1 Trigger for Slow Moving Particles*", DØnote # 3431.
24. T. Sjöstrand, Comp. Phys. Comm. **82**, 74 (1994), S. Mrenna, Comp. Phys. Comm. **101**, 232 (1997).
25. J. Conway, talk given at the SUSY-Higgs Workshop meeting, Fermilab, May 14-16, 1998. See also www.physics.rutgers.edu/~jconway/soft/shw/shw.html.
26. S. Jadach, J.H. Kuhn and Z. Was, Comp. Phys. Comm. **64**, 275 (1990), *ibid.* **76**, 361 (1993).
27. L. Garren, STDHEP manual, http://www-pat.fnal.gov/stdhep.html
28. CDF Technical Design Report, preprint FERMILAB-PUB-96/390-E.
29. D. Toback, Ph.D. thesis, University of Chicago, 1997. F. Abe et al., Phys. Rev. Lett. **81**, 1791 (1998). F. Abe et al., submitted to Phys. Rev. D, FERMILAB-PUB-98/206-E.
30. DØ Collaboration, B. Abbott *et al.*, Phys. Rev. Letters, **80**, 442 (1998).
31. H. Baer, M. Brhlik, C. Chen and X. Tata, Phys. Rev. **D55**, 4463 (1997).
32. B. Abbott *et al.* Phys. Rev. Lett. **80**, 442 (1998).
33. C. H. Chen and J. F. Gunion, Phys. Lett. **B420**, 77 (1998); Phys. Rev. **D58**, 075005 (1998).
34. "Report of the Beyond the MSSM Subgroup for the Tevatron Run II SUSY/Higgs Workshop", hep-ph/0006162 and these proceedings.
35. K. Matchev, talk given at SUSY'98, Oxford, England, http://hepnts1.rl.ac.uk/SUSY98; S. Thomas, talks presented at the SUSY/Higgs Run II workshops, Batavia, IL, May 1998, Sept. 1998.
36. K. Matchev and S. Thomas, hep/ph-9908482, to appear in Phys. Rev. D.
37. K. Matchev and S. Thomas, SU-ITP-99-46.
38. S. Ambrosanio, G.L. Kane, G.D. Kribs, S.P. Martin and S. Mrenna, Phys. Rev. **D54**, 5395 (1996).
39. J. Bagger, K. Matchev, D. Pierce, and R.-J. Zhang, Phys. Rev. D **55** 3188 (1997).
40. Presented at the Summary Meeting of the Physics at Run II – Supersymmetry/Higgs Workshop, 1998.

41. DØ Collaboration, B. Abbott *et al.*, Phys. Rev. Letters, **82**, 42 (1999).
42. T. Han and R. Sobey, Phys. Rev. D **52**, 6302 (1995).
43. F. Abe *et al.*, Phys. Rev. Lett. **74**, 1941 (1995).
44. B. Abbott *et al.*, Phys. Rev. D **57** R3817 (1998).
45. G. Landsberg, private communication.
46. S. Abachi *et al.*, Phys. Rev. Lett. **78**, 3640 (1997).
47. S. Abachi *et al.*, Phys. Rev. **D56**, 6742 (1997).
48. B. Abbott *et al.*, Phys. Rev. Lett. **82** 29 (1999).
49. The CDF Collaboration, Phys. Rev. D **58**, (1998) 051101.
50. J. L. Feng and T. Moroi, Phys. Rev. **D58**, 035001 (1998).
51. S. P. Martin and J. D. Wells, Phys. Rev. **D59**, 035008 (1999).
52. L. Groer, Ph.D. Thesis, Rutgers University, 1998.
53. F. Abe et al., The CDF Collaboration, Phys. Rev. Lett. **79**, 357 (1997).
54. DØ Collaboration, B. Abbott *et al.*, Phys. Rev. Letters, **80**, 1591 (1998).
55. K. Maeshima, in *Proceedings of the 28th International Conference on High Energy Physics*, edited by Z. Ajduk and A. K. Wroblewski (World Scientific, Singapore), 1997, FERMILAB–CONF–96–412–E.
56. F. Abe et al., The CDF Collaboration, Phys. Rev. Lett. **80**, 5275 (1998).
57. U. Sarid and S. Thomas, hep-ph/9909349, Phys. Rev. Lett. **85** (2000) 1178.
58. C.-L. Chou and M. Peskin, hep-ph/9909536, Phys. Rev. D **61** (2000) 055004.
59. J. Valls, in *Proceedings of the 29th International Conference on High-Energy Physics (ICHEP '98)*, (Vancouver, Canada, July, 1998), FERMILAB-CONF-98-292-E,.
60. P. Azzi, in *Proceedings of XXXII Rencontres de Moriond, QCD and High Energy Hadronic Interactions*, 1997, FERMILAB–CONF–97/148–E.
61. J. Bjorken, private communication.
62. M. Drees and X. Tata, Phys. Lett. B **252** (1990) 695; H. Baer, K. Cheung, and J. Gunion, hep-ph/9806361, Phys. Rev. D **59** (1999) 075002,
63. F. Abe, *et al.*, Phys. Rev. Lett. **80**, 2779 (1998)
64. T. Han, D. Marfatia, R.-J. Zhang, MADPH-99-1123, hep-ph/9906508.
65. A. Brignole, F. Feruglio, M.L. Mangano, and F. Zwirner, Nucl. Phys. B **526** 136 (1998) and private communication.
66. T. Affolder *et al.* [CDF Collaboration], hep-ex/0003026.
67. S. Dimopoulos, G.F. Giudice and A. Pomarol, Phys. Lett. **B389**, 37 (1996).
68. G.F. Giudice and R. Rattazzi, Nucl. Phys. **B511**, 25 (1997).
69. E. Poppitz and S.P. Trivedi, Phys. Lett. **B401**, 38 (1997).
70. I. Jack, D.R.T. Jones, S.P. Martin, M.T. Vaughn and Y. Yamada, Phys. Rev. **D50**, 5481 (1994), and references therein.
71. S. Dimopoulos, M. Dine, S. Raby and S. Thomas, Phys. Rev. Lett. **76**, 3494 (1996).
72. A.G. Cohen, D.B. Kaplan and A.E. Nelson, hep-ph/9706275, Phys. Lett. **B412**, 301 (1997).
73. S. Dimopoulos and G.F. Giudice, hep-ph/9507282, Phys. Lett. **B357**, 573 (1995); A.G. Cohen, D.B. Kaplan and A.E. Nelson, hep-ph/9607394, Phys. Lett. **B388**, 588 (1996); hep-ph/9507282, S. Ambrosanio and J.D. Wells, hep-ph/9902242.
74. J. Gunion, H. Haber, G. Kane, and S. Dawson, *The Higgs Hunter's Guide* (Addison-Wesley, New York, 1990) Chp. 4.